



CZECH TECHNICAL UNIVERSITY IN PRAGUE

FACULTY OF BIOMEDICAL ENGINEERING

**Novel approaches in evaluation of lung ventilation distribution
using electrical impedance tomography**

**Nové přístupy ve vyhodnocování distribuce plicní ventilace
pomocí elektrické impedanční tomografie**

Master Thesis

Study Programme: Biomedical and clinical technology
Branch of Study: Biomedical engineer

Author: Bc. Vladimír Sobota
Supervisor: prof. Ing. Karel Roubík, Ph.D.

Kladno 2016

Department of Biomedical Technology

Academic year: 2015/2016

D i p l o m a T h e s i s a s s i g n m e n t

Student: **Bc. Vladimír Sobota**
Study branch: Biomedical engineer
Title: **Novel approaches in evaluation of lung ventilation distribution using electrical impedance tomography**
Title in Czech: **Nové přístupy ve vyhodnocování distribuce plicní ventilace pomocí elektrické impedanční tomografie**

Instructions for processing:

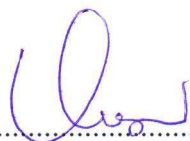
Compare the parameters derived from electrical impedance tomography that describe regional distribution of lung ventilation. Implement the algorithms for calculation of these parameters in MATLAB environment and use them for evaluation of data obtained in animal experiments. Analyze the results with respect to the parameters that were published in current research literature.

References:

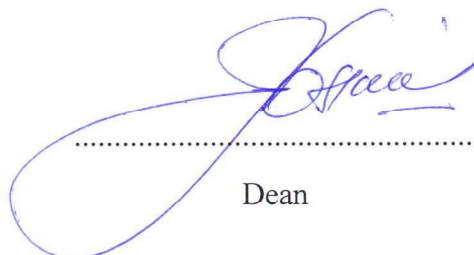
- [1] Holder D., Electrical impedance tomography: Methods, history and applications, ed. 2, IOP Publishing Ltd., 2005, 456 s., ISBN 978-0-7503-0952-3
- [2] Steffen Leonhardt, Burkhard Lachmann, Electrical impedance tomography: the holy grail of ventilation and perfusion monitoring? Intensive Care Medicine, vol. 38, no. 12, 2012, 12 s.
- [3] A. Adler, M. B. Amato, J. H. Arnold, R. Bayford, M. Bodenstein, S. H. Böhm, B. H. Brown, I. Frerichs, O. Stenqvist, et al. Whither lung EIT: Where are we, where do we want to go and what do we need to get there? Physiological Measurement, vol. 33, no. 5. 2012, 679-694 s.
- [4] M. van Heerde, K. Roubik, V. Kopelent, M. C. J. Kneyber and D. G. Markhorst, Spontaneous breathing during high-frequency oscillatory ventilation improves regional lung characteristics in experimental lung injury, Acta Anaesthesiol Scand, vol. 54, no. 1, 2010, 1248-1256 s.

Validity of Thesis Assignment:
Supervisor:

20. 8. 2017
Prof. Ing. Karel Roubík, Ph.D.



Head of Department



Dean

In Kladno 23. 02. 2016

Katedra biomedicínské techniky

Akademický rok: 2015/2016

Z a d á n í d i p l o m o v é p r á c e

Student: **Bc. Vladimír Sobota**
Studijní obor: Biomedicínský inženýr
Téma: **Nové přístupy ve vyhodnocování distribuce plicní ventilace pomocí elektrické impedanční tomografie**
Téma anglicky: Novel approaches in evaluation of lung ventilation distribution using electrical impedance tomography

Z á s a d y p r o v y p r a c o v á n í :

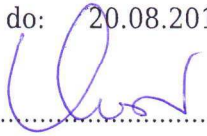
Inovujte parametry, které popisují regionální distribuci plicní ventilace a které jsou vypočítávány na základě elektrické impedanční tomografie. Implementujte v prostředí MATLAB algoritmy pro výpočet těchto parametrů a vyhodnoťte jimi data získaná v průběhu animálních experimentů. Analyzujte výsledky vzhledem k parametrům publikovaným v současné odborné literatuře.

Seznam odborné literatury:

- [1] A. Adler, M. B. Amato, J. H. Arnold, R. Bayford, M. Bodenstein, S. H. Böhm, B. H. Brown, I. Frerichs, O. Stenqvist, et al. , Whither lung EIT: Where are we, where do we want to go and what do we need to get there? , Physiological Measurement, ročník 33, číslo 5, 2012, 679-694 s.
- [2] Steffen Leonhardt, Burkhard Lachmann, Electrical impedance tomography: the holy grail of ventilation and perfusion monitoring?, Intensive Care Medicine, ročník 38, číslo 12, 2012
- [3] M. van Heerde, K. Roubik, V. Kopelent, M. C. J. Kneyber and D. G. Markhorst, Spontaneous breathing during high-frequency oscillatory ventilation improves regional lung characteristics in experimental lung injury, Acta Anaesthesiol Scand, ročník 54, číslo 1, 2010, 1248-1256 s.

Vedoucí: **prof. Ing. Karel Roubík, Ph.D.**

Zadání platné do: 20.08.2017


.....
vedoucí katedry / pracoviště


.....
děkan

V Kladně dne 20.01.2015

Acknowledgement

This master thesis partially reflects several years of my research interest in electrical impedance tomography. Most of that time, I was a student member of the Non-conventional Ventilatory Team, based at Faculty of Biomedical Engineering, Czech Technical University in Prague. I would like to thank to prof. Ing. Karel Roubík, Ph.D., the head of the team and my supervisor, for all the support, guidance and valuable advices that I received throughout those years. My gratitude also belongs to all the team members that contributed to create a great research environment for my work and encouraged me to present my results at international conferences.

Special thanks also go to Priv.-Doz. Dr.med. Michael Czaplik for supervision of my internship at the Department of Anaesthesiology, University Hospital RWTH Aachen, Germany, where I prepared the background for the theoretical part of this work. I would also like to thank the employees of the animal laboratory of the Department of Physiology, First Faculty of Medicine, Charles University, where the animal trials were performed, especially to MUDr. Mikuláš Mlček, Ph.D.

Finally, I would like to thank to my parents who have been supporting me throughout my studies. This work would hardly be created without their encouragement and without the help of all the persons mentioned above.

The research described in this study was supported by the grants of Czech Technical University in Prague SGS14/216/OHK4/3T/17 and SGS16/258/OHK4/3T/17 and by the grant of the Ministry of the Interior VG20102015062.

Declaration

Hereby I declare that I have completed the thesis entitled **Novel approaches in evaluation of lung ventilation distribution using electrical impedance tomography** independently and that I have included a full list of used references.

I have no objections to the usage of this work in compliance with §60 of Act No. 121/2000 Coll. on copyright, rights related to copyright and on the amendment of certain laws (copyright act).

Kladno, May 20th, 2016

.....

signature

Prohlášení

Prohlašuji, že jsem diplomovou práci s názvem **Nové metody ve vyhodnocování distribuce plicní ventilace pomocí elektrické impedanční tomografie** vypracoval samostatně a použil k tomu úplný výčet citací použitých pramenů, které uvádím v seznamu přiloženém k této práci.

Nemám závažný důvod proti užití tohoto školního díla ve smyslu §60 Zákona č.121/2000 Sb., o právu autorském, o právech souvisejících s právem autorským a o změně některých zákonů (autorský zákon).

V Kladně dne 20. května 2016

.....

podpis

Abstract

Electrical impedance tomography (EIT) is a promising bedside imaging modality for monitoring of lung ventilation. The information provided by EIT is rather complex and sometimes difficult to interpret. Therefore, several methods were developed for evaluation of EIT data. This work has three main objectives. Firstly, to compare the already published methods that describe regional distribution of lung ventilation. Secondly, to analyse different methods for calculation of Center of ventilation (*CoV*) and to evaluate the effects of image segmentation upon its values. The third aim is to investigate whether the setting of ventilatory parameters can affect the values of EIT-derived regional time constants (τ). Based on the requirements for a specific ventilatory manoeuvre, the published methods were divided into two groups and their prerequisites were compared. The algorithms for calculation of both *CoV* and τ were implemented and the EIT data obtained during animal trials were evaluated. The results show that there are statistically significant differences between the values provided by different algorithms for calculation of *CoV*. It has been shown that the setting of ventilatory parameters significantly affects the values of τ . Thus, to ensure interindividual comparability of these methods, a certain level of standardization is necessary.

Keywords

Electrical impedance tomography, EIT, image segmentation, center of ventilation, regional time constants, mechanical ventilation

Abstrakt

Elektrická impedanční tomografie (EIT) je neinvazivní zobrazovací technika pro monitorování plicní ventilace. Informace, které EIT poskytuje, jsou poměrně komplexní a občas i obtížně interpretovatelné. Proto bylo vyvinuto mnoho různých metod pro vyhodnocování EIT dat. Tato práce má tři základní cíle. Prvním cílem je porovnat publikované metody, které popisují regionální distribuci plicní ventilace. Druhým cílem je porovnat algoritmy pro výpočet Centra ventilace (CoV) a vyšetřit, jakým způsobem jsou jimi získané hodnoty ovlivňovány segmentací obrazu. Třetím cílem je pak zjistit vliv ventilačních parametrů na metodu regionálních časových konstant (τ). Publikované metody byly podle požadavků na nastavení ventilátoru rozděleny do dvou skupin a byly porovnány jejich vstupní předpoklady. Byly implementovány algoritmy pro výpočet CoV a τ , pomocí nichž byla vyhodnocena data získaná v průběhu animálních experimentů. Výsledky ukazují, že existují statisticky významné rozdíly mezi hodnotami vypočítanými na základě různých metod pro výpočet CoV . Zároveň bylo prokázáno, že nastavení ventilačních parametrů může statisticky významně ovlivnit hodnoty τ . Pro zajištění porovnatelnosti výsledků mezi jedinci tak bude zřejmě nutná jejich částečná standardizace.

Klíčová slova

Elektrická impedanční tomografie, EIT, segmentace obrazu, centrum ventilace, regionální časové konstanty, umělá plicní ventilace

Contents

1	Introduction	13
1.1	Principles of EIT	14
1.2	Current issues in EIT data evaluation	17
1.3	Objectives of the work	19
2	Methods of EIT data evaluation	20
2.1	Breath-by-breath methods	20
2.1.1	Regions of interest	20
2.1.2	Row and column sums	21
2.1.3	Difference images	22
2.1.4	Center of ventilation	22
2.1.5	Silent Spaces	23
2.1.6	Global inhomogeneity index	24
2.1.7	Regional intratidal gas distribution	25
2.1.8	Regional filling characteristics	26
2.1.9	Regional time constants	27
2.2	Methods requiring ventilation maneuver	30
2.2.1	Regional ventilation delay	30
2.2.2	Regional opening and closing pressure	30
2.2.3	Regional pressure-volume curves	32
2.2.4	Regional compliance	32
3	Pre-processing of fEIT data and lung segmentation	36
3.1	Selection of the reference frame	36
3.2	Lung segmentation	37

3.2.1	Segmentation based on standard deviation	38
3.2.2	Segmentation based on linear regression coefficient	38
3.2.3	Lung Area Estimation algorithm	40
4	Implementation part	45
4.1	Comparison of methods for calculation of Center of ventilation	45
4.1.1	Methods	46
4.1.2	Results	49
4.1.3	Discussion	51
4.2	Regional time constants	54
4.2.1	Methods	55
4.2.2	Results	57
4.2.3	Discussion	60
5	Conclusion	63
A	Approval of Institutional Review Board	72
B	MEDICON 2016 conference paper	74
C	POSTER 2016 conference paper	81
D	CD contents	88

Abbreviations

aEIT	absolute electrical impedance tomography
ARDS	acute respiratory distress syndrome
AU	arbitrary units
COPD	chronic obstructive pulmonary disease
CU	Charles University
EIT	electrical impedance tomography
fEIT	functional electrical impedance tomography
FFM	First Faculty of Medicine
IM	intramuscular
IV	intravenous
LAE	lung area estimation
PV	pressure-volume (curve)
RFCh	regional filling characteristics
ROI	region of interest
RVD	regional ventilation delay
TV	tidal variation

Symbols

\mathbf{B}	sensitivity matrix
CoG	center of gravity
CoV	center of ventilation
C	compliance of the respiratory system
C_p	pixel compliance
CVP	central venous pressure
ΔZ	change of relative impedance
ΔZ_{norm}	normalized change of relative impedance
E_i	energy distribution of the i -th pixel
f	frequency
f_h	heart frequency

FiO_2	fraction of inspired oxygen
f_s	sampling frequency
\mathbf{g}_{dat}	vector of input voltages
\mathbf{g}_{n}	vector of normalized voltages
\mathbf{g}_{ref}	vector of reference voltages
GI	global inhomogeneity index
H_{cumul}	cumulated hyperdistension
H_p	relative alveolar hyperdistension
ID	inner diameter
$I:E$	inspiration-to-expiration ratio
k	linear regression coefficient
$PaCO_2$	partial pressure of carbon dioxide in arterial blood
pH	measure of acidity or alkalinity of a substance
$PEEP$	positive end-expiratory pressure
P_{plateau}	plateau pressure
R	resistance of the respiratory system
R^2	coefficient of determination
R_{cumul}	cumulated collapse
$R_{E,i}$	ratio of energy distributions for the i -th pixel
R_p	relative alveolar collapse
RCP	regional closing pressure
ROP	regional opening pressure
RR	respiratory rate
SD	standard deviation
t	time
th	threshold value of LAE algorithm
TV_{xy}	tidal variation value of the pixel with coordinates x, y
τ	regional time constant
τ_{global}	global time constant
V_T	tidal volume
$\hat{\mathbf{x}}$	vector of relative impedance values

Remarks to the used symbols and units

This work adopts the nomenclature that is commonly used in international medical journals. Therefore, a non-SI pressure unit “millimeter of mercury” (mmHg) is used for central venous pressure (*CVP*) and for the partial pressure of carbon dioxide in arterial blood (*PaCO₂*). Similarly, a unit “centimeter of water” (cmH₂O) is used for positive end-expiratory pressure (*PEEP*).

In order to avoid the risk of confusion between the lower-case letter “l” and the numeral “1” (one), capital letter “L” is used a symbol for liter.

Chapter 1

Introduction

In the last two decades, electrical impedance tomography (EIT) made a huge progress from an experimental technology to imaging modality for clinical use. It is a safe, radiation-free method that allows a long-term bedside monitoring of patients, mainly at intensive care units. Many clinical studies have shown that EIT could offer a considerable alternative to conventional imaging modalities, especially in monitoring of lung ventilation and perfusion [1, 2].

The experimental use of EIT in monitoring of lung functions soon revealed several areas where EIT provides valuable clinical information. Probably the most intensively studied topic is the optimization of mechanical ventilation by means of EIT, especially titration of positive end-expiratory pressure (*PEEP*) [3, 4, 5]. Encouraging findings were also presented in estimation of regional lung parameters [6, 7] and in quantification of pulmonary edema [8]. In neonatology, promising results were achieved in assessment of maturational changes in lungs [9, 10] and in evaluation of the effect of body positioning upon ventilation distribution [11]. New insights brought by EIT are also expected in monitoring of cardiac output [12] and in assessment of pulmonary embolism [2, 13].

It is believed that EIT will probably cause a revolution in mechanical ventilation [14]. Some authors even refer to it as to the “Holy Grail” of ventilation and perfusion monitoring [15, 16]. However, there is still no gold standard in processing the information provided by EIT. Thus, development of new approaches for evaluation of EIT is still relevant and engages many researchers from around the world.

1.1 Principles of EIT

Dielectric properties of biological tissues are dependent on the tissue composition and on the frequency of the applied electric current. The concentration of electrolytes in intracellular and extracellular fluids, the presence of lipids, cell size or the amount of water are the most influential attributes affecting the tissue impedance [17]. In lung tissue, the dielectric properties are also influenced by the amount of air in alveoli. With increasing air content, the structures of lung parenchyma are stretched, decreasing their thickness while increasing the length of the pathways for electric current at the same time [18, 19]. As a result, electrical impedance of lung tissue increases. When bioimpedance measurements are performed using alternating current of several different frequencies, electrical conductivity of body tissues can be determined and the particular tissues and their state can be distinguished, as shown in Fig. 1.1.

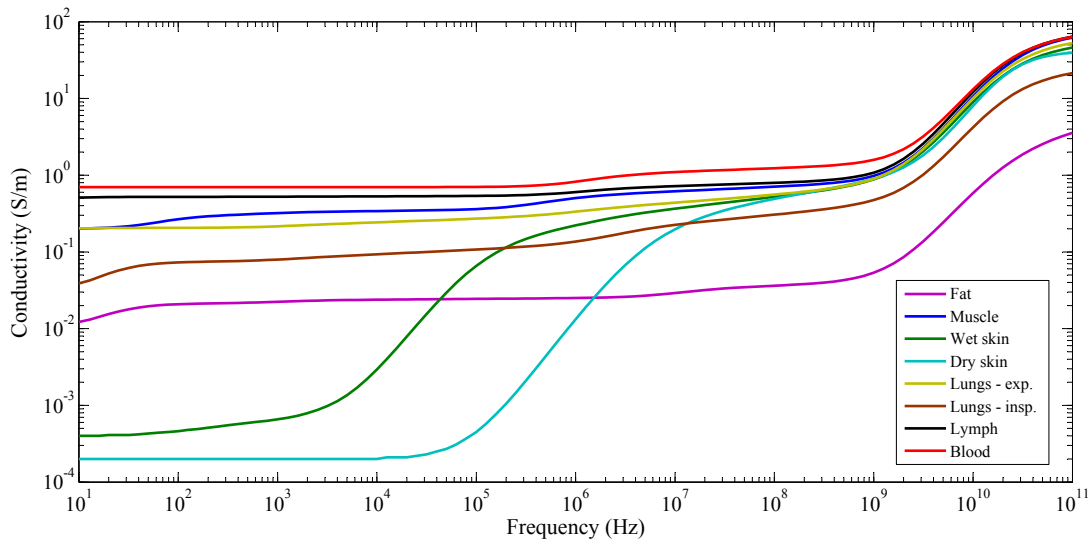


Figure 1.1: The dependency of tissue conductivity upon the frequency of applied alternating current for selected tissues. Modified from [20].

The fundamental idea of EIT is to determine the spatial distribution of conductivity inside an inhomogeneous volume conductor. For this purpose, array of electrodes attached to the surface of the conductor is used. Electric current is applied consecutively through selected electrode pairs and the resulting voltages are measured by the remaining pairs. From the patterns for the electric current application and voltage measurements that were developed [21], the method called “Neighboring” is probably the most widely used one and is implemented in available clinical devices. In Fig. 1.2, its principle

is depicted at a cylindrical volume conductor with 16 electrodes. Alternating current is applied using two neighboring electrodes and 13 resulting voltages are measured between the remaining 14 electrodes. Consequently, the next set of 13 voltages is obtained, using the adjacent pair of electrodes. This pattern is repeated for all 16 electrode pairs used as a current source, resulting in $13 \times 16 = 208$ voltage values that are used for image reconstruction.

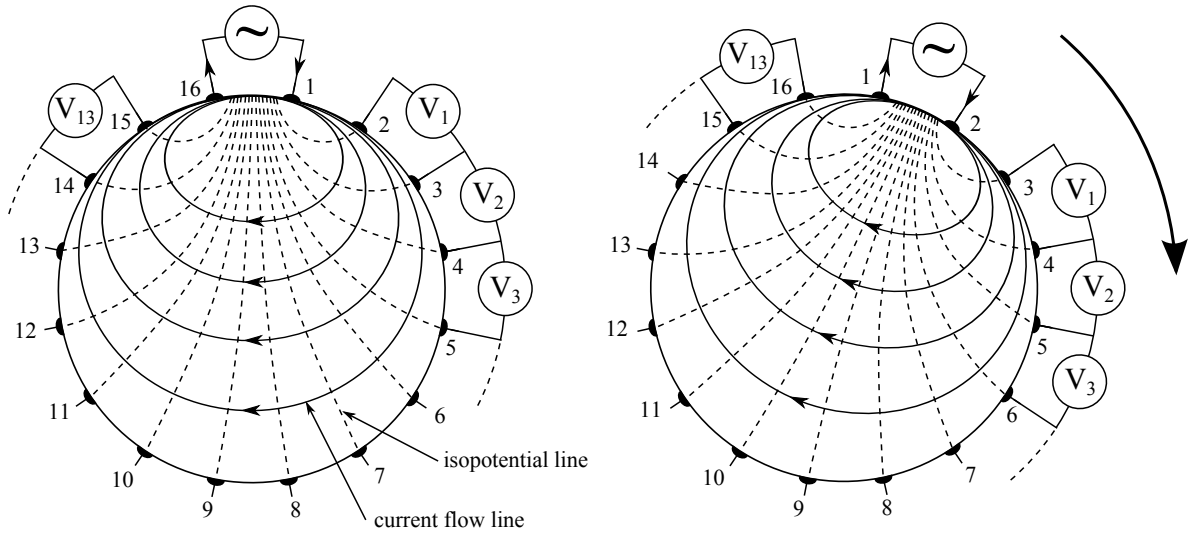


Figure 1.2: Neighboring method illustrated at a cylindrical volume conductor with 16 electrodes equidistantly attached to its surface in one cross-sectional plane. Modified from [20].

The image reconstruction problem of EIT is relatively difficult. In an inhomogeneous volume conductor, electric current spreads along non-linear streamlines and its path can not be easily assumed. This makes the reconstruction problem severely ill-posed, which means that to find the distribution of conductivity, a system of equations in which each measurement is related to each voxel must be solved [22]. Moreover, from 208 voltages that are obtained in the Neighboring method with 16 electrodes, more than 1000 image elements need to be reconstructed. Therefore, the equation system is also underdetermined and finding the solution is even more complicated.

Historically, there are two approaches in reconstruction of EIT images. The older one, referred to as “absolute EIT” (aEIT), calculates the regional distribution of tissue conductivity or resistivity within the selected tomographic plane. However, detailed knowledge about the size and shape of the patient’s chest is required for the reconstruction algorithm [16, 23]. As obtaining of such information in clinical use can be both troublesome and time-consuming, a concept of “functional EIT” (fEIT) was developed.

In this approach, the vector of input voltage data \mathbf{g}_{dat} is normalized using a reference set of measurements \mathbf{g}_{ref} , resulting in a vector of normalized voltages \mathbf{g}_n [24]:

$$\mathbf{g}_n = \frac{\mathbf{g}_{\text{dat}} - \mathbf{g}_{\text{ref}}}{\mathbf{g}_{\text{ref}}}. \quad (1.1)$$

The main advantage of fEIT is that the reconstruction algorithm does not require any knowledge about the geometry of the patient's chest. However, the price paid is the loss of absolute impedance information. In consequence, only relative impedance changes expressed in arbitrary units (AU) remain visible [16].

For the purposes of this work, EIT system PulmoVista 500 (Dräger Medical, Lübeck, Germany) was used for data acquisition. It is the first commercially available EIT device dedicated for clinical praxis and adopts the principles of fEIT. Bioimpedance measurements are performed using 16 electrodes embedded in a silicone belt that is placed around the patient's chest between the 4th and 6th intercostal space [17]. The application of electric current and subsequent voltage measurements are performed according to the Neighboring method. The frequency of the alternating current is selected from the range 80 kHz – 130 kHz, reaching the maximum amplitude of 9 mA.

Finite element method based Newton-Rhapson algorithm is used for image reconstruction in PulmoVista 500. The tomographic plane is divided into 340 triangular elements, considering homogeneous and isotropic biological properties for each element [17]. The values of relative impedance are calculated by multiplication of the normalized voltages \mathbf{g}_n with a sensitivity matrix \mathbf{B} :

$$\hat{\mathbf{x}} = \mathbf{B}\mathbf{g}_n, \quad (1.2)$$

where $\hat{\mathbf{x}}$ is a vector of relative impedance values assigned to the triangular elements. The implementation of the algorithm into the form of matrix multiplication allows minimization of computing time. Thus, real-time imaging with relatively high temporal resolution is possible. In PulmoVista 500, the image acquisition rate is 50 Hz.

When the distribution of relative impedance within the tomographic plane is calculated, the triangular elements are co-registered into rectangular ones. The artefacts close to the boundary are suppressed and Gaussian filter is applied to smooth the image [17]. This process is depicted in Fig. 1.3. The resulting images provided by PulmoVista 500 have a spatial resolution of 32×32 pixels and are visualized using a color scale.



Figure 1.3: Transformation of triangular mesh into EIT image. Left: the values of relative impedance are assigned to triangular elements. Middle: triangular mesh is co-registered into rectangular elements and the artefacts that are close to the boundary are damped. Right: a Gaussian filter is used to smooth the image. Adopted from [17].

Due to the relatively high frame rate, fEIT systems are capable to provide time courses of relative impedance which are obtained as a sum of pixel values in time. When all the pixels from the EIT image are used (summed up), the time course is referred to as “global impedance waveform,” hence the sum of pixels from a defined region is referred to as “local impedance waveform.” An example of global impedance waveform of one breath cycle is depicted in Fig. 1.4.

To visualize the distribution of tidal volume in lungs, Tidal Variation (TV) images are often used. In fEIT, the term “Tidal Variation” refers to the difference between end-inspiratory and end-expiratory point on the impedance waveform, expressed in AU [16]. Thus, TV image is obtained as a difference between end-inspiratory image (the image that corresponds with the local maximum on the global impedance waveform) and the previous end-expiratory image (the image that corresponds with the local minimum). In the example presented in Fig. 1.4 the TV image would be calculated as a difference between the images *a* and *d*.

1.2 Current issues in EIT data evaluation

When compared to conventional imaging modalities, EIT images are rather blurred and suffer from low spatial resolution. Therefore, the information provided by EIT may be sometimes difficult to interpret [26]. To improve the assessment of regional lung ventilation, several methods were developed for evaluation of EIT data [27]. Due to relatively high acquisition rates of EIT systems, the image processing algorithms used in these methods are able to consider also the dynamic behaviour of impedance

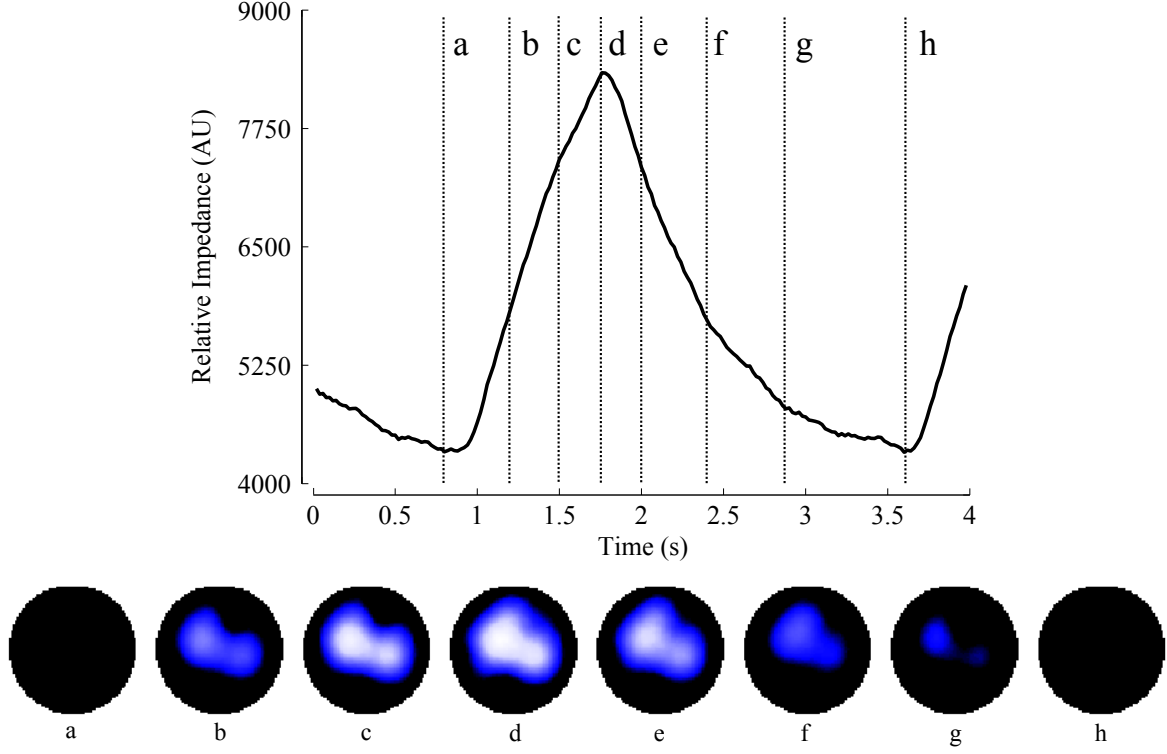


Figure 1.4: Global impedance waveform of one single breath. Positions *a-h* correspond with the respective EIT images. The image *d* visualizes regional distribution of lung ventilation at the end of inspiratory phase, hence the images *a* and *h* represent the end of expiratory phase. Adopted from [25].

changes. As a result, regional values of the parameters that describe the overall state of the lungs can be estimated [6, 28].

Although there are many promising methods that were presented, none of them became a gold standard. Moreover, sometimes there are even inconsistencies in their use that lead to confusion [29]. For example, the algorithms for calculation of an EIT-derived index Center of ventilation are often used for obtaining of a very similar index called Center of gravity.

The methods for evaluation of EIT data still undergo rapid development [27]. This can be illustrated in the example of regional time constants that are derived from the fitting of impedance waveforms by exponential functions. This approach was originally used for evaluation of the data obtained during a special ventilation manoeuvre [30, 31]. However, recent feasibility study has shown that it is also possible to use this method on breath-by-breath basis. [32]. Nevertheless, there is an assumption that the values of regional time constants that are determined according to this study can be affected by the setting of ventilatory parameters.

1.3 Objectives of the work

There are three main objectives of this work. Firstly, to investigate and compare the methods for EIT data evaluation with a particular focus on the approaches that are used for assessment of regional distribution of lung ventilation. Secondly, to compare different methods for calculation of Center of ventilation and to evaluate the effects of image segmentation upon its values. The third aim of this work is to investigate whether the setting of ventilatory parameters can affect the values of EIT-derived regional time constants.

Chapter 2

Methods of EIT data evaluation

The approaches for evaluation of lung ventilation can be basically divided into two groups. The methods from the first group can be used on breath-by-breath basis and does not require any change of ventilator setting. On the other hand, the second group contains methods in which a specific ventilation maneuver is necessary and some of them even combine EIT data with information provided by ventilator. This chapter offers an overview of commonly used and the most promising methods.

2.1 Breath-by-breath methods

2.1.1 Regions of interest

Analysis of local distribution of lung ventilation by means of regions of interest (ROI) is probably one of the oldest methods that have been used in EIT. The image is segmented into several coherent ROIs and for each region a proportion of impedance changes is calculated as a percentage. Similarly, local impedance waveform can be obtained for each ROI. The ROIs determined as simple geometrical objects are referred to as “arbitrary” (see Fig. 2.1) while the ROIs that are defined on the basis of pixel values are referred to as “functional” [33]. Determination of functional ROIs can be understood as lung segmentation and is further described in chapter 3. Sometimes, both functional and arbitrary ROIs can be combined, as shown in Fig. 2.1.

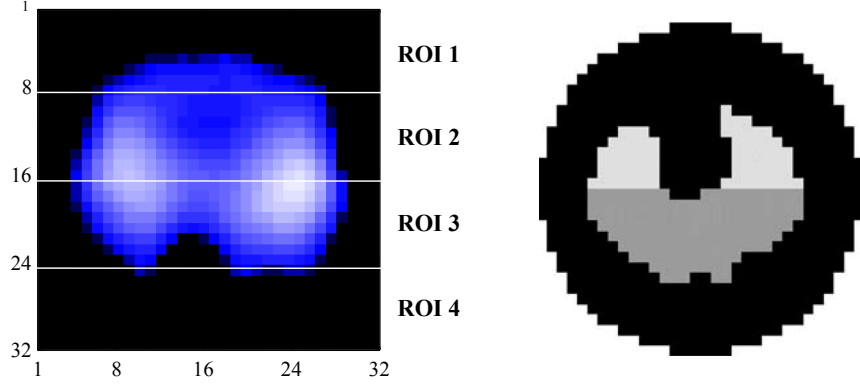


Figure 2.1: Arrangement of arbitrary regions of interest (ROIs) as horizontal layers (left) and combination of both functional and arbitrary ROIs (right). Adopted from [34] and [35].

2.1.2 Row and column sums

Segmentation of EIT images into several arbitrary ROIs may be too coarse when more precise assessment of regional ventilation is necessary. Calculation of row and column sums is able to circumvent this problem, because each row and column in the image is considered as a ROI. Using normalized relative impedance, this approach allows inter-individual comparisons by means of error bars, as shown in Fig. 2.2. However, individual body constitution and chest geometry should be taken into account in evaluation of data obtained in different subjects.

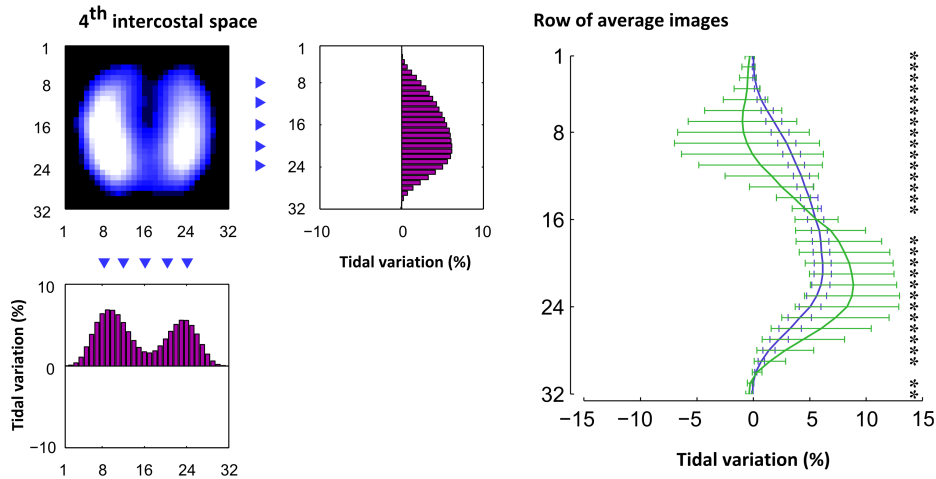


Figure 2.2: Row and columns sums obtained from tidal variation image (left) and comparison of two regional ventilation distributions using error bars (right). Adopted from [36].

2.1.3 Difference images

Two images depicting regional distribution of lung ventilation can be directly compared by means of difference images. In this approach, the images are subtracted pixel by pixel and the differences are color-coded, allowing visual assessment of ventilation differences, as shown in Fig. 2.3. This method is beneficial especially in evaluation of changes in regional lung ventilation induced by optimization of ventilatory setting or in monitoring of the effects of patient positioning [17].

When images from different individuals are used, the method has similar limitations as row and column sums. Firstly, the magnitudes of relative impedance changes are incomparable between different subjects [17]. Thus, the pixel values expressed in arbitrary units should be normalized and only impedance changes that correspond with comparable physiological processes can be evaluated. Secondly, regional distribution of lung ventilation is substantially influenced by body constitution of each individual. Thus, only subjects with similar anatomy can be compared by means of difference images.

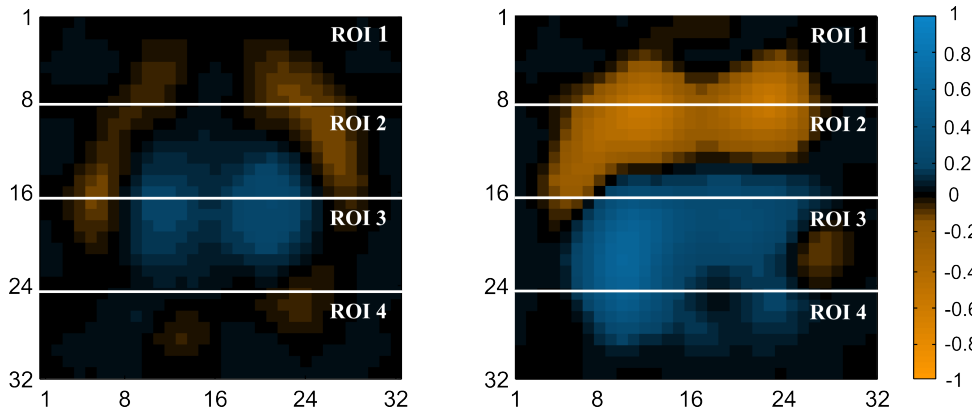


Figure 2.3: Example of difference images with highlighted regions of interest. Pixel values are color-coded using a special color scale. Adopted from [36].

2.1.4 Center of ventilation

In the approaches described above, the distribution of relative impedance within the tomographic plane is expressed by several numbers (ROIs), by bar graph (row and column sums) or visualized in images. However, especially in guiding of mechanical ventilation, it is desirable to describe the changes in regional lung ventilation as a single number.

Center of ventilation (CoV) was introduced in 1998 as index for quantification of ventral-to-dorsal changes of ventilation distribution [37]. Although the definitions of CoV differ among authors, it is mostly calculated as a “geometrical center” of ventilatory induced impedance changes [38] or as a weighted mean of row sums obtained from the TV image [39]. It can be obtained separately for each lung [40, 38] as well as for both lungs together [39]. The position of CoV is usually expressed as a percentage of the chest diameter, as shown in Fig. 2.4.

Center of gravity (CoG) is an EIT-derived index that is very similar to CoV . However, CoG is often obtained along both vertical and horizontal axis [41]. Thus, it is not a plane but a point with given coordinates. Ventral-to-dorsal shifts in regional ventilation can be also described by Impedance ratio, defined as a ratio between impedance changes in the ventral and the dorsal half of EIT image [42].

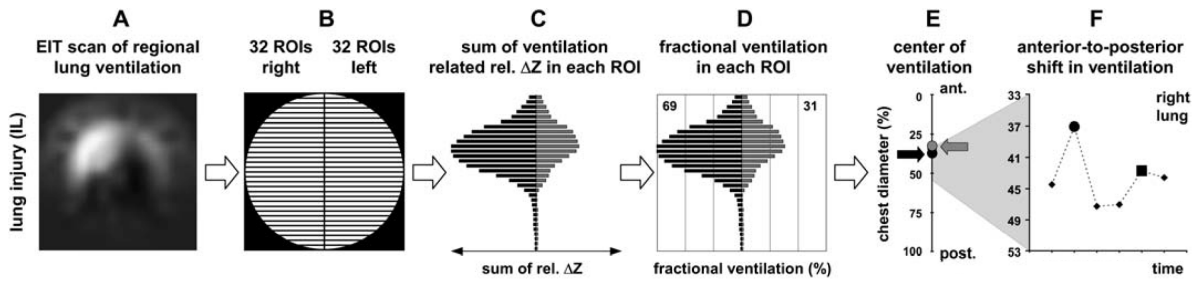


Figure 2.4: Determination of Center of Ventilation (CoV). Tidal variation image (A) is segmented using a circular mask (B) that splits the image vertically in two equal halves, each having 32 regions of interest (ROIs). Row sums are obtained for each half (C) and are expressed as a percentage of the total sum (D). CoV is calculated as a weighted mean of the row sums (E) and plotted in time (F). Adopted from [38].

2.1.5 Silent Spaces

To analyze distribution of ventilation in TV images, several approaches were developed in Swisstom EIT devices [43]. The images are segmented using two arbitrary lung-shaped ROIs. Based on the pixel values in these ROIs, image histogram is obtained and subsequently weighted by the number of pixels in each category, as shown in Fig. 2.5. The pixels from the lowest histogram category correspond with poorly ventilated areas and are called as “Silent Spaces”. CoV is obtained and a line called “ventilation horizon” passing through the CoV perpendicularly to the gravity vector is constructed. Silent Spaces located below the ventilation horizon are then considered as collapsed lung regions

while the Silent Spaces above the ventilation horizon are considered as overdistended, as shown in Fig. 2.6. This approach allows optimization of ventilatory setting based on minimization of insufficiently ventilated lung areas.

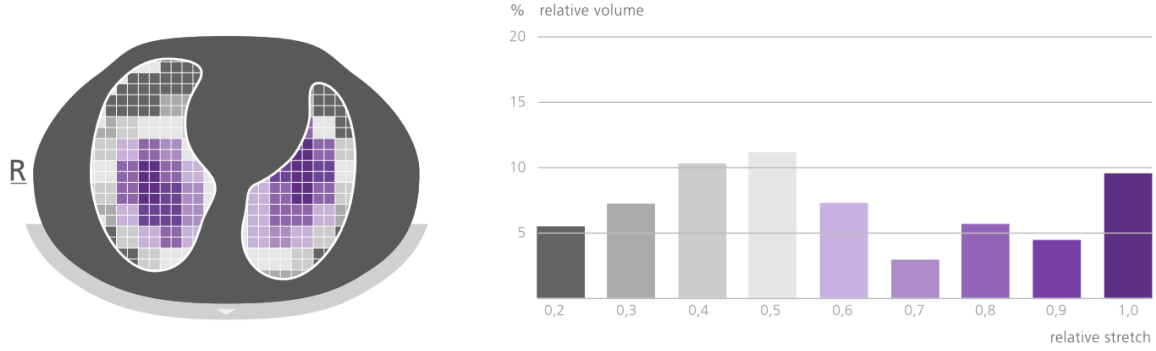


Figure 2.5: Weighted image histogram. The tidal variation image is segmented using two arbitrary lung-shaped regions of interest (left). Subsequently, image histogram is obtained and weighted by the number of pixels in each category (right). The pixels from the lowest category are depicted as dark gray. Adopted from [43].

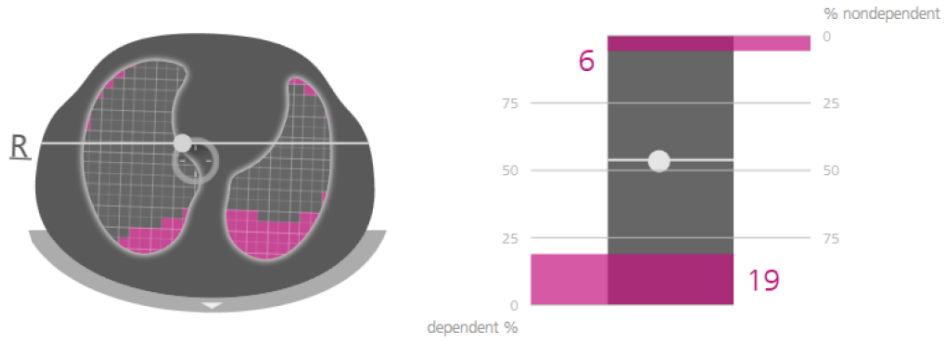


Figure 2.6: Silent Spaces. Center of ventilation is calculated from the tidal variation image (left) and the pixels from the lowest weighted histogram category are considered as “Silent Spaces” (left). Ventilation horizon, the line perpendicular to the gravity vector that passes through the *CoV*, divides the Silent Spaces into dependent and non-dependent ones (right). Adopted from [43].

2.1.6 Global inhomogeneity index

Another approach to characterize distribution of lung ventilation by a single number is Global inhomogeneity (*GI*) index [44]. TV image is segmented using functional ROI and *GI* is calculated according to the formula [44]:

$$GI = \frac{\sum_{x,y \in \text{lungs}} |DI_{xy} - \text{median}(DI_{\text{lung}})|}{\sum_{x,y \in \text{lungs}} DI_{xy}}, \quad (2.1)$$

where DI_{xy} is the differential impedance value of the TV image with coordinates x, y and DI_{lung} represents values of all pixels contained in the ROI.

It has been shown that GI is a useful tool for optimization of $PEEP$, as shown in Fig. 2.7 [3]. However, several methodical aspects have to be considered when using this index. Although GI allows comparisons between different individuals [3, 44, 45], its values are strongly affected by the threshold used for ROI determination [44]. Thus, only GI values obtained in TV images that were segmented using the same method and threshold criterion can be directly compared. From the clinical point of view, a certain degree of ventilation heterogeneity may be considered as physiological. Therefore, it is rather questionable whether GI should be used as an optimization criterion for mechanical ventilation of healthy lungs [46].

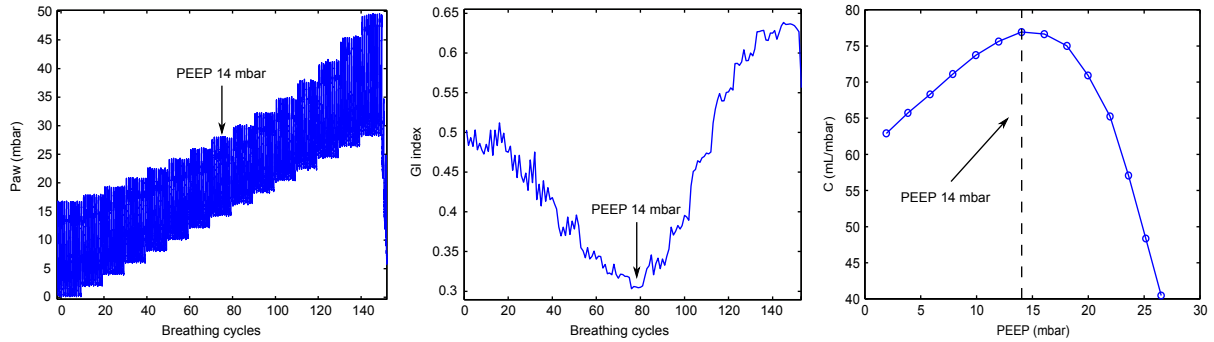


Figure 2.7: Global inhomogeneity (GI) index. When increasing changes in $PEEP$ are performed (left), minimum value of GI indicates the best $PEEP$ setting (middle), corresponding with the maximum dynamic compliance (right). Modified from [3].

2.1.7 Regional intratidal gas distribution

Regional intratidal gas distribution is an approach that uses inspiratory phase of the breath cycle [47]. The inspiration is divided into several intervals of equal volume and for each interval an EIT image representing the volume change is obtained. Consequently, the images are divided into ROIs and a proportion of relative impedance change expressed as percentage is obtained for each ROI and image, as shown in Fig. 2.8. This method provides patterns that represent regional ventilation distribution in each phase of the inspiratory phase. On their basis, dynamics of regional ventilation can be assessed [47].

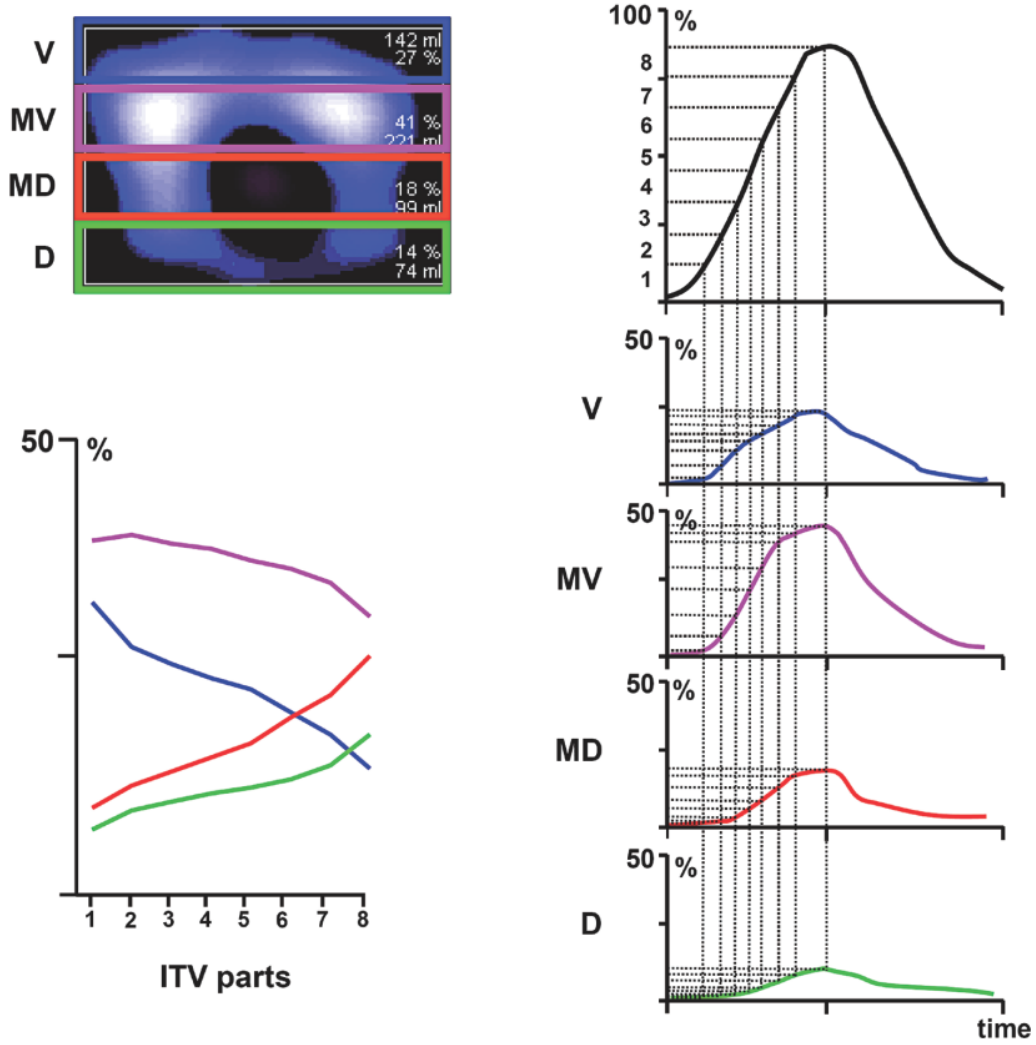


Figure 2.8: Regional intratidal gas distribution. Regions of interest (ROIs) were determined as horizontal layers (top left), identified as ventral (V), mid-ventral (MV), mid-dorsal (MD) and dorsal (D). The inspiratory phase was divided into eight iso-volume parts (right). Consequently, proportion of relative impedance changes expressed as percentage is plotted for each part and ROI (bottom left). Adopted from [47].

2.1.8 Regional filling characteristics

An approach called Regional filling characteristics (RFCh) describes similar phenomena as regional intratidal gas distribution. EIT data from inspiratory phase of breath cycle are used and for each pixel, its impedance waveform is plotted against the global impedance waveform. Polynomial function of the second degree is fitted to the data and the value of quadratic coefficient is assigned to each pixel, as shown in Fig. 2.9 [48]. Image rows in which the mean value of quadratic coefficient is positive and higher than a certain threshold at the same time (the polynomial has a convex shape) are considered

as overinflated, while the rows in which the mean value of quadratic coefficient is negative and below a certain threshold (the fitted polynomial function is concave) are considered as recruitable [40].

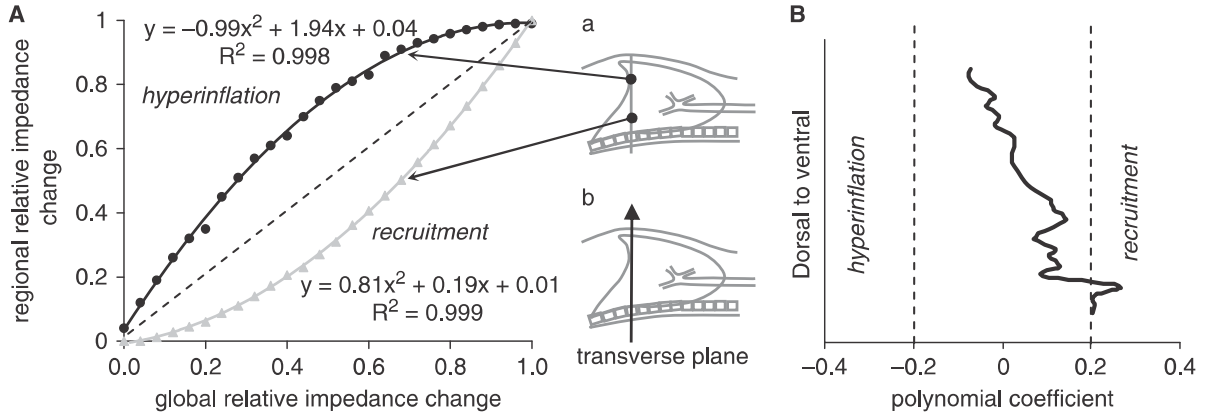


Figure 2.9: Determination of regional filling characteristics. Regional impedance waveforms of two pixels are plotted against the global impedance waveform and quadratic coefficients are determined (A). Mean values of quadratic coefficient are obtained for each image row and the values below the threshold (-0.2) are considered as hyperinflated, while the values higher than 0.2 are considered as recruitable (B). Adopted from [40].

2.1.9 Regional time constants

Regional time constants method is another approach for visualization of regional dynamics of lung aeration. This method is based on fitting of impedance waveforms by exponential functions and subsequent evaluation of acquired time constants. Generally, we can divide the currently published methods in two types, based on the ventilatory setting during EIT data acquisition.

There are studies, where exponential [30] or bi-exponential [31] functions were fitted to local impedance waveforms obtained during stepwise increase of airway pressure in both conventional [31] and high-frequency oscillatory ventilation [30]. This kind of analysis allows assessment of surfactant treatment [30] and is capable to identify differences between healthy patients and the patients with acute respiratory distress syndrome (ARDS), as shown in Fig. 2.10 [31].

Another approach does not require any special ventilation maneuver and allow analysis on breath-by-breath basis. Subjects are mechanically ventilated and regional impedance waveforms depicting expiratory phase of breath cycle are fitted by exponential curves,

yielding time constants that are consequently visualized as color-coded maps [28, 32, 49]. Promising results were presented in recent feasibility studies, showing that different lung pathologies can be distinguished by regional time constants [32, 50].

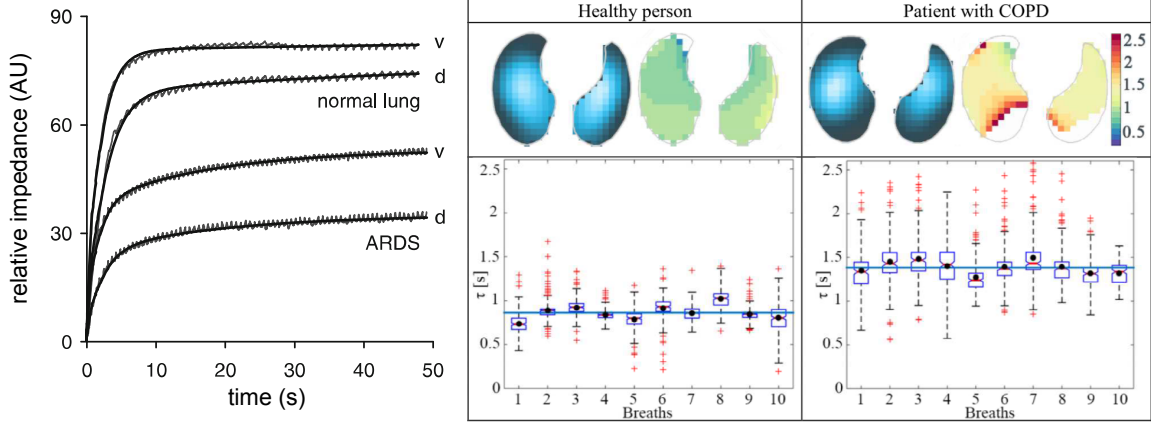


Figure 2.10: Regional time constants obtained during stepwise increase of airway pressure (left) allow identification of differences between normal lungs and the lungs with acute respiratory distress syndrome ARDS. Determination on the breath-by-breath basis yields in visualization of color-coded maps of time constants (middle and right). Subsequently, lung pathologies like chronic obstructive pulmonary disease (COPD) can be distinguished. Adopted from [31] and [32].

An overview of prerequisites for the breath-by-breath EIT methods described in this section is presented in Tab. 2.1.

Table 2.1: Overview of frequently used breath-by-breath methods for EIT data evaluation. The prerequisites that are necessary for the method are marked with \bullet , for optional prerequisites is the symbol stated in round brackets. When arbitrary and functional region of interest (ROI) are stated at the same time, the method can be used with both image segmentation approaches.

Method	TV image	Whole breath cycle		Image segmentation	
		Inspiratory phase	Expiratory phase	Arbitrary ROI	Functional ROI
Arbitrary ROIs [33]	\bullet			—	—
Functional ROIs [33]	\bullet			—	—
Row and column sums [36]	\bullet			(\bullet)	(\bullet)
Difference images [36]	\bullet			(\bullet)	(\bullet)
Center of ventilation [40, 38]	\bullet			(\bullet)	(\bullet)
Center of gravity [41]	\bullet			(\bullet)	(\bullet)
Impedance ratio [42]	\bullet			\bullet	
Silent spaces [43]	\bullet			\bullet	
Global inhomogeneity index [44]	\bullet				\bullet
Regional intratidal gas distribution [47]		\bullet		\bullet	
Regional filling characteristics [48, 40]		\bullet			\bullet
Regional time constants [28, 32]			\bullet		\bullet

2.2 Methods requiring ventilation maneuver

2.2.1 Regional ventilation delay

Similarly to regional time constants, local ventilation dynamics can be assessed by regional ventilation delay (RVD). It requires EIT data acquired during slow inflation maneuver [51, 52] or during a step increase of airway pressure in a duration of 1 min [53]. Local impedance waveforms are obtained for each ROI or pixel and the delay between the beginning of the lung inflation and the time when relative impedance reaches a certain threshold is determined, as shown in Fig. 2.11. RVD values may be further visualized as color-coded maps, as shown in Fig. 2.12. This allows assessment of temporal inhomogeneity of tidal ventilation [52] and subsequent evaluation of recruitment maneuver efficiency [51].

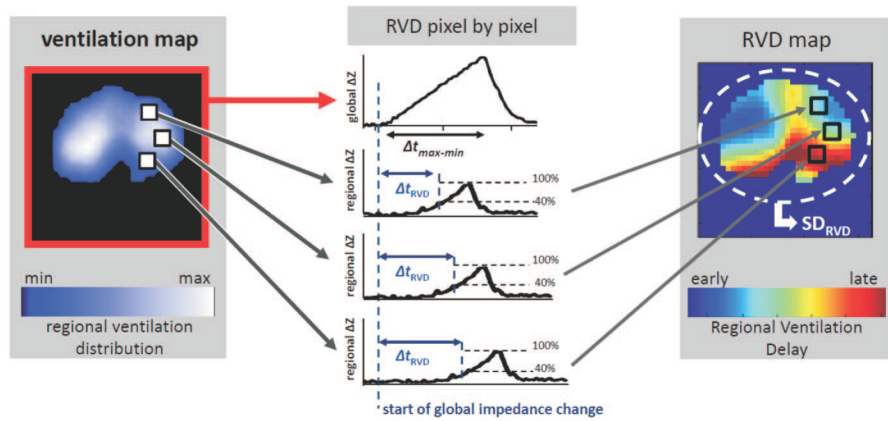


Figure 2.11: Calculation of regional ventilation delay demonstrated on impedance waveforms of three selected pixels (left). The time before the start of inflation and the point where the impedance waveform reaches a certain threshold is determined (middle) and subsequently visualized as a color-coded map (right). Adopted from [52].

2.2.2 Regional opening and closing pressure

An interesting combination of EIT and ventilatory data was presented in methods for determination of regional opening pressure (ROP) and regional closing pressure (RCP) [54]. EIT data and continuously measured pressure values are obtained during a low flow inflation and deflation pressure-volume maneuver. Subsequently, functional ROI is obtained and for each pixel within the ROI the impedance waveform is smoothed by fitting to a fourth order polynomial. ROP is determined as a pressure that corresponds

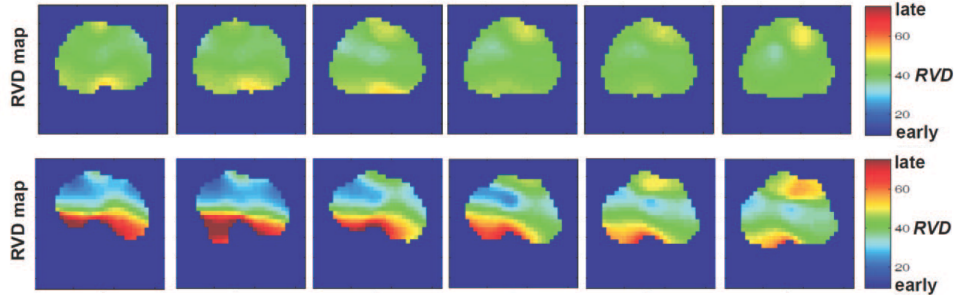


Figure 2.12: Comparison of regional ventilation delay maps obtained in healthy animal (top row) and in the animal with artificially induced lung injury (bottom row). $PEEP$ was set in a range from 0 to 25 cmH₂O with a step of 5 cmH₂O (from left to right). Adopted from [52].

with the time at which the relative impedance in the inflation phase reaches 10% of the maximum of impedance waveform. The value of RCP is determined analogously in the deflation phase, as depicted in Fig. 2.13. It has been shown that the values of ROP are significantly higher in patients with acute lung injury when compared to patients with healthy lungs [54]. Both ROP and RCP can be visualized as color-coded maps.

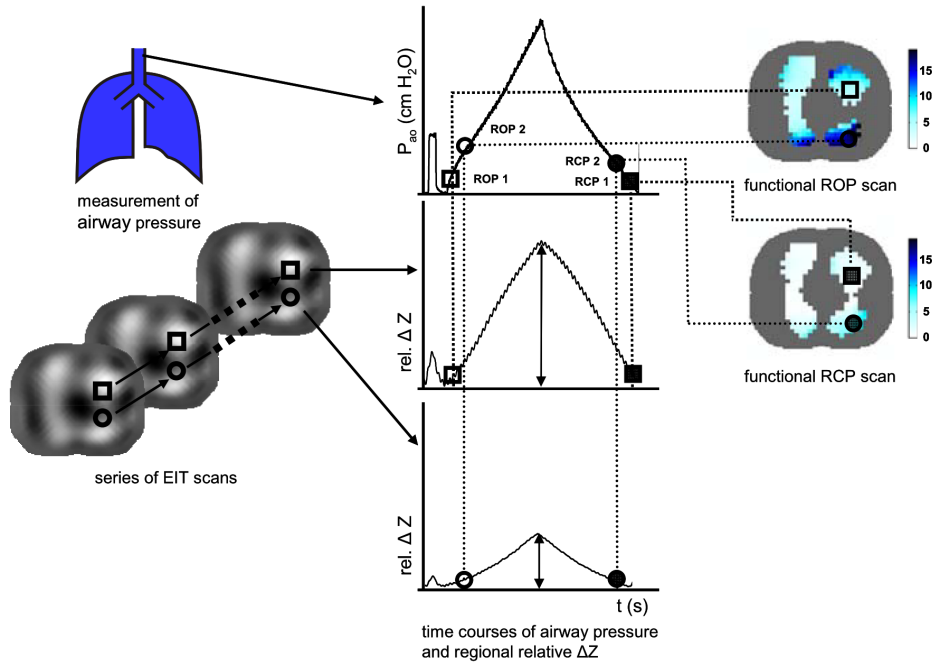


Figure 2.13: Determination of regional opening pressure (ROP) and regional closing pressure (RCP), demonstrated at two selected pixels (marked as a square and a circle). ROP is determined as a pressure value that corresponds with a time point in the inflation phase in which the impedance waveform reaches 10% of the maximum (marked as an unfilled square and circle). RCP is determined analogously in the deflation phase of the maneuver (marked as a filled square and circle). Adopted from [54].

2.2.3 Regional pressure-volume curves

As a good agreement has been found between tidal volume and the corresponding changes of relative impedance [1, 55], several studies have shown that reconstruction of regional pressure-volume (PV) curves is feasible by means of EIT [56, 57]. For this purpose, EIT data should be acquired during an inflation-deflation maneuver [57]. When incremental and subsequent decremental changes in *PEEP* are performed and regional PV curves are obtained at each level, optimal *PEEP* setting can be found as shown in Fig. 2.14 [56].

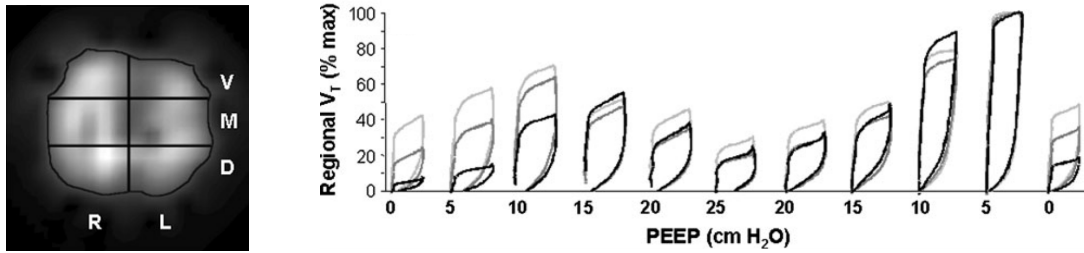


Figure 2.14: Regional pressure-volume curves determined for three regions of interest during stepwise changes of *PEEP*. Light gray, dark gray and black curves correspond with ventral (V), medial (M) and dorsal (D) regions of interest. Optimal setting of *PEEP* was determined as 5 cmH₂O. Adopted from [56].

2.2.4 Regional compliance

Similarly to regional PV curves, regional dynamic compliance can be obtained by means of EIT. The main prerequisite for its computation is an EIT dataset acquired during mechanical ventilation in pressure-controlled mode. For each pixel, compliance can be calculated as follows [6]:

$$C_p = \frac{\Delta Z}{P_{\text{plateau}} - PEEP}, \quad (2.2)$$

where C_p is a pixel compliance and ΔZ is the change of relative impedance that corresponds with a difference between the plateau pressure P_{plateau} and *PEEP*. This approach allows individual optimization of *PEEP* during *PEEP* titration. Obtaining the C_p for each *PEEP* value, the setting for which the most of the pixels have the “best” (highest) compliance can be identified, as shown in Fig. 2.15 [6].

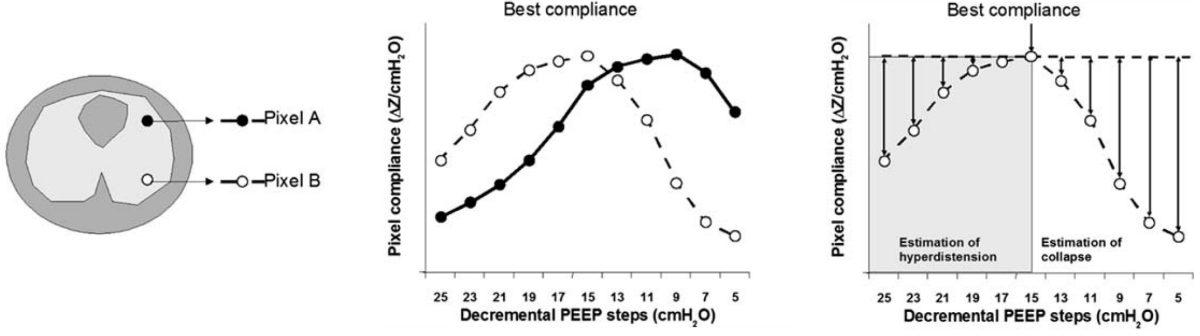


Figure 2.15: Identification of the optimal setting of *PEEP* by means of EIT-derived regional compliance. In two selected pixels (left), regional compliance was obtained for each *PEEP* value (middle). While the pixel *A* reaches the “best” (highest) compliance at *PEEP* of 10 cmH₂O, the pixel *B* has the highest compliance for the *PEEP* of 16 cmH₂O (right). Therefore, this setting is considered as optimal. Adopted from [6].

Based on the regional compliance, regional alveolar collapse can be estimated for each pixel as [6]:

$$R_p = \frac{(C_{p,\max} - C_p) \cdot 100}{C_{p,\max}}, \quad (2.3)$$

where R_p is a relative collapse of the pixel expressed as a percentage, $C_{p,\max}$ is the highest compliance value of the particular pixel determined during the *PEEP* titration and C_p is the current pixel compliance. When estimating the overall alveolar collapse for the entire lung, cumulated collapse R_{cumul} can be obtained according to the formula [6]:

$$R_{\text{cumul}} = \frac{\sum_{p=1}^{N_p} (R_p \cdot C_{p,\max}) \cdot 100}{\sum_{p=1}^{N_p} C_{p,\max}}. \quad (2.4)$$

Analogously to the definition of regional collapse, alveolar hyperdistension can be estimated as:

$$H_p = \frac{(C_{p,\max} - C_p) \cdot 100}{C_{p,\max}}, \quad (2.5)$$

where H_p is a relative alveolar hyperdistension expressed as a percentage. However, only the C_p values obtained at the *PEEP* level that is higher than the level of $C_{p,\max}$ are used. Cumulated hyperdistension H_{cumul} can be defined analogously to cumulated collapse:

$$H_{\text{cumul}} = \frac{\sum_{p=1}^{N_p} (H_p \cdot C_{p,\max}) \cdot 100}{\sum_{p=1}^{N_p} C_{p,\max}}. \quad (2.6)$$

For assessment of regional distribution of collapsed and hyperdistended lung regions, the values of R_p and H_p can be visualized as color-coded maps as shown in Fig. 2.16.

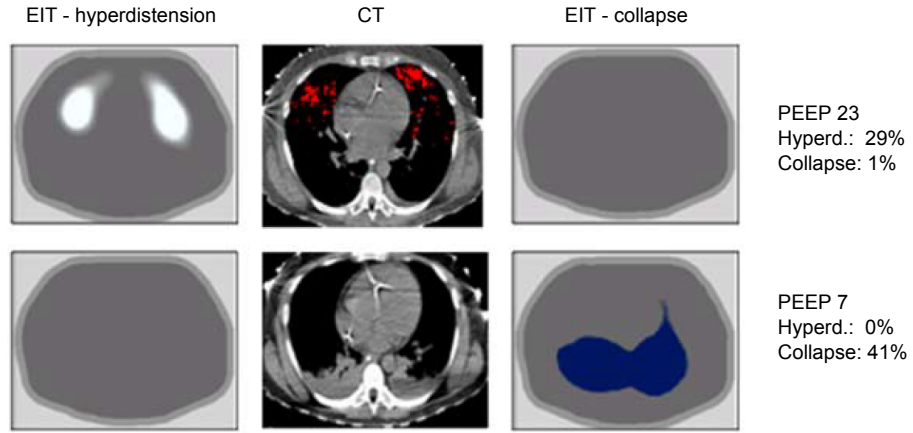


Figure 2.16: Visualization of hyperdistended (left column) and collapsed (right column) lung regions for two different *PEEP* settings in a patient with pneumonia. For comparison, corresponding CT images are presented in the middle column. Adopted from [6].

An overview of prerequisites for the EIT methods that require specific ventilation maneuver is presented in Tab. 2.2.

Table 2.2: Overview of frequently used methods for EIT data evaluation that require ventilation maneuver. The prerequisites that are necessary for the method are marked with •, for optional prerequisites is the symbol stated in round brackets. When arbitrary and functional region of interest (ROI) are stated at the same time, the method can be used with both image segmentation approaches.

Method	Ventilation maneuver		Ventilator data		Image segmentation	
	Slow inflation deflation maneuver	PEEP steps	Continuous data	One param. for each breath	Arbitrary ROI	Functional ROI
Regional ventilation delay [51, 52, 53]	•				•	•
Regional time constants [30, 31]	•				•	•
Regional opening and closing pressures [54]		•	•			•
Regional pressure- -volume curves [56, 57]	•	(•)	•			•
Regional compliance [6]		•		•		•
Estimation of recruitable alveolar collapse [6]		•		•		•
Estimation of alveolar hypertension [6]		•		•		•

Chapter 3

Pre-processing of fEIT data and lung segmentation

The methods described in the previous chapter require a certain degree of data pre-processing. That includes selection of the reference set of voltage measurements for reconstruction of fEIT images and their subsequent segmentation. The first section of this chapter describes how the reference frame can be determined and what are the consequences of its selection with a focus on the implementation used in PulmoVista 500. The section dedicated to image segmentation deals with determination of functional ROI that can be also understood as lung segmentation.

3.1 Selection of the reference frame

As was mentioned in the section 1.1, a vector of reference measurements \mathbf{g}_{ref} is necessary for reconstruction of fEIT images. This vector is frequently determined by choosing a particular set of reference voltages, referred to as “reference frame” or “baseline frame”, or by calculation of average voltage values over a certain time period [16]. In PulmoVista 500, the baseline frame is determined as a frame that represents the end of expiration of the last detected breath [17]. When the acquired data are analysed in Dräger EIT Data Analysis Tool (Dräger Medical, Lübeck, Germany), the baseline frame is automatically chosen as an end-expiratory frame that corresponds with the lowest value on the global impedance waveform [58]. However, manual setting of the baseline frame still remains possible.

Selection of the baseline frame has consequences that should be considered. Firstly, when a long-term fEIT monitoring is performed and the whole record is divided into several files, a common baseline frame should be used for reconstruction of the record. Otherwise, discontinuities in the impedance waveforms may occur, as shown in Fig. 3.1.

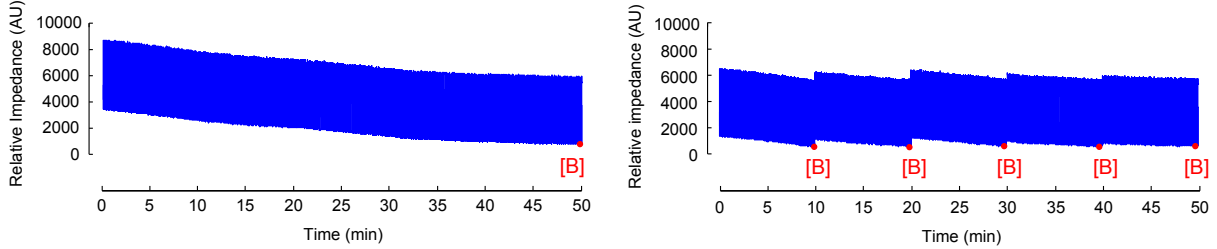


Figure 3.1: The effect of baseline setting in long-term EIT measurements. Left: a common baseline frame (the position is marked as “[B]”) was used for the reconstruction of several parts of one measurements. Right: each part of the measurement was reconstructed using its own baseline file.

Figure 3.1 shows that the point on the impedance waveform that represents the baseline frame has a zero value. This comes from the equation 1.1, where the vector of normalized voltages \mathbf{g}_n is equal to zero vector in the case of baseline frame. As a consequence, the resulting fEIT image has all the pixel values equal to zero, yielding a zero point on the global impedance waveform.

Determination of the baseline frame may also affect visualization of fEIT images. Since the point representing the baseline frame always has a zero value, deliberate selection of the reference frame to the point that does not correspond with global minimum results in existence of negative values on the impedance waveform. The images represented by these points have negative pixel values and when visualized, different colors are assigned to these pixels. This may lead to rather difficult assessment of regional distribution of lung ventilation, as shown in Fig. 3.2.

3.2 Lung segmentation

Rough estimation of lung area is a necessary prerequisite for several methods that were described in chapter 2. The segmentation approaches are mainly based on the fact that the bioimpedance changes induced by ventilation activity are much greater than the impedance changes caused by any other physiological process in the thorax. Therefore, the pixels that represent lungs have relatively large variation of relative

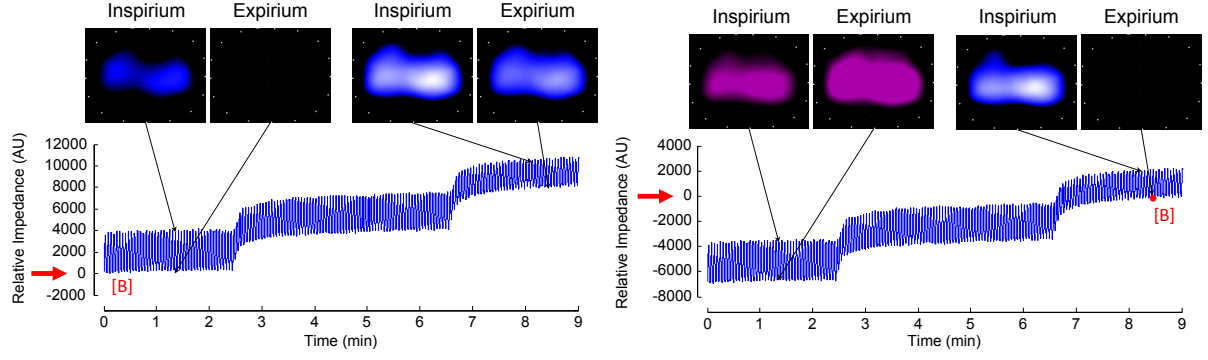


Figure 3.2: The effect of the baseline setting upon visualization of fEIT images. The data were reconstructed using the baseline frame (the position is marked as “[B]”) that represents global minimum of the impedance waveform (left) and that was deliberately selected as a point that does not correspond with global minimum (right). Although visualized differently, the fEIT images depict the same distributions of lung ventilation.

impedance values in time when compared to cardiac-related or thoracic regions [17].

3.2.1 Segmentation based on standard deviation

The identification of lung boundaries based on standard deviation (SD) of pixel values in time was introduced in 1995 [59] and is probably one of the most intuitive methods for lung segmentation. For each pixel, SD is calculated using the relative impedance waveform of the pixel, resulting in a map of SD values. The pixels with SD higher than a certain threshold are then considered as lung regions. The most widely accepted edge criteria are determined as 20%–35% of maximum SD [33]. The effect of thresholding upon determination of lung area in TV images is depicted in Fig. 3.3.

Although the impedance changes caused by ventilation are normally about 10 times greater than the cardiac-related impedance changes [17], this segmentation approach in many cases can not distinguish the pixels that represent lung regions from the cardiac-related pixels, especially when lower segmentation thresholds are used. This phenomena is demonstrated in the images in Fig. 3.3.

3.2.2 Segmentation based on linear regression coefficient

Another approach for determination of functional ROIs was introduced in 1997 [60] and is based on the values of linear regression coefficient (k). For each pixel, k is calculated using the relative impedance waveform as a dependent variable and the global impedance

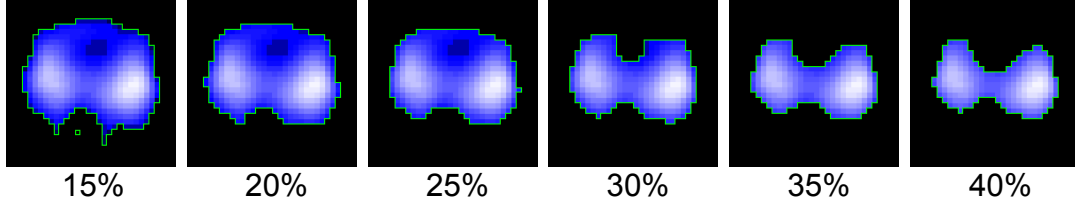


Figure 3.3: Determination of lung area in a tidal variation (TV) image based on pixel SD . The edge criterion used for the segmentation were determined as a percentage of maximum SD value. In this particular subject (mechanically ventilated healthy pig), the threshold values in a range 15%–25% of maximum SD does not allow to distinguish cardiac-related pixels from the pixels that represent lung regions.

waveform as an independent variable [33]. Lung regions are then identified as pixels with values of k larger than a certain threshold. The threshold criteria are usually determined similarly to the SD -based approach, as 20%–35% of maximum k . An example of segmentation of TV image with differently applied thresholds is demonstrated in Fig. 3.4.

This method is considered as more suitable for lung segmentation than the SD -based method, because there is a linear relationship between the local and global impedance data in the ventilated lung regions [33]. As a consequence, the cardiac related pixels are eliminated more successfully as presented in Fig. 3.4.

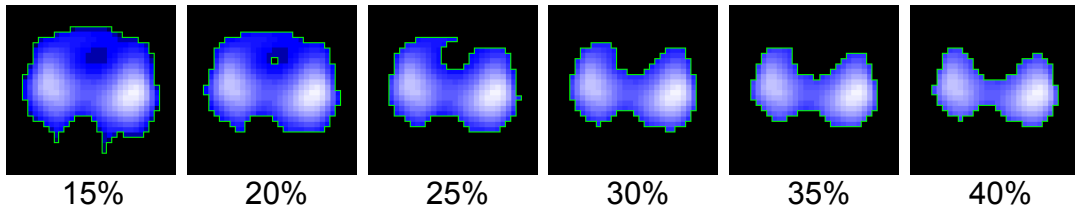


Figure 3.4: Determination of lung area in a tidal variation (TV) image based on linear regression coefficient (k). The edge criterion used for segmentation were determined as a percentage of maximum k . When compared with the corresponding regions of interest from the Fig. 3.3, the cardiac-related pixels (located in ventral part of the image) are excluded more successfully. The most pronounced differences can be observed for the thresholds 25% and 30%.

For the purposes of this work, the method based on linear regression coefficient was enhanced by computation of coefficient of determination (R^2). For each image point, both pixel impedance waveform and global impedance waveform were normalized, and R^2 was calculated. Subsequently, the values of R^2 were thresholded, resulting in a mask. The functional ROI determined on the basis of k was then multiplied with that mask

pixel by pixel, yielding in the final ROI. The whole process is schematically depicted in Fig. 3.6.

The local impedance changes of pixels that represent cardiac activity have a poor correlation (low values of R^2) with global impedance changes that are predominantly caused by lung ventilation. Therefore, adding the criterion of R^2 improves to exclude cardiac-related pixels from the functional ROI, even when the magnitude of their impedance changes is relatively high. The effect of threshold criterion of R^2 upon the segmentation of TV image is demonstrated in Fig. 3.5.

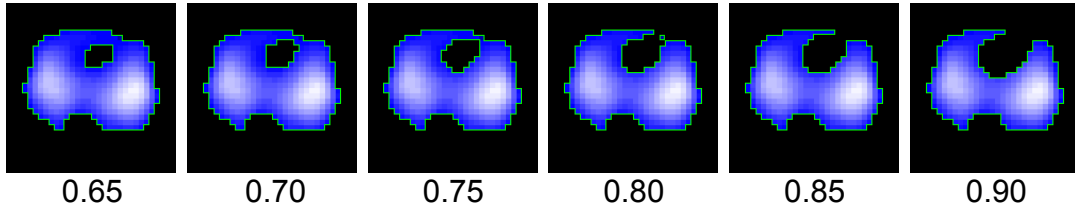


Figure 3.5: Different threshold criteria for coefficient of determination (R^2) in segmentation of tidal variation image. The number of excluded pixels associated with cardiac activity increases with the threshold value. The threshold for linear regression coefficient (k) was set to 20% of maximum k .

3.2.3 Lung Area Estimation algorithm

The segmentation methods described above are able to determine only ventilated lung areas. However, in case of lung atelectasis, pneumothorax or lung cancer there are no changes of air content in the impaired lung regions that would cause bioimpedance changes. To overcome this problem and further improve determination of lungs in fEIT images, Lung Area Estimation (LAE) algorithm was introduced in 2009 [61].

The method is based on the approach of linear regression coefficient, but uses further data processing. Functional ROI is determined using the threshold criterion of 20% of maximum k . The lung area is mirrored from left to right and is combined with the original ROI by a logical OR operation [62]. This process results in a functional ROI that is symmetrical along vertical axis.

Since heart rate has a different frequency than spontaneous or conventional mechanical ventilation, the pixels that represent cardiac activity can be identified using analysis in frequency domain, as shown in Fig. 3.7.

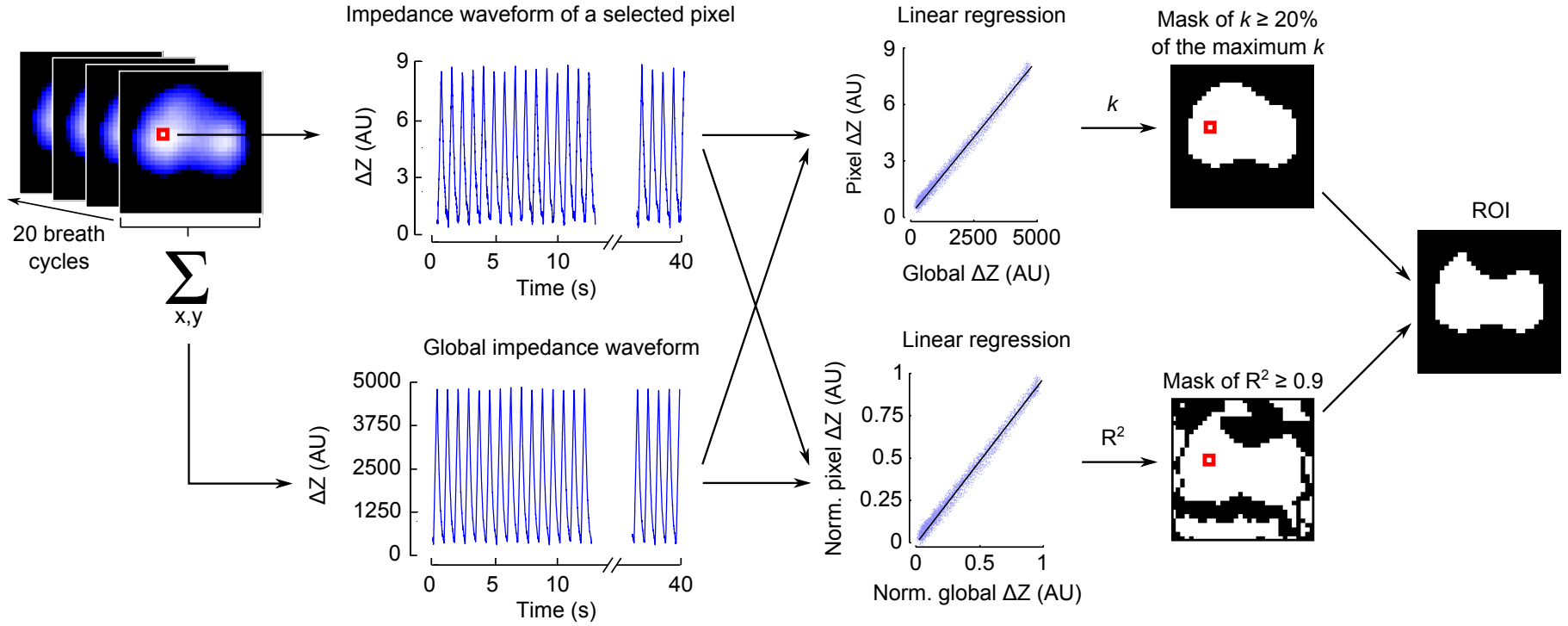


Figure 3.6: Determination of lung area based on linear regression coefficient (k) and on coefficient of determination (R^2). For each pixel, k is calculated using the pixel impedance waveform as a dependent variable and the global impedance waveform as an independent variable. Using a given threshold criterion (in this example 20% of the maximum k), a mask is obtained. This mask is the same as the region of interest (ROI) that is provided by the original k -based method for image segmentation. Normalizing both the pixel impedance waveform and the global impedance waveform, R^2 is obtained for each pixel. The values of R^2 are then thresholded, yielding in a mask. The final ROI is obtained as an intersection of both masks.

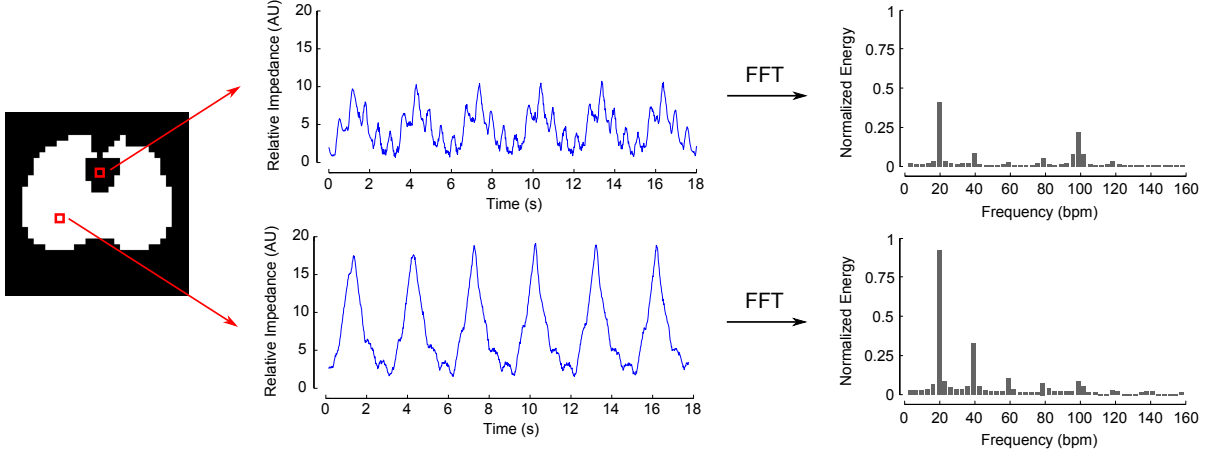


Figure 3.7: Relative impedance waveform and corresponding energy spectrum of cardiac-related pixel (top) and of the pixel that belongs into ventilated lung area (bottom).

For each pixel, energy distribution $E_i(f)$ of the relative impedance waveform is obtained and the pixel is considered as cardiac related if

$$\frac{\sum_{f=0}^{0.8f_h} E_i(f)}{\sum_{0.8f_h}^{f_s/2} E_i(f)} < th, \quad (3.1)$$

where f stands for the frequency, f_h for heart frequency, f_s for sampling frequency, i is the pixel index and th is an individually determined threshold [62]. Let $R_{E,i}$ be a ratio:

$$R_{E,i} = \frac{\sum_{f=0}^{0.8f_h} E_i(f)}{\sum_{0.8f_h}^{f_s/2} E_i(f)} \quad (3.2)$$

and $R_{E,1:N}$ a vector of all $R_{E,i}$ sorted in ascending order. The values in the vector are filtered using five-point moving average window and the threshold th is determined as the first $R_{E,i}$ value in $R_{E,1:N}$ that satisfies $R_{E,i+1} - R_{E,i} < 0.0014, i \in \langle 1, N \rangle$. The difference $R_{E,i+1} - R_{E,i}$ should not be above 0.004 for $i \in \langle 1, 40 \rangle$, otherwise this value is considered as a noise and ignored [62]. Determination of the threshold value is demonstrated in Fig. 3.1.

LAE method is probably the most sophisticated algorithm for fEIT image segmentation that has been published so far. Mirroring of the lung area allows assessment of non-ventilated lung regions that occur only in one lung. This can be beneficial, especially in evaluation of ventilation homogeneity [44, 62]. However, when injured lung

regions are situated symmetrically in both lungs, the LAE method may not be able to discover these regions [62].

Identification of cardiac-related pixels based on frequency analysis can be rather precise when individually set threshold is used. Nevertheless, determination of the threshold value in LAE algorithm is not optimal for all subjects and may lead to exclusion of ventilated lung regions, as demonstrated in Fig. 3.9. Therefore, the issue of finding the universal method for separation of respiratory and cardiac-related areas still remains unresolved and will be essential for further use of this method [62].

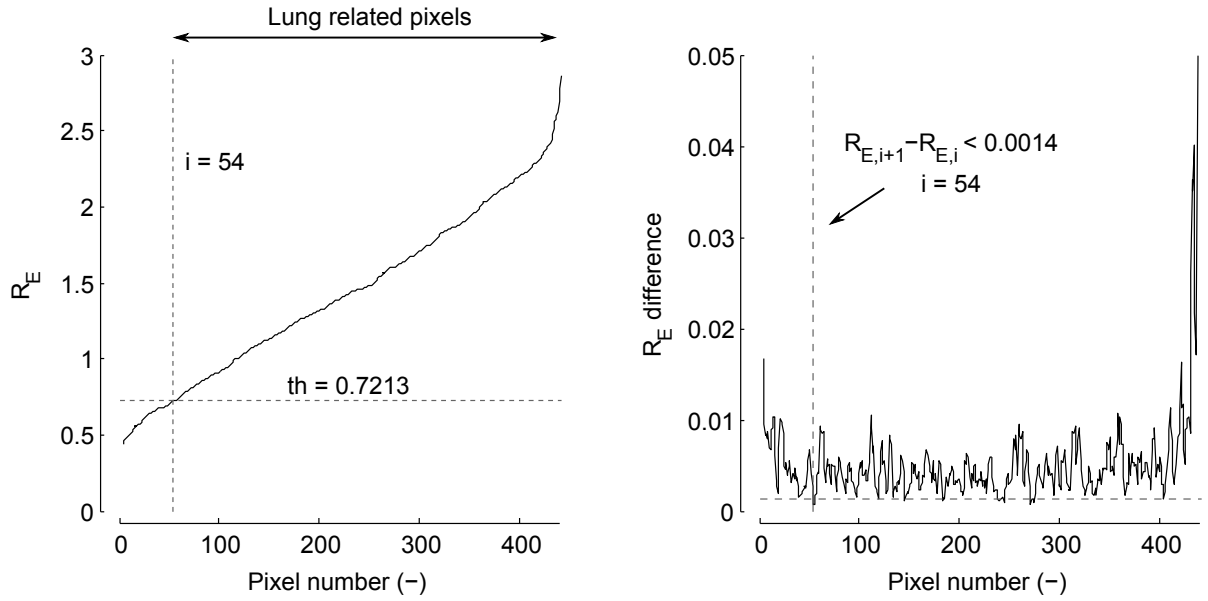


Figure 3.8: Determination of the threshold for cardiac-related pixels in lung area estimation algorithm. The ratios $R_{E,i}$ are sorted in ascending order (left), five-point moving average filter is applied and approximate derivative of $R_{E,i}$ is obtained (right). A first pixel index i that satisfies the condition $R_{E,i+1} - R_{E,i} < 0.0014$ is determined ($i = 54$) and the corresponding $R_{E,i}$ value is considered as a threshold ($th = 0.7213$).

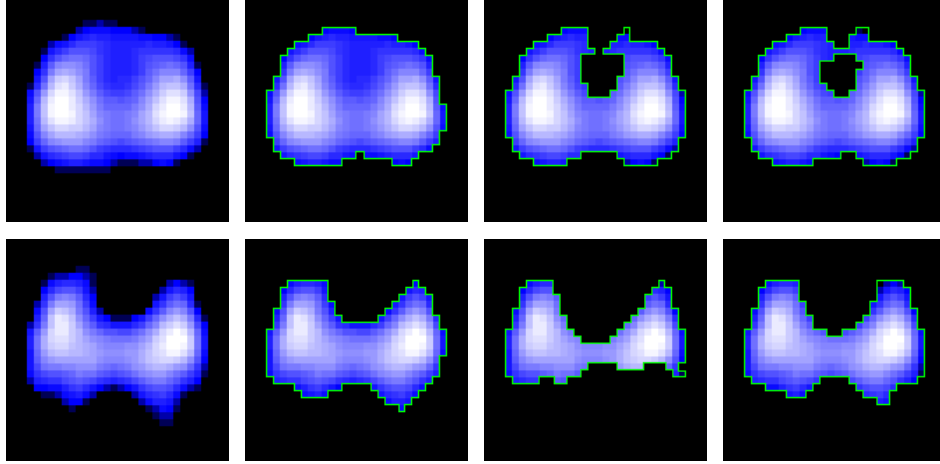


Figure 3.9: Comparison of lung regions determined in two subjects (healthy pigs). From left to right: color-coded image of tidal variation without any lung segmentation; identification of the lung area using the method based on linear regression coefficient (k) with threshold set to 20% of maximum k ; lung area estimation (LAE) algorithm with the threshold criterion $R_{E,i+1} - R_{E,i} < 0.0014$; LAE method with the threshold defined as $R_{E,i+1} - R_{E,i} < 0.01$. The original setting of the threshold in LAE may cause exclusion of dorsal parts of ventilated lung regions (bottom row, the second image from right). When the threshold criterion is modified and the lung area is estimated properly in this subject (bottom row, right) the same setting leads to reduction of cardiac related region in another subject (top row, right).

Chapter 4

Implementation part

The implementation part of this work consists of two studies that were performed to investigate practical aspects of use for the methods described in the chapter 2. The first study compares the methods for calculation of Center of ventilation and evaluates the influence of image segmentation upon its values. The second study investigates how the setting of ventilatory parameters affects the values of regional time constants.

4.1 Comparison of methods for calculation of Center of ventilation

As was already mentioned in the section 2.1.4, Center of ventilation (*CoV*) describes shifts in regional lung ventilation in ventral-to-dorsal direction. It has a high potential in clinical use and was therefore adopted by many research groups [63, 64]. Nevertheless, the definitions of *CoV* are not consistent among authors. In several studies, *CoV* is defined as a weighted mean of the row sums [39, 45, 63, 64] but there are also studies where it is obtained as “the point where the sum of fractional ventilation is 50% of the summed fractional ventilation” [40]. Moreover, in one study published in 2014, it is defined as a ratio between the dorsal and total fractional ventilation [4]. Some authors even refer to *CoV* but they obtain it along both vertical and horizontal axis [43] which is equivalent to the approach of Center of gravity (*CoG*) index [41].

Unfortunately, different definitions of *CoV* are not the only inconsistency in its use. Segmentation of EIT images from which the *CoV* is calculated also varies. Initially, circular mask was applied to the EIT image and the resulting area was divided

into several regions of interest (ROI) [40, 38]. However, some authors use functional segmentation of the images based on linear regression coefficient [45] or on pixel SD [64]. Finally, there are studies where CoV was calculated without any previous image segmentation [39].

As there are different definitions of CoV published, used together with various image segmentations applied, it can be assumed that the resulting CoV values and thus the evaluation of regional lung ventilation may differ.

The aim of this study is to compare the values of CoV that were obtained by different methods of computation, applied in variously segmented images.

4.1.1 Methods

The study protocol was approved by the Institutional Review Board of the First Faculty of Medicine, Charles University in Prague (FFM CU) and is in accordance with Act No. 246/1992 Coll., on the protection of animals against cruelty. The measurements were performed at the accredited animal laboratory of the FFM CU. Four crossbred Landrace female pigs (*Sus scrofa domestica*) with a body weight of 48 ± 2 kg were used.

Anesthesia and preparation

The animals were premedicated with azaperone (2 mg/kg IM). Anesthesia was initiated with ketamine hydrochloride (20 mg/kg IM) and atropine sulphate (0.02 mg/kg IM), followed by boluses of morphine (0.1 mg/kg IV) and propofol (2 mg/kg IV). A cuffed endotracheal tube (ID 7.5 mm) was used for intubation. Anesthesia was maintained with propofol (8 to 10 mg/kg/h IV) in combination with morphine (0.1 mg/kg/h IV) and heparin (40 U/kg/h IV). To suppress spontaneous breathing, myorelaxant pipecuronium bromide (4 mg boluses every 45 min) was administered during mechanical lung ventilation. Initially, rapid infusion of 1 000 mL of saline was administered intravenously, followed by a continuous IV administration of 250 mL/h to reach and maintain central venous pressure of 6 to 7 mmHg.

Mixed venous blood oxygen saturation and continuous cardiac output were measured by Vigilance (Edwards Lifesciences, Irvine, CA, USA) monitor. Arterial blood gases, i.e. arterial partial pressure of oxygen (PaO_2), carbon dioxide ($PaCO_2$) and pH , were continuously measured by CDI 500 (Terumo, Tokyo, Japan). The arterio-venous

extracorporeal circuit for CDI 500 monitor was established between the femoral artery and the femoral vein using a mechanical blood pump (peristaltic roller pump with a blood flow set to 400 mL/min).

In one animal, repeated whole lung lavage (normal saline, 30–40 mL/kg, 37°C) was performed to induce the surfactant deficiency similar to ARDS [40].

Ventilation

Conventional ventilator Hamilton G5 (Hamilton Medical AG, Bonaduz, Switzerland) was used in the CMV mode with the following setting: respiratory rate 18 min⁻¹, fraction of inspired oxygen (FiO_2 21%), inspiration-to-expiration ratio ($I:E$) 1:2 with initial *PEEP* 5 cmH₂O and pressure limit set to 40 cmH₂O. The initial V_T was set to 8.5 mL/kg of the actual body weight and was titrated to reach normocapnia ($PaCO_2$ 40 ± 3 mmHg). During the study protocol four increasing *PEEP* steps of 5 cmH₂O were performed in animals with healthy lungs and three increasing *PEEP* steps of 4 cmH₂O with initial value of 10 cmH₂O were performed in the ARDS model. Each *PEEP* level was maintained at least for 3 minutes.

EIT measurements

EIT system PulmoVista 500 was used for data acquisition. The electrode belt (size S) was attached to the chest of the animal at the level of the 6th intercostal space. The frequency of the applied current was set to 110 kHz with amplitude of 9 mA. EIT images were recorded continuously with a frame rate of 50 Hz during the entire *PEEP* maneuver.

Data Processing

The acquired data were pre-processed in Dräger EIT Data Analysis Tool 6.1. Baseline frame was set automatically for each animal as a frame that corresponds with the global minimum of impedance waveform. Reconstructed data were processed in MATLAB 2014b (MathWorks, Natick, MA, USA).

At each *PEEP* level, data from 30 consecutive breaths were used for analysis. The breaths were selected in the phases where the values of end-expiratory lung impedance were the most stable. TV images were calculated as a difference between end-inspiratory

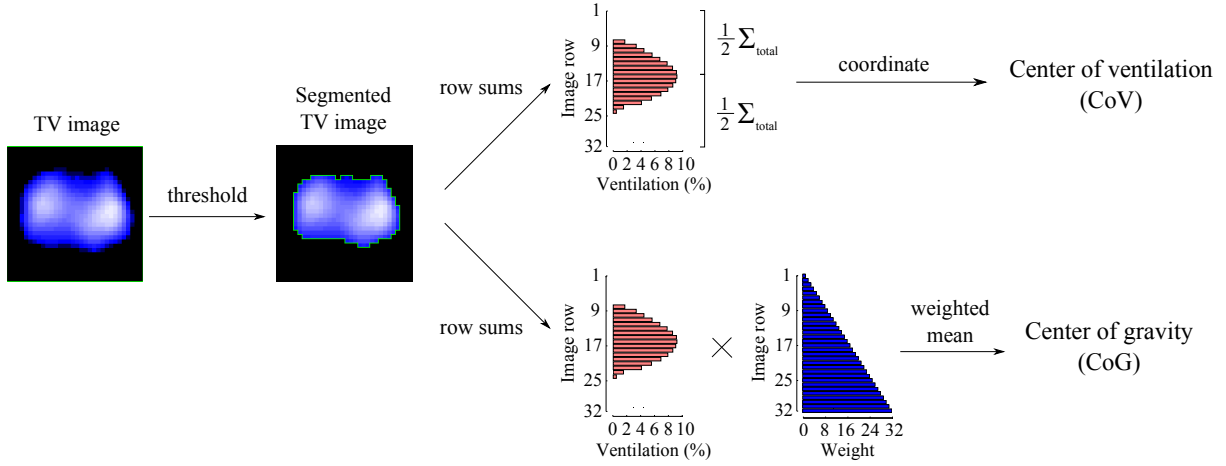


Figure 4.1: Computation of Center of ventilation (*CoV*) and Center of gravity (*CoG*). Tidal variation (TV) images were segmented and functional region of interest was defined. Row sums were obtained from the segmented TV image. *CoV* was calculated as a coordinate that divides the row sums in two equal halves. *CoG* was calculated as a weighted mean of the row sums.

and end-expiratory EIT images. In total, 30 TV images were obtained for each *PEEP* level.

Functional ROI was defined, based on *SD* of individual pixel values in time, as described in section 3.2.1. Six threshold levels ranging from 15% to 40% of maximum pixel *SD* with 5% step were used for image segmentation. For each set of 30 TV images, a common ROI was applied. The *CoG* index was defined as a weighted mean of row sums obtained from TV image [41]:

$$CoG = \frac{1}{N+1} \cdot \frac{\sum_{x=1}^N \sum_{y=1}^N y \cdot TV_{xy}}{\sum_{x=1}^N \sum_{y=1}^N TV_{xy}}, \quad (4.1)$$

where N stands for both the number of pixel rows and pixel columns in the TV image ($N = 32$ for EIT images provided by PulmoVista 500) and TV_{xy} stands for the value of the pixel with coordinates x, y .

For the purposes of this study, *CoV* was defined as a vertical coordinate that divides the sum of fractional ventilation in two equal halves [40] (Fig. 4.1). The implementation of the algorithm for calculation of *CoV* can be summarized as follows:

1. Normalize the pixel values in the TV image:

$$TV_{xy}^* = \frac{TV_{xy}}{\sum_{x=1}^N \sum_{y=1}^N TV_{xy}} \cdot 100, \quad (4.2)$$

where TV_{xy}^* expresses the value of the original pixel TV_{xy} as a percentage of the total sum of the TV image.

2. Calculate row sums of the normalized TV image and save them into the array \mathbf{r} .
3. Find the highest index $n \in \mathbb{N}$ for which holds:

$$\sum_{i=1}^n \mathbf{r}_i \leq 50. \quad (4.3)$$

4. Calculate the ratio p :

$$p = \frac{50 - \sum_{i=1}^n \mathbf{r}_i}{r_n}. \quad (4.4)$$

5. Calculate the value of CoV:

$$\text{CoV} = \frac{n + p + 0.5}{N + 1}. \quad (4.5)$$

For calculation of both CoV and CoG , a coordinate system with the top left pixel represented by coordinates $x = 1, y = 1$ was used. In the following text the abbreviations “ CoV ” and “ CoG ” refer to the indices described above and the unabbreviated term “Center of ventilation” represents the index in general.

Paired two-tailed t-test was used for evaluation of statistical differences between CoV and CoG . The values of both indices obtained at different $PEEP$ levels were visualized as a box plot.

4.1.2 Results

EIT data from 4 animals were studied. The highest $PEEP$ step was omitted in two subjects due to their hemodynamic instability. In total 510 TV images were analyzed.

In general, the values of CoV were significantly higher ($p < 0.05$) than the corresponding values of CoG in all subjects. As shown in Tab. 4.1, there were four cases where the difference between CoV and CoG was not statistically significant and three cases where the mean value of CoG was higher than the corresponding mean value of CoV .

Box plots were created for each animal to visualize the effect of image segmentation upon values of both CoV and CoG . Figure 4.2 shows typical values of these indices during incremental $PEEP$ steps. Both CoV and CoG move dorsally when a higher $PEEP$ level is applied. When calculated from segmented TV images, variation in values of both indices decreases with higher threshold.

Table 4.1: The differences $CoV-CoG$ (mean \pm SD). Statistically insignificant differences (paired t-test, $p > 0.05$) are marked as *. The cases where the mean value of CoG is higher than the value of CoV are marked as \dagger . Repeated whole lung lavage was performed in pig 4.

Pig	<i>PEEP</i> level (cmH ₂ O)	Threshold (% of max. <i>SD</i>)					
		15	20	25	30	35	40
1	5	0.290 \pm 0.049	0.315 \pm 0.043	0.361 \pm 0.045	0.392 \pm 0.053	0.509 \pm 0.047	0.509 \pm 0.040
	10	0.477 \pm 0.089	0.434 \pm 0.046	0.387 \pm 0.028	0.383 \pm 0.057	0.308 \pm 0.048	0.308 \pm 0.043
	15	0.348 \pm 0.112	0.193 \pm 0.058	0.166 \pm 0.012	0.191 \pm 0.027	0.090 \pm 0.027	0.090 \pm 0.027
	20	0.507 \pm 0.333	0.034 \pm 0.179*	0.062 \pm 0.054	0.098 \pm 0.036	0.047 \pm 0.036	0.047 \pm 0.031
	25	1.131 \pm 0.434	0.539 \pm 0.374	0.088 \pm 0.243*	0.066 \pm 0.093	0.057 \pm 0.051	0.057 \pm 0.049
2	5	0.770 \pm 0.122	0.823 \pm 0.112	0.908 \pm 0.110	0.845 \pm 0.101	0.719 \pm 0.091	0.719 \pm 0.086
	10	1.158 \pm 0.063	1.174 \pm 0.054	0.972 \pm 0.050	0.635 \pm 0.056	0.513 \pm 0.055	0.513 \pm 0.044
	15	0.851 \pm 0.056	0.314 \pm 0.023	0.186 \pm 0.026	0.138 \pm 0.025	0.080 \pm 0.021	0.080 \pm 0.019
	20	0.507 \pm 0.017	0.093 \pm 0.026	0.026 \pm 0.028	-0.001 \pm 0.030 \dagger *	-0.039 \pm 0.029 \dagger	-0.039 \pm 0.033 \dagger
3	5	0.193 \pm 0.122	0.186 \pm 0.121	0.181 \pm 0.118	0.186 \pm 0.117	0.052 \pm 0.122	0.052 \pm 0.110*
	10	0.498 \pm 0.098	0.448 \pm 0.098	0.407 \pm 0.103	0.355 \pm 0.105	0.221 \pm 0.107	0.221 \pm 0.102
	15	0.647 \pm 0.106	0.532 \pm 0.063	0.358 \pm 0.050	0.320 \pm 0.055	0.198 \pm 0.057	0.198 \pm 0.059
	20	0.460 \pm 0.233	0.307 \pm 0.159	0.246 \pm 0.067	0.240 \pm 0.040	0.146 \pm 0.041	0.146 \pm 0.036
4	10	0.304 \pm 0.206	0.351 \pm 0.199	0.234 \pm 0.129	0.166 \pm 0.078	0.106 \pm 0.081	0.106 \pm 0.084
	14	0.528 \pm 0.255	0.497 \pm 0.231	0.385 \pm 0.176	0.341 \pm 0.138	0.264 \pm 0.127	0.264 \pm 0.113
	18	1.116 \pm 0.474	1.088 \pm 0.479	0.930 \pm 0.448	0.730 \pm 0.392	0.449 \pm 0.312	0.449 \pm 0.237
	22	1.338 \pm 0.376	1.197 \pm 0.387	1.051 \pm 0.380	0.742 \pm 0.324	0.311 \pm 0.220	0.311 \pm 0.134

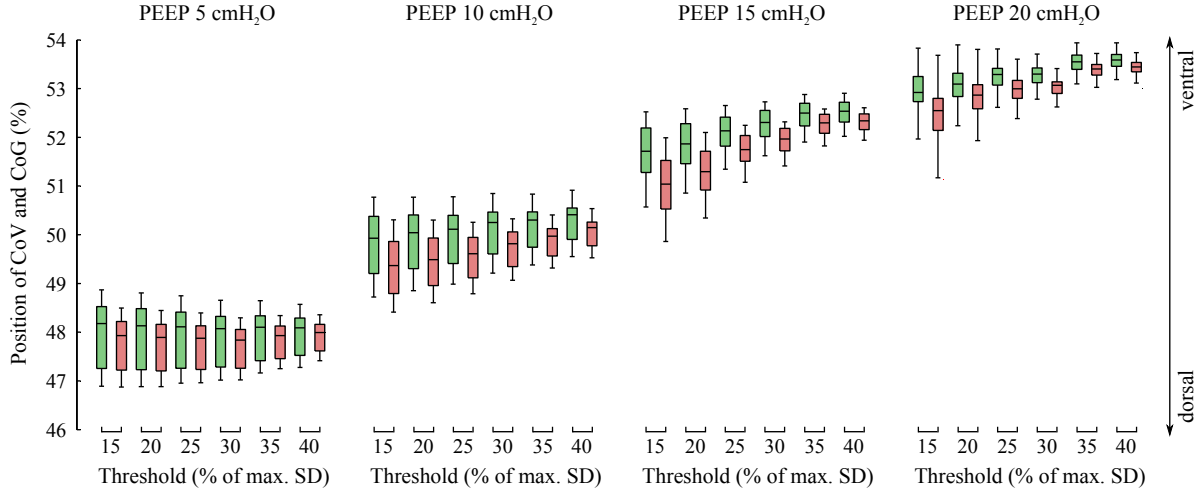


Figure 4.2: Values of Center of ventilation (red) and Center of gravity (green) calculated from EIT images that were segmented using thresholds in the range of 15% – 40% of maximum pixel standard deviation (SD). The data obtained at four different *PEEP* levels are presented as box-and-whisker plot (minimum – lower quartile – median – upper quartile – maximum).

The effect of image segmentation upon the values of *CoV* and *CoG* is rather small when the indices are calculated from mean TV image, as illustrated in Fig. 4.3 and 4.4. The influence of *PEEP* upon both indices is much higher when compared to the changes caused by application of different image segmentation thresholds.

4.1.3 Discussion

The results of this study show, that in general, there is a statistically significant difference between the values obtained using different methods for calculation of Center of ventilation. Both presented algorithms for its calculation show relatively low sensitivity to lung segmentation.

Although statistically significant, the differences between the values of *CoV* and *CoG* presented in this study are mostly at the edge of clinical relevance or even negligible. However, as shown in Fig. 4.5, there might be considerable differences in some subjects.

When functional ROI is applied to the TV image, the variation in values of both *CoV* and *CoG* and the difference between their mean values decrease with an increasing threshold level of lung segmentation. This is mainly due to the fact that the pixels with low change of relative impedance in time represent poorly ventilated lung regions or tissues that does not participate in ventilation at all. When these pixels are excluded

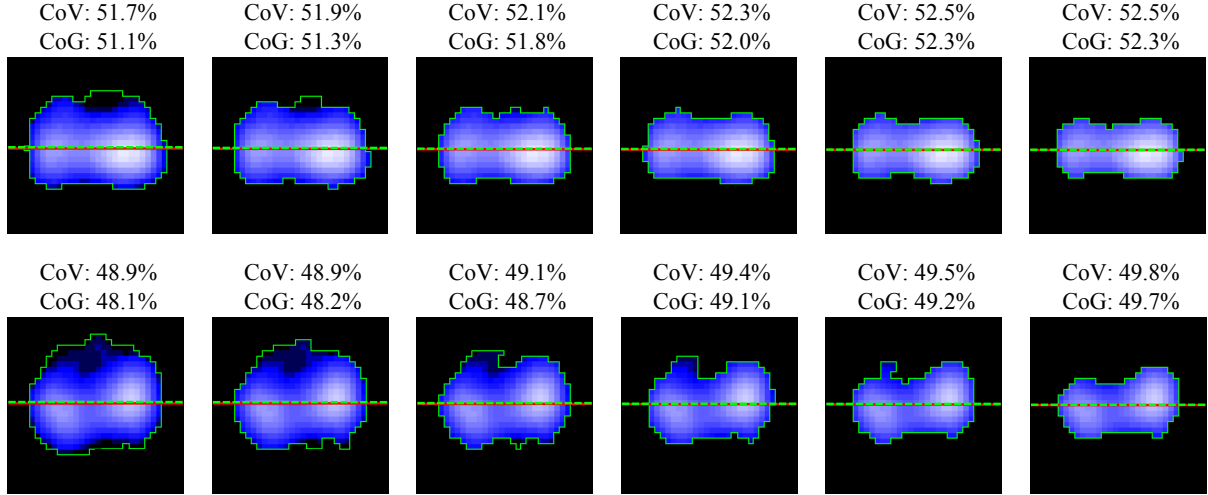


Figure 4.3: The effect of thresholding upon mean tidal variation (TV) images. The threshold criteria were set in the range from 15% to 40% in 5% steps (from left to right). The position of Center of ventilation (CoV) and Center of gravity (CoG) is depicted with red solid line and green dashed line, respectively. The top row depicts the mean TV image obtained in healthy animal with $PEEP$ set to 15 cmH₂O. The bottom row shows the mean TV image of the animal with induced acute respiratory distress syndrome, using a $PEEP$ of 14 cmH₂O. Each of the images was obtained as a mean of 30 consecutive TV images.

from the ROI, only the lung regions that substantially contribute to ventilation are used for the calculation. In a consequence, this may result in cases where CoV and CoG switch their positions when a high segmentation threshold is applied, as shown in Tab. 4.1. Similarly, the mean difference between CoV and CoG values substantially decreases when large insufficiently ventilated lung regions are omitted from the calculation due to the use of high segmentation threshold, as shown in the values of the ARDS model in Tab. 4.1.

Contrary to the effect of lung segmentation, when incremental $PEEP$ steps are performed, the lung area that is predominantly ventilated moves dorsally. Therefore, the changes of both CoV and CoG values caused by $PEEP$ setting are more pronounced.

For the purposes of this study the values of both CoV and CoG were presented as a percentage as this is probably the most common way [38, 39, 64]. However, the expression as a value from the interval $(1, N)$, where N stands for the number of an image row is also possible and correct [41].

To enable the comparison of two different approaches for calculation of Center of ventilation, the published algorithms were modified to provide the value of 50%

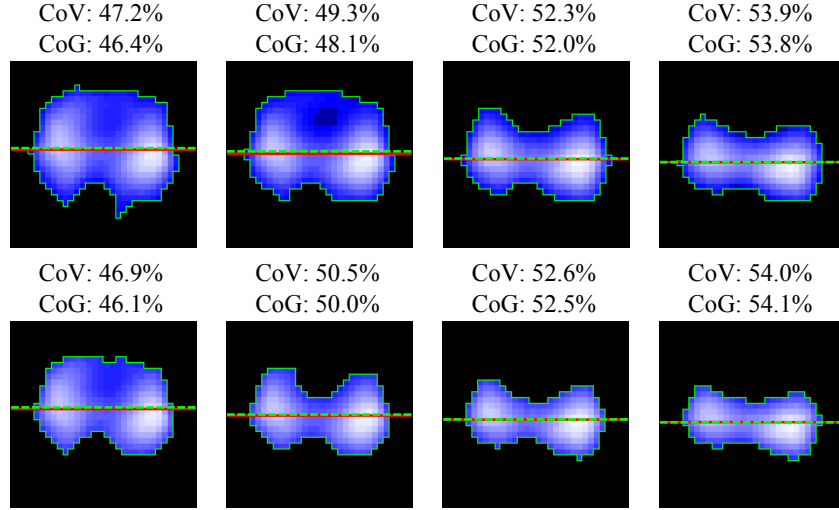


Figure 4.4: The effect of *PEEP* and lung segmentation upon mean tidal variation (TV) images. Distribution of ventilation at four *PEEP* levels (5 to 20 cmH₂O with a step of 5 cmH₂O, from left to right). Top row: the threshold level set to 20% of maximum *SD*, bottom row: the threshold level set to 35% of maximum *SD*. The position of Center of ventilation (*CoV*) and Center of gravity (*CoG*) is depicted with red solid line and green dashed line, respectively. The pixel values of the image were obtained as a mean of 30 consecutive TV images.

for a homogeneous image and also for images that are symmetrical along vertical axis. Both algorithms are also shift invariant for the structures with vertical symmetry (top row of Fig. 4.5). Therefore, the biggest differences between *CoV* and *CoG* occur for the images with a substantial horizontal asymmetry as shown in the bottom row of Fig. 4.5.

The abbreviation “*CoV*” was used for the method presented by van Heerde et al. [40] as it is in our opinion closer to the original idea of geometrical center of ventilation [37, 38]. The methods for calculation of this index presented in [39, 45, 63, 64] are closer to the idea of Center of gravity index [41]. Therefore, abbreviation “*CoG*” was used for this method. The method presented by Blankman et al. [4] was not evaluated in this study.

Segmentation of TV images based on *SD* values of individual pixels is one of the most common approaches used for definition of functional ROI [33]. For this method, there is a recommended range of threshold values from 20% to 35% of maximum pixel *SD*. The threshold values ranging from 15% to 40% were used to assess also the effect of ROIs that are produced by setting of the threshold criteria outside the recommended range.

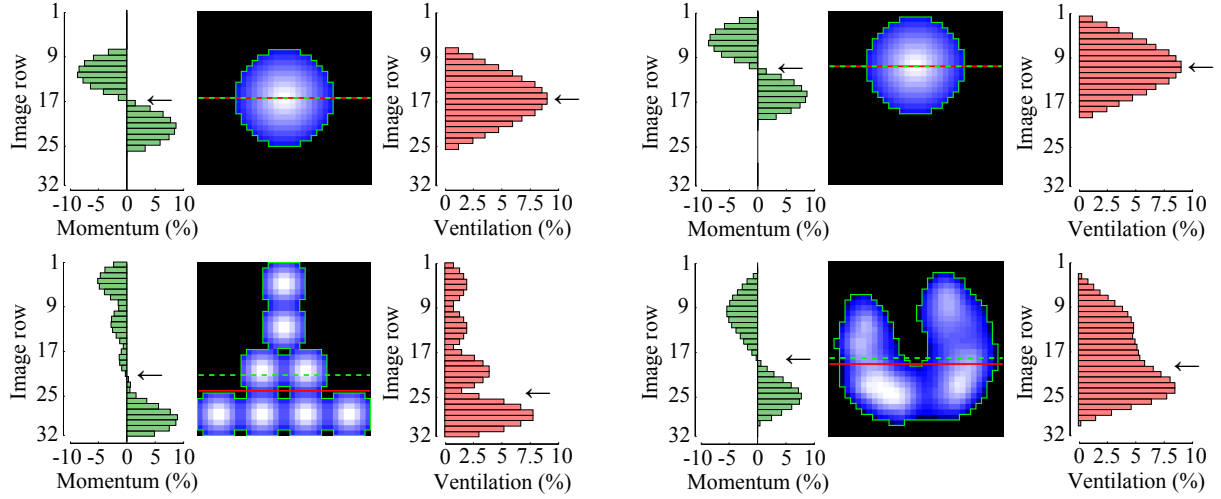


Figure 4.5: The position of Center of ventilation (CoV) and Center of gravity (CoG) for the image structures that are symmetrical (top row) and asymmetrical (bottom row) along vertical axis. For each image, the left bar graph represents the distribution of momentum (weighted means) along vertical axis and the right bar graph shows the row sums in the normalized tidal variation (TV) image. The right bottom image is an example of TV image obtained in a spontaneously breathing healthy volunteer. The position of CoV and CoG is depicted with red solid line and green dashed line, respectively.

4.2 Regional time constants

Monitoring of regional lung aeration dynamics is probably one of the most promising areas for clinical use of EIT. It has been shown that EIT-derived regional time constants (τ) determined during spirometry may provide clinically valuable information in assessment of therapy effects [28]. Similarly, recently published feasibility studies [32, 50] suggested that τ obtained on breath-by-breath basis in mechanically ventilated patients can be used to distinguish lung pathologies such as acute respiratory distress syndrome (ARDS) or chronic obstructive pulmonary disease (COPD).

While obtaining of τ during spirometry requires fEIT data recorded during defined ventilation manoeuvre (forced expiration performed in Tiffeneau test), ventilatory parameters are set individually for each patient. Therefore, there is an assumption that the values of τ determined during mechanical ventilation may be influenced by the setting of ventilatory parameters.

The aim of this study is to investigate whether the setting of ventilatory parameters can affect the values of EIT-derived regional time constants.

4.2.1 Methods

The study protocol was approved by the Institutional Review Board of FFM CU and is in accordance with Act No. 246/1992 Coll., on the protection of animals against cruelty. The measurements were performed at an accredited animal laboratory. Three crossbred Landrace female pigs (*Sus scrofa domestica*) with a body weight of 47 ± 2 kg were used.

Anaesthesia and preparation

The animals were premedicated with azaperone (2 mg/kg IM), followed by anesthesia with ketamine hydrochloride (20 mg/kg IM) and atropine sulphate (0.02 mg/kg IM). When placed on the operating table, initial boluses of morphine (0.1 mg/kg IV) and propofol (2 mg/kg IV) were administered. A cuffed endotracheal tube (*ID* 7.5 mm) was used for intubation. Anesthesia was maintained with propofol (8 to 10 mg/kg/h IV) in combination with heparin (40 U/kg/h IV) and morphine (0.1 mg/kg/h IV). Myorelaxant pipecuronium bromide (4 mg boluses every 45 min) was administered during mechanical lung ventilation to suppress spontaneous breathing. Initial rapid infusion of 1 000 mL of normal saline was administered intravenously, followed by a continuous IV drip of 250 mL/h to reach and maintain central venous pressure of 6 to 7 mmHg.

Heart rate, arterial blood pressure, central venous pressure, body temperature and ECG were monitored using MU-631 RK (Nihon Kohden, Tokyo, Japan) patient monitor. Continuous cardiac output and mixed venous blood oxygen saturation were measured by Vigilance monitor. Arterial blood gases, i.e. PaO_2 , $PaCO_2$ and pH , were measured continuously by CDI 500. The arterio-venous extracorporeal circuit for CDI 500 monitor was established between the femoral artery and the femoral vein using peristaltic roller pump with a blood flow set to 400 mL/min.

Ventilation

Conventional ventilator Engström (Datex-Ohmeda, GE Healthcare, Finland) was used in the VCV mode with the following initial setting: RR 18 min⁻¹, FiO_2 21%, $I:E$ 1:2, $PEEP$ 5 cmH₂O and pressure limit set to 40 cmH₂O. V_T was set to 8.5 mL/kg of the actual body weight and was titrated to reach normocapnia ($PaCO_2$ 40 ± 3 mmHg).

Study protocol

After animal preparation, myorelaxation and instrumentation, calibration of the EIT system was performed. A steady phase of 30 minutes was introduced. The study protocol consisted of three phases separated by stabilization periods. In each phase, several different settings of the selected ventilatory parameter were used while keeping the values of remaining ventilatory parameters unchanged. Each setting was kept at least for 2 minutes. The stabilization periods lasted from 3 to 4 minutes. In the first phase, the values of V_T were set in a range from 6 to 12 mL/kg with a step of 2 mL/kg. In the second phase, six different values of RR were used, ranging from 12 to 22 breaths per minute with a step of 2. Changes of $I:E$ were performed in the third phase, setting the values of the parameter to 1:1, 1:1.5, 1:2, 1:2.5 and 1:3. The study protocol is summarized in Fig. 4.6.

In the ARDS subject, different setting of ventilatory parameters was used to prevent severe hypercapnia and hypoxemia. $PEEP$ was set to 15 cmH₂O during the whole protocol. In the first phase, RR was set to 30 min⁻¹ and the highest value of V_T (12 mL/kg) was omitted. In the second phase, RR was set to 30, 35, 40, 45 and 50 min⁻¹ with V_T of 8 mL/kg. The third phase was performed with RR set to 30 min⁻¹ and V_T of 8 mL/kg.

Time →

	Steady phase	Phase 1: Changes of V_T				Stabilization	Phase 2: Changes of RR						Stabilization	Phase 3: Changes of $I:E$				
V_T (mL/kg)	8	6	8	10	12	8	10	10	10	10	10	10	8	10	10	10	10	10
RR (min ⁻¹)	20	20	20	20	20	20	12	14	16	18	20	22	20	20	20	20	20	20
$I:E$ (-)	1:2	1:2	1:2	1:2	1:2	1:2	1:2	1:2	1:2	1:2	1:2	1:2	1:2	1:1	1:1.5	1:2	1:2.5	1:3

Figure 4.6: Study design and the settings of ventilatory parameters during the protocol. For each phase, the changes in parameter setting are highlighted by light gray background of the parameter value. V_T —tidal volume; RR —respiratory rate; $I:E$ —inspiratory-to-expiratory time ratio.

Data analysis and statistics

The acquired EIT data were pre-processed using Dräger EIT Data Analysis Tool 6.1. Baseline frames were set automatically for each animal as frames that correspond with global minima of impedance waveforms. Reconstructed data were processed in MATLAB 2014b. For each ventilatory setting, a data set representing 20 consecutive breaths was created and used for analysis.

Functional region of interest (ROI) was determined in each data set, using the modified

approach of linear regression coefficient, as described in section 3.2.2. The threshold level was set as 20% of the maximum value. Determination of the ROI is schematically depicted in Fig. 3.6.

The obtained functional ROI was applied to each data set. For each pixel inside the ROI, impedance waveform was segmented in time domain, resulting in 20 separated breath cycles from which one mean breath cycle was calculated. An expiratory phase was determined in the mean breath cycle and the part with the values higher than 75% of the mean breath amplitude was cropped [32]. The resulting part of the expiratory phase was normalized and fitted with an exponential curve:

$$\Delta Z_{\text{norm}} = e^{-\frac{t}{\tau}}, \quad (4.6)$$

where ΔZ_{norm} is normalized relative impedance, t is time and τ is a time constant. Only the values of τ that resulted from a curve fitting with $R^2 > 0.6$ were analyzed [32]. The whole procedure of obtaining the time constants is depicted in Fig. 4.7.

For each ventilatory setting the values of τ were visualized as color-coded maps and as a box-and-whisker-plot. To allow pairwise comparisons within each pig, only the pixels with nonzero τ for all ventilatory settings were used for statistical analysis. The Shapiro-Wilk test was used to confirm the normality of evaluated data. The differences between the values of τ were assessed by repeated measures ANOVA. A value of $p < 0.05$ was considered as statistically significant. The statistical analysis was performed with STATISTICA (StatSoft, Inc., Tulsa, OK, USA).

4.2.2 Results

EIT data from 3 animals were analyzed according to the study protocol. In one healthy animal the values of RR were set to 12, 15, 18, 20, 22 and 24 min^{-1} in the second phase of the protocol to investigate greater range of settings. In total, 44 data sets were analyzed.

In general, the values of τ differed significantly in each phase of the protocol as shown in Fig. 4.8. There were only three cases where the changes in τ were statistically insignificant with $p > 0.05$ and one case with $p > 0.01$. The box plots in Fig. 4.8 show that V_T has an increasing effect upon values of τ while the effect of RR is exactly the opposite.

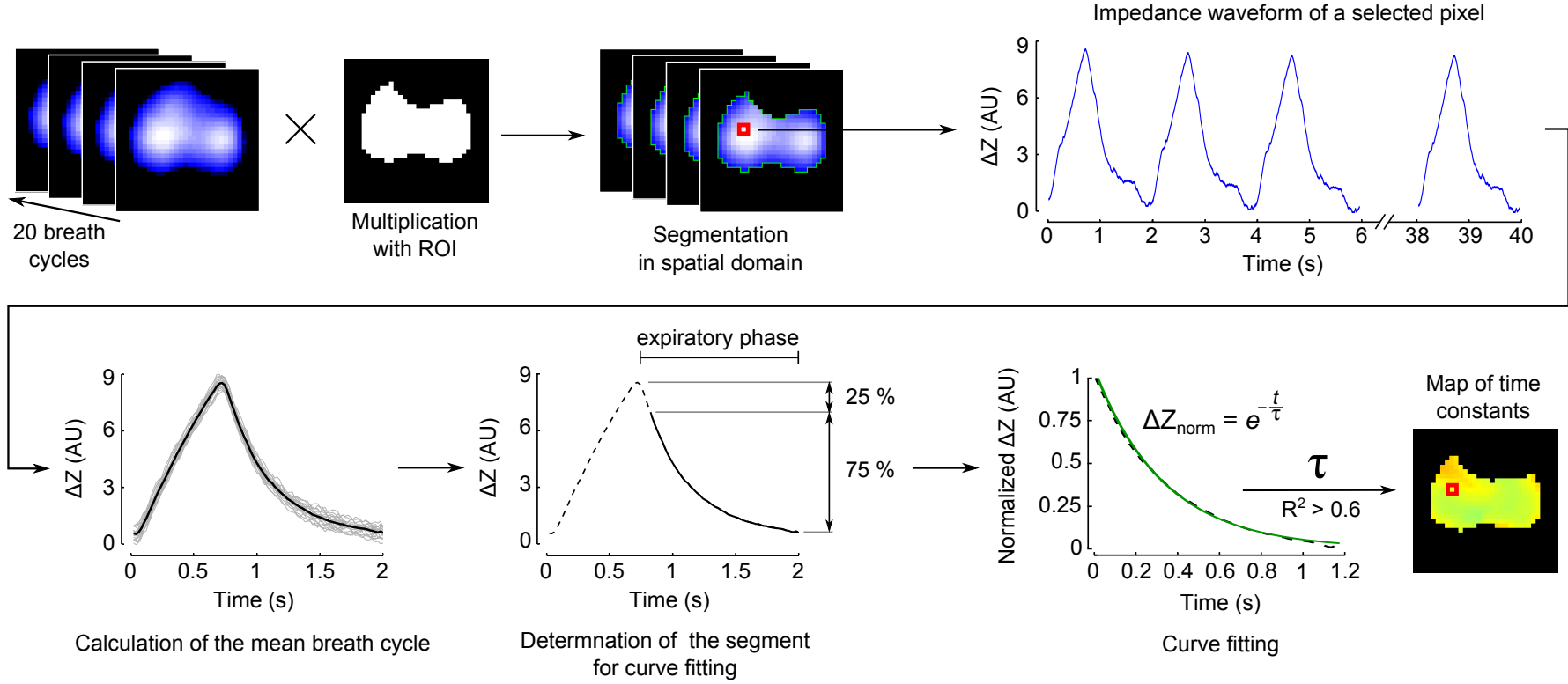


Figure 4.7: Data processing scheme. EIT data set is segmented in spatial domain by multiplication of each frame with the region of interest (ROI). Impedance waveform of each pixel within the ROI is divided in 20 separated breath cycles from which one mean breath cycle is calculated. The expiratory phase of the mean breath cycle is determined and the part with the values lower than 75% of the mean breath amplitude is fitted with an exponential curve. The values of time constants (τ) obtained from the curve fitting with coefficient of determination (R^2) higher than 0.6 are visualized as a map of time constants.

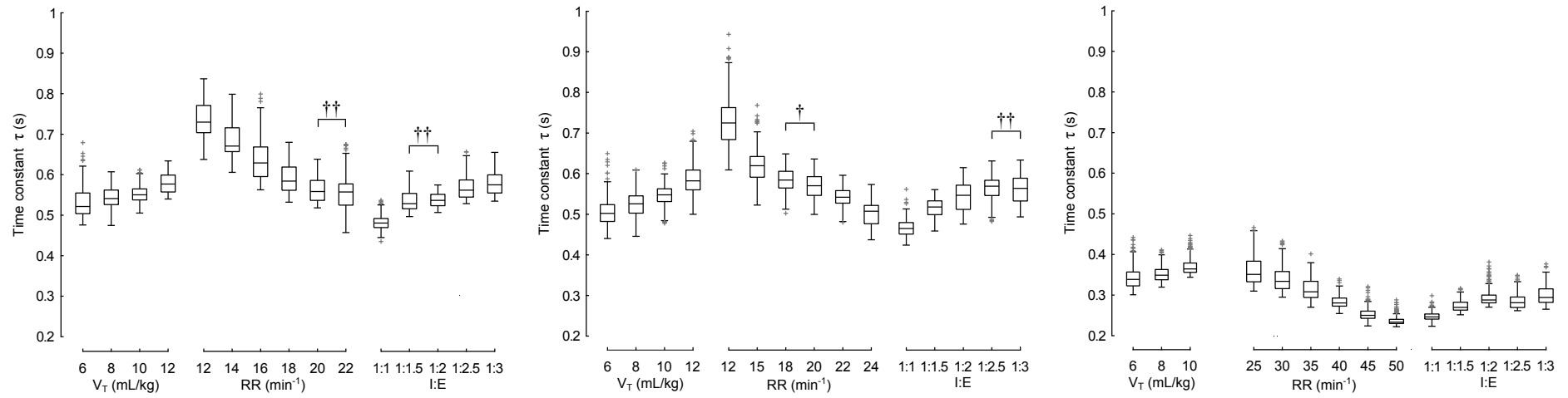


Figure 4.8: Values of regional time constants (τ) for different ventilatory settings. The top and the middle graph represent the values obtained in healthy animals, the bottom graph presents τ calculated in the animal with induced acute respiratory distress syndrome. Statistically insignificant differences are marked as \dagger ($p > 0.01$) and $\dagger\dagger$ ($p > 0.05$). V_T —tidal volume; RR —respiratory rate; $I:E$ —inspiratory-to-expiratory ratio.

Similarly, the values of τ are higher when the value of $I:E$ is increased on the side of expiratory time. In the ARDS animal, τ was significantly lower as shown in Fig. 4.8 and in the color-coded maps presented in Fig. 4.9 and 4.10.

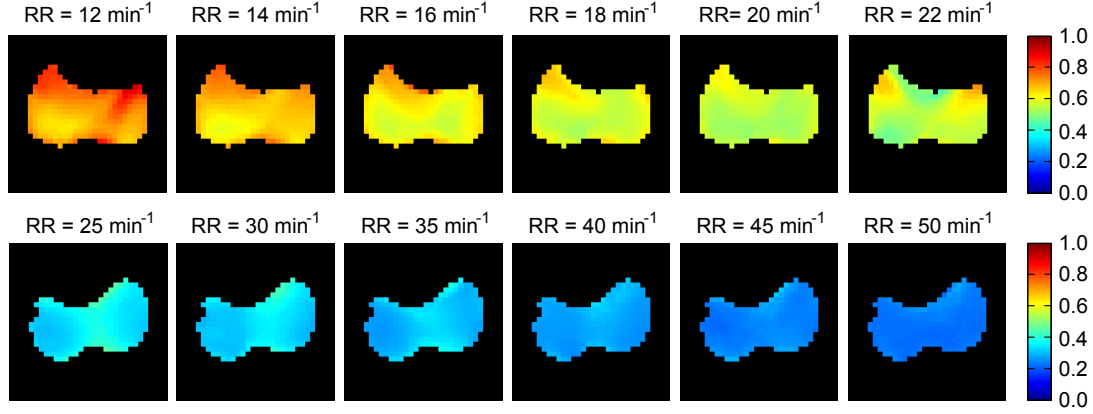


Figure 4.9: Color-coded maps of time constants obtained during the second phase of the study protocol. Top row: changes of respiratory rate (RR) in healthy animal— $PEEP$ 5 cmH₂O, tidal volume (V_T) 10 mL/kg, $I:E$ 1:2. Bottom row: animal with induced acute respiratory distress syndrome— $PEEP$ 15 cmH₂O, V_T 8 mL/kg, $I:E$ 1:2.

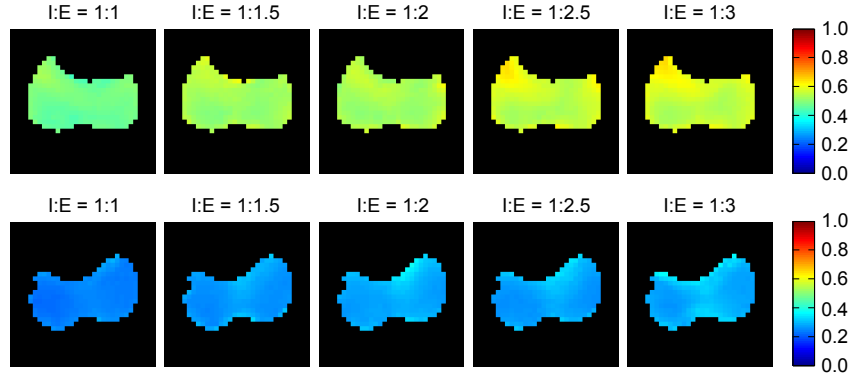


Figure 4.10: Color-coded maps of time constants obtained during the third phase of the study protocol. Top row: changes of inspiratory-to-expiratory ratio ($I:E$) in healthy animal— $PEEP$ 5 cmH₂O, V_T 10 mL/kg, RR 20 min⁻¹. Bottom row: animal with induced acute respiratory distress syndrome— $PEEP$ 15 cmH₂O, V_T 8 mL/kg, RR 30 min⁻¹.

4.2.3 Discussion

The main result of this study is that values of regional EIT-derived time constants are affected by setting of ventilatory parameters. Statistically significant changes

of τ were observed for different settings of V_T , RR and $I:E$ in healthy animals as well as in the animal with artificially induced ARDS.

The values of τ obtained in healthy animals are comparable with the values presented in recently published study [32]. However, more pronounced decrease of τ was observed in the ARDS animal. This was probably caused by relatively high values of RR during the whole study protocol. Because the results show that RR has a decreasing effect upon τ , it is rather difficult to distinguish how much the values of τ are affected by the ventilatory setting and what is the effect of the lung injury itself.

The EIT-derived regional time constant τ can be considered as a regional analogy of the global time constant τ_{global} . Using a mathematical model of respiratory system, τ_{global} can be obtained as a product:

$$\tau_{\text{global}} = RC, \quad (4.7)$$

where R is a resistance of the respiratory system and C is its compliance [28]. In lungs with ARDS, C is reduced, resulting in lower τ_{global} . Contrary to this, obstructive diseases cause an increase of R that leads to higher τ_{global} . Therefore, lung pathologies such as ARDS and COPD can be distinguished using τ . Similarly, the mathematical model of respiratory system can be used to describe how the setting of ventilatory parameters affects the mechanical impedance of the lungs [65].

Despite the observed dependency of τ upon ventilatory settings, we do not reject the idea that different lung pathologies could be distinguished by assessment of regional dynamics of lung aeration as determined by EIT. However, the results indicate that a defined ventilatory maneuver or ventilatory setting is necessary to obtain comparable values for different subjects.

There are numerous outliers above the box plots depicted in Fig. 4.8, especially in the graph of the ARDS animal. Analysis of the maps of time constants presented in Fig. 4.9 and 4.10 showed that the corresponding pixels are predominantly located at the ventral edge of the ROI. Therefore, the high values of τ in these pixels are probably caused by the presence of cardiac-related artifacts in the impedance waveforms.

Although the original idea of regional time constants considered calculation of τ on a breath-to-breath basis, we decided to use mean breath cycles for our calculations. The main advantage of this approach is that averaging attenuates the artifacts in the impedance waveforms that are related to cardiac activity and lung perfusion.

A modified approach for calculation of ROI was used in this study. Multiplication of the original ROI with the mask that is based on the values of R^2 resulted in most of the cases in neglecting of cardiac-related pixels. In a consequence, there were only few pixels where the value of τ was omitted due to poor curve fitting ($R^2 < 0.6$).

Even though the study was performed using the data from three animals only, we do not consider this number insufficient. Rather than evaluation of τ in individual animals, the aim of this study was to assess the changes caused by different ventilatory settings. Thus, the applied range of selected ventilatory parameters was more important for the study design than the total number of evaluated subjects. For this reason, a higher number of animals involved in the study would be ethically inappropriate.

Chapter 5

Conclusion

Electrical impedance tomography offers a new perspective in monitoring of lung ventilation. Using the evaluation methods that were developed, it allows assessment of regional lung filling in both spatial and temporal domain. Based on the requirements for a specific ventilatory manoeuvre, the methods were divided into two groups. In this work, two approaches were investigated more into depth.

The study that was performed to compare the methods for calculation of Center of ventilation shows, that there are statistically significant differences between the values provided by different algorithms. Although the differences are mostly at the edge of clinical relevance or even negligible, the study suggest that there could be cases where the assessment of ventral-to-dorsal shifts in lung ventilation is compromised. Both algorithms that were investigated are relatively insensitive to image segmentation.

The second study shows that the setting of ventilatory parameters significantly affects the values of regional time constants, as defined in the recently published feasibility study. In consequence, assessment of lung pathologies by means of regional time constants may be compromised when various ventilatory settings are applied.

Bibliography

- [1] J. A. Victorino, J. B. Borges, V. N. Okamoto, G. F. J. Matos, M. R. Tucci, M. P. R. Caraméz, H. Tanaka, F. S. Sipmann, D. C. B. Santos, C. S. V. Barbas, C. R. R. Carvalho, and M. B. P. Amato, “Imbalances in regional lung ventilation: a validation study on electrical impedance tomography,” *American Journal of Respiratory and Critical Care Medicine*, vol. 169, no. 7, pp. 791–800, Apr. 2004.
- [2] I. Frerichs, J. Hinz, P. Herrmann, G. Weisser, G. Hahn, M. Quintel, and G. Hellige, “Regional lung perfusion as determined by electrical impedance tomography in comparison with electron beam CT imaging,” *IEEE transactions on medical imaging*, vol. 21, no. 6, pp. 646–652, Jun. 2002.
- [3] Z. Zhao, D. Steinmann, I. Frerichs, J. Guttman, and K. Möller, “PEEP titration guided by ventilation homogeneity: a feasibility study using electrical impedance tomography,” *Critical Care (London, England)*, vol. 14, no. 1, p. R8, 2010.
- [4] P. Blankman, D. Hasan, G. Erik, and D. Gommers, “Detection of ‘best’ positive end-expiratory pressure derived from electrical impedance tomography parameters during a decremental positive end-expiratory pressure trial,” *Critical Care (London, England)*, vol. 18, no. 3, p. R95, 2014.
- [5] J. Karsten, C. Grusnick, H. Paarman, M. Heringlake, and H. Heinze, “Positive end-expiratory pressure titration at bedside using electrical impedance tomography in post-operative cardiac surgery patients,” *Acta Anaesthesiologica Scandinavica*, vol. 59, no. 6, pp. 723–732, Jul. 2015.
- [6] E. L. V. Costa, J. B. Borges, A. Melo, F. Suarez-Sipmann, C. Toufen, S. H. Böhm, and M. B. P. Amato, “Bedside estimation of recruitable alveolar collapse

- and hyperdistension by electrical impedance tomography,” *Intensive Care Medicine*, vol. 35, no. 6, pp. 1132–1137, Jun. 2009.
- [7] Z. Zhao, R. Fischer, I. Frerichs, U. Müller-Lisse, and K. Möller, “Regional ventilation in cystic fibrosis measured by electrical impedance tomography,” *Journal of Cystic Fibrosis: Official Journal of the European Cystic Fibrosis Society*, vol. 11, no. 5, pp. 412–418, Sep. 2012.
- [8] C. J. C. Trepte, C. R. Phillips, J. Solà, A. Adler, S. A. Haas, M. Rapin, S. H. Böhm, and D. A. Reuter, “Electrical impedance tomography (EIT) for quantification of pulmonary edema in acute lung injury,” *Critical Care (London, England)*, vol. 20, no. 1, p. 18, 2016.
- [9] B. H. Brown, R. A. Primhak, R. H. Smallwood, P. Milnes, A. J. Narracott, and M. J. Jackson, “Neonatal lungs: maturational changes in lung resistivity spectra,” *Medical & Biological Engineering & Computing*, vol. 40, no. 5, pp. 506–511, Sep. 2002.
- [10] K. Buzkova and J. Suchomel, “Use of electrical impedance tomography for quantitative evaluation of disability level of bronchopulmonary dysplasia,” in *E-Health and Bioengineering Conference (EHB), 2013*, Iasi, Romania, Nov. 2013, pp. 1–4.
- [11] P. S. van der Burg, F. H. de Jongh, M. Miedema, I. Frerichs, and A. H. van Kaam, “The effect of prolonged lateral positioning during routine care on regional lung volume changes in preterm infants,” *Pediatric Pulmonology*, vol. 51, no. 3, pp. 280–285, Mar. 2016.
- [12] R. Pikkemaat, S. Lundin, O. Stenqvist, R.-D. Hilgers, and S. Leonhardt, “Recent advances in and limitations of cardiac output monitoring by means of electrical impedance tomography,” *Anesthesia and Analgesia*, vol. 119, no. 1, pp. 76–83, Jul. 2014.
- [13] V. Sobota and J. Suchomel, “Monitoring of pulmonary embolism using electrical impedance tomography: A case study,” in *E-Health and Bioengineering Conference (EHB)*, Iasi, Romania, Nov. 2013, pp. 1–4.

- [14] J.-M. Constantin, S. Perbet, J. Delmas, and E. Futier, “Electrical impedance tomography: so close to touching the holy grail,” *Critical Care (London, England)*, vol. 18, no. 4, p. 164, 2014.
- [15] J. H. Arnold, “Electrical impedance tomography: on the path to the Holy Grail,” *Critical Care Medicine*, vol. 32, no. 3, pp. 894–895, Mar. 2004.
- [16] S. Leonhardt and B. Lachmann, “Electrical impedance tomography: the holy grail of ventilation and perfusion monitoring?” *Intensive Care Medicine*, vol. 38, no. 12, pp. 1917–1929, 2012.
- [17] E. Teschner and M. Imhoff, “Electrical impedance tomography: The realization of regional ventilation monitoring,” Drägerwerk AG & Co. KGaA, 2011.
- [18] P. Nopp, E. Rapp, H. Pfützner, H. Nakesch, and C. Ruhsam, “Dielectric properties of lung tissue as a function of air content,” *Physics in Medicine and Biology*, vol. 38, no. 6, pp. 699–716, Jun. 1993.
- [19] P. Nopp, N. D. Harris, T. X. Zhao, and B. H. Brown, “Model for the dielectric properties of human lung tissue against frequency and air content,” *Medical & Biological Engineering & Computing*, vol. 35, no. 6, pp. 695–702, Nov. 1997.
- [20] V. Sobota, “The use of electrical impedance tomography for monitoring changes in fluid balance,” Bachelor thesis, Czech Technical University in Prague, Faculty of Biomedical Engineering, May 2013.
- [21] J. Malmivuo and R. Plonsey, *Bioelectromagnetism - Principles and Applications of Bioelectric and Biomagnetic Fields*. New York: Oxford University Press, 1995.
- [22] D. S. Holder, *Electrical Impedance Tomography: methods, history and applications*. Philadelphia: Institute of Physics Pub., 2005.
- [23] G. Hahn, A. Just, T. Dudykevych, I. Frerichs, J. Hinz, M. Quintel, and G. Hellige, “Imaging pathologic pulmonary air and fluid accumulation by functional and absolute EIT,” *Physiological Measurement*, vol. 27, no. 5, pp. S187–198, May 2006.
- [24] D. C. Barber, “Quantification in impedance imaging,” *Clinical Physics and Physiological Measurement*, vol. 11 Suppl A, pp. 45–56, 1990.

- [25] J. Suchomel and V. Sobota, “A model of end-expiratory lung impedance dependency on total extracellular body water,” in *Journal of Physics: Conference Series*, vol. 434, Heilbad Heiligenstadt, Germany, Apr. 2013, pp. 1–4.
- [26] C. Putensen, H. Wrigge, and J. Zinserling, “Electrical impedance tomography guided ventilation therapy,” *Curr. Opin. Crit. Care*, vol. 13, no. 3, pp. 344–350, Jun. 2007.
- [27] A. Adler, M. Amato, J. Arnold, R. Bayford, M. Bodenstein, S. Böhm, B. Brown, I. Frerichs, O. Stenqvist, N. Weiler, and G. Wolf, “Whither lung EIT: Where are we, where do we want to go and what do we need to get there?” *Physiological Measurement*, vol. 33, no. 5, pp. 679–694, 2012.
- [28] R. Pikkemaat, K. Tenbrock, S. Lehmann, and S. Leonhardt, “Electrical impedance tomography: New diagnostic possibilities using regional time constant maps,” *Applied Cardiopulmonary Pathophysiology*, vol. 16, pp. 212–225, 2012.
- [29] I. Frerichs, T. Becher, and N. Weiler, “Methodology of electrical impedance tomography-derived measures of regional lung ventilation,” *Critical Care*, vol. 18, no. 6, pp. 1–1, 2014.
- [30] M. Miedema, F. H. de Jongh, I. Frerichs, M. B. van Veenendaal, and A. H. van Kaam, “Regional respiratory time constants during lung recruitment in high-frequency oscillatory ventilated preterm infants,” *Intensive Care Medicine*, vol. 38, no. 2, pp. 294–299, Feb. 2012.
- [31] S. Pulletz, M. Kott, G. Elke, D. Schädler, B. Vogt, N. Weiler, and I. Frerichs, “Dynamics of regional lung aeration determined by electrical impedance tomography in patients with acute respiratory distress syndrome,” *Multidisciplinary Respiratory Medicine*, vol. 7, no. 1, p. 44, 2012.
- [32] P. L. Róka, A. D. Waldmann, B. Müller, F. Ender, S. H. Böhm, W. Windisch, S. Strassmann, and C. Karagiannidis, “Breath-by-breath regional expiratory time constants by electrical impedance tomography – a feasibility study,” in *Proceedings of the 16th International Conference on Biomedical Applications of Electrical Impedance Tomography*, Neuchâtel, Switzerland, Jun. 2015, p. 50.

- [33] S. Pulletz, H. R. van Genderingen, G. Schmitz, G. Zick, D. Schädler, J. Scholz, N. Weiler, and I. Frerichs, “Comparison of different methods to define regions of interest for evaluation of regional lung ventilation by EIT,” *Physiological Measurement*, vol. 27, no. 5, p. S115, 2006.
- [34] K. Roubík, V. Sobota, and M. Laviola, “Selection of the baseline frame for evaluation of electrical impedance tomography of the lungs,” in *2nd International Conference on Mathematics and Computers in Sciences and in Industry (MCSI)*, Sliema, Malta, Aug. 2015.
- [35] H. R. van Genderingen, A. J. van Vught, and J. R. C. Jansen, “Estimation of regional lung volume changes by electrical impedance pressures tomography during a pressure-volume maneuver,” *Intensive Care Medicine*, vol. 29, pp. 233–240, 2003.
- [36] M. Masopustová, V. Sobota, Z. Marešová, J. Ráfl, and M. Rožánek, “Changes of the electrode plain position within the recommended area affect significantly the results of ventilation analysis using EIT,” in *The 6th Biomedical Engineering Conference of Young Biomedical Engineers and Researchers (YBERC)*, Bratislava, Slovakia, Jul. 2014.
- [37] I. Frerichs, G. Hahn, W. Golisch, M. Kurpitz, H. Burchardi, and G. Hellige, “Monitoring perioperative changes in distribution of pulmonary ventilation by functional electrical impedance tomography,” *Acta Anaesthesiologica Scandinavica*, vol. 42, no. 6, pp. 721–726, Jul. 1998.
- [38] I. Frerichs, P. A. Dargaville, H. van Genderingen, D. R. Morel, and P. C. Rimensberger, “Lung volume recruitment after surfactant administration modifies spatial distribution of ventilation,” *American Journal of Respiratory and Critical Care Medicine*, vol. 174, no. 7, pp. 772–779, Oct. 2006.
- [39] O. C. Radke, T. Schneider, A. R. Heller, and T. Koch, “Spontaneous breathing during general anesthesia prevents the ventral redistribution of ventilation as detected by electrical impedance tomography: a randomized trial,” *Anesthesiology*, vol. 116, no. 6, pp. 1227–1234, Jun. 2012.
- [40] M. van Heerde, K. Roubik, V. Kopelent, M. Kneyber, and D. Markhorst, “Spontaneous breathing during high-frequency oscillatory ventilation improves

- regional lung characteristics in experimental lung injury,” *Acta Anaesthesiologica Scandinavica*, vol. 54, no. 10, pp. 1248–1256, 2010.
- [41] H. Luepschen, T. Meier, M. Grossherr, T. Leibecke, J. Karsten, and S. Leonhardt, “Protective ventilation using electrical impedance tomography,” *Physiological Measurement*, vol. 28, no. 7, pp. S247–260, Jul. 2007.
- [42] P. W. Kunst, G. Vazquez de Anda, S. H. Böhm, T. J. Faes, B. Lachmann, P. E. Postmus, and P. M. de Vries, “Monitoring of recruitment and derecruitment by electrical impedance tomography in a model of acute lung injury,” *Critical Care Medicine*, vol. 28, no. 12, pp. 3891–3895, Dec. 2000.
- [43] “Swisstom BB² Silent Spaces – clinically meaningful electrical impedance tomography,” Swisstom AG, Landquart, Switzerland, 2015. [Online]. Available: http://www.swisstom.com/wp-content/uploads/BB2-White-Paper_2ST800-104_Rev.000.pdf
- [44] Z. Zhao, K. Möller, D. Steinmann, I. Frerichs, and J. Guttman, “Evaluation of an electrical impedance tomography-based Global Inhomogeneity Index for pulmonary ventilation distribution,” *Intensive Care Medicine*, vol. 35, no. 11, pp. 1900–1906, Nov. 2009.
- [45] Z. Zhao, S. Pulletz, I. Frerichs, U. Müller-Lisse, and K. Möller, “The EIT-based global inhomogeneity index is highly correlated with regional lung opening in patients with acute respiratory distress syndrome,” *BMC Research Notes*, vol. 7, no. 1, 2014.
- [46] E. L. Costa and M. B. Amato, “Can heterogeneity in ventilation be good?” *Critical Care*, vol. 14, no. 2, pp. 1–2, 2010.
- [47] K. Lowhagen, S. Lundin, and O. Stenqvist, “Regional intratidal gas distribution in acute lung injury and acute respiratory distress syndrome—assessed by electric impedance tomography,” *Minerva Anesthesiologica*, vol. 76, no. 12, pp. 1024–1035, Dec. 2010.
- [48] I. Frerichs, T. Dudykevych, J. Hinz, M. Bodenstein, G. Hahn, and G. Hellige, “Gravity effects on regional lung ventilation determined by functional EIT during

- parabolic flights,” *Journal of Applied Physiology (Bethesda, Md.: 1985)*, vol. 91, no. 1, pp. 39–50, Jul. 2001.
- [49] A. D. Waldmann, S. H. Böhm, W. Windisch, S. Strassmann, and C. Karagiannidis, “Electrical impedance tomography: Robustness of a new pixel wise regional expiratory time constant calculation,” in *Proceedings of the 36th International Symposium on Intensive Care and Emergency Medicine*, Brussels, Belgium, Mar. 2015, p. 255.
- [50] —, “Comparison of regional and global expiratory time constants measured by electrical impedance tomography,” in *Proceedings of the 36th International Symposium on Intensive Care and Emergency Medicine*, Brussels, Belgium, Mar. 2015, p. 254.
- [51] H. Wrigge, J. Zinserling, T. Muders, D. Varelmann, U. Günther, C. von der Groeben, A. Magnusson, G. Hedenstierna, and C. Putensen, “Electrical impedance tomography compared with thoracic computed tomography during a slow inflation maneuver in experimental models of lung injury,” *Critical Care Medicine*, vol. 36, no. 3, pp. 903–909, Mar. 2008.
- [52] T. Muders, H. Luepschen, J. Zinserling, S. Greschus, R. Fimmers, U. Guenther, M. Buchwald, D. Grigutsch, S. Leonhardt, C. Putensen, and H. Wrigge, “Tidal recruitment assessed by electrical impedance tomography and computed tomography in a porcine model of lung injury*,” *Critical Care Medicine*, vol. 40, no. 3, pp. 903–911, Mar. 2012.
- [53] Z. Zhao, I. Frerichs, S. Pulletz, U. Müller-Lisse, and K. Möller, “The influence of image reconstruction algorithms on linear thorax EIT image analysis of ventilation,” *Physiological Measurement*, vol. 35, no. 6, pp. 1083–1093, Jun. 2014.
- [54] S. Pulletz, A. Adler, M. Kott, G. Elke, B. Gawelczyk, D. Schädler, G. Zick, N. Weiler, and I. Frerichs, “Regional lung opening and closing pressures in patients with acute lung injury,” *Journal of Critical Care*, vol. 27, no. 3, pp. 323.e11–18, Jun. 2012.
- [55] A. Adler, R. Amyot, R. Guardo, J. H. T. Bates, and Y. Berthiaume, “Monitoring changes in lung air and liquid volumes with electrical impedance tomography,” *Journal of Applied Physiology*, vol. 83, no. 5, pp. 1762–1767, Nov. 1997.

- [56] P. A. Dargaville, P. C. Rimensberger, and I. Frerichs, “Regional tidal ventilation and compliance during a stepwise vital capacity manoeuvre,” *Intensive Care Medicine*, vol. 36, no. 11, pp. 1953–1961, Nov. 2010.
- [57] I. Frerichs, P. A. Dargaville, and P. C. Rimensberger, “Regional respiratory inflation and deflation pressure-volume curves determined by electrical impedance tomography,” *Physiological Measurement*, vol. 34, no. 6, pp. 567–577, Jun. 2013.
- [58] “Instruction manual – dräger eit data analysis tool,” Dräger Medical GmbH, 2011.
- [59] G. Hahn, I. Sipinkova, F. Baisch, and G. Hellige, “Changes in the thoracic impedance distribution under different ventilatory conditions,” *Physiological Measurement*, vol. 16, no. 3A, pp. A161–A173, 1995.
- [60] G. Kühnel, G. Hahn, I. Frerichs, T. Schröder, and G. Hellige, “Neue verfahren zur verbesserung der abbildungsqualität bei funktionellen eit-tomogrammen der lunge,” *Biomedizinische Technik*, vol. 42, pp. 470–471, 1997.
- [61] Z. Zhao, K. Moller, D. Steinmann, and J. Guttmann, “Determination of lung area in EIT images,” in *2009 3rd International Conference on Bioinformatics and Biomedical Engineering*, Jun. 2009, pp. 1–4.
- [62] Z. Zhao, D. Steinmann, D. Müller-Zivkovic, M. Jörg, I. Frerichs, J. Guttmann, and K. Möller, “A lung area estimation method for analysis of ventilation inhomogeneity based on electrical impedance tomography,” *Journal of X-Ray Science and Technology*, vol. 18, pp. 171–182, 2010.
- [63] A. Schibler, M. Yuill, C. Parsley, T. Pham, K. Gilshenan, and C. Dakin, “Regional ventilation distribution in non-sedated spontaneously breathing newborns and adults is not different,” *Pediatric Pulmonology*, vol. 44, no. 9, pp. 851–858, 2009.
- [64] M. Schaefer, V. Wania, B. Bastin, U. Schmalz, P. Kienbaum, M. Beiderlinden, and T. Treschan, “Electrical impedance tomography during major open upper abdominal surgery: A pilot-study,” *BMC Anesthesiology*, vol. 14, 2014.
- [65] M. Rožánek and K. Roubík, “Mathematical model of the respiratory system – comparison of the total lung impedance in the adult and neonatal lung,” in *International Journal of Biomedical Sciences*, vol. 2, 2007, pp. 249–252.

Appendix A

Approval of Institutional Review Board

A statement of Institutional Review Board of First Faculty of Medicine, Charles University that approved the use animals for experimental purposes.

UNIVERZITA KARLOVA V PRAZE

1. lékařská fakulta

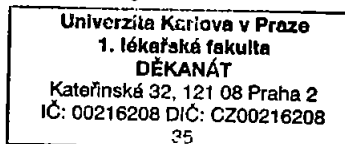
Děkanát - Kateřinská 32, 121 08 Praha 2



Vyjádření odborné komise pro práci s pokusnými zvířaty

Odborná komise Univerzity Karlovy v Praze, 1. lékařské fakulty projednala projekt pokusů – název projektu: „Experimentální studie Centra pro multifyzikální snímání a multidimensionální zpracování signálů životních funkcí. Úkoly: Analýza tranzientních reakcí na stimulus; Integrovaný systém pro hemometabolické monitorování; Zpracování signálů elektrické impedační tomografie.“ předložený MUDr. Mikulášem Mlčkem a vyslovila souhlas s použitím pokusných zvířat.

Doc. MUDr. Drahomíra Křenová, CSc.
předsedkyně odborné komise



V Praze : 13. května 2013

TELEFON
224 968 147

IČ
00216208

DIČ
CZ00216208

E-MAIL
drahomira.krenova@lf1.cuni.cz

Appendix B

MEDICON 2016 conference paper

A conference paper presented at the XIV Mediterranean Conference on Medical and Biological Engineering and Computing, March 31th – April 2nd, 2016, Paphos, Cyprus.

Center of Ventilation—Methods of Calculation using Electrical Impedance Tomography and the Influence of Image Segmentation

V. Sobota¹ and K. Roubik¹

¹ Faculty of Biomedical Engineering, Czech Technical University in Prague, Kladno, Czech Republic

Abstract— Electrical impedance tomography (EIT) is a promising non-invasive, radiation-free imaging modality. Using EIT-derived index Center of Ventilation (CoV), ventral-to-dorsal shifts in distribution of lung ventilation can be assessed. The methods of CoV calculation differ among authors and so does the segmentation of EIT images from which the CoV is calculated. The aim of this study is to compare the values of CoV obtained using different algorithms, applied in variously segmented EIT images. An animal trial (n=4) with anesthetized mechanically ventilated pigs was conducted. In one animal, acute respiratory distress syndrome (ARDS) was induced by repeated whole lung lavage. Incremental steps in positive end-expiratory pressure (PEEP), each with a value of 5 cmH₂O (or 4 cmH₂O in the ARDS model), were performed to reach total PEEP level of 25 cmH₂O (or 22 cmH₂O in the ARDS model). EIT data were acquired continuously during this PEEP trial. From each PEEP level, 30 tidal variation (TV) images were used for analysis. Functional regions of interest (ROI) were defined based on the standard deviation (SD) of pixel values, using threshold 15%–35% of maximum pixel SD. The results of this study show that there might be statistically significant differences between the values obtained using different methods for calculation of CoV. The differences occurred in healthy animals as well as in the ARDS model. Both investigated algorithms are relatively insensitive to the image segmentation.

Keywords— center of ventilation, center of gravity, electrical impedance tomography, EIT, region of interest

I. INTRODUCTION

Electrical impedance tomography (EIT) is an imaging modality that provides information about regional lung ventilation. It is based on the application of small alternating currents using skin electrodes attached to the patient's chest and the consequent measurement of resulting voltages. It can offer a non-invasive, radiation-free bedside alternative to computed tomography in monitoring of tidal volume (V_T) distribution and lung aeration inhomogeneity [1].

Due to the physical principle used, EIT images suffer from low spatial resolution [2], [3] and the information provided

by EIT is rather complex and may be difficult to interpret [3]. Therefore, several indices and measures were developed to assess lung ventilation [4].

One of the most widely used indices in EIT data processing is called Center of Ventilation (CoV) and was introduced for the first time in 1998 by Frerichs et al. [5]. It describes shifts in distribution of lung ventilation in ventral-to-dorsal direction. In that study, it was defined as a weighted mean of geometrical centers of the right and the left lung. In 2006, the same research group presented a modified approach for its calculation where CoV was calculated separately for both left and right lung [6].

Since CoV has proven to be a useful index in assessment of regional lung ventilation, it was adopted by many research groups [7]–[12]. However, the definitions of CoV are not consistent among these studies. Some authors define CoV as a weighted mean of the row sums [7], [9], [11], [12]. Van Heerde et al. defined CoV as “the point where the sum of fractional ventilation was 50% of the summed fractional ventilation” [8] and Blankman et al. computed it as a ratio between dorsal and total fractional ventilation [10]. Similarly to CoV, Center of Gravity (CoG) index was introduced in 2007 as a weighted mean of image row sums [13].

Unfortunately, different definitions of CoV are not the only inconsistency in its use. Segmentation of EIT images from which the CoV is calculated also varies. Initially, circular mask was applied to the EIT image and the resulting area was divided into several regions of interest (ROI) [6], [8]. However, some authors use functional segmentation of the images, defined as 20% of maximum regression coefficient obtained between global and local relative impedance [11] or as 20% of the maximum standard deviation (SD) of the pixel value in certain time period [12]. Finally, there are studies where CoV was calculated without any previous image segmentation [9].

As there are different definitions of CoV published, used together with various EIT image segmentation, we hypothesized that the resulting CoV values and thus the evaluation of regional lung ventilation may differ.

The aim of this study is to compare the values of CoV obtained using different methods of its computation, applied in variously segmented images.

II. METHODS

The study protocol was approved by the Institutional Review Board of the First Faculty of Medicine, Charles University in Prague (FFM CU) and is in accordance with Act No. 246/1992 Coll., on the protection of animals against cruelty. The measurements were performed at an accredited animal laboratory of the FFM CU.

Four crossbred Landrace female pigs (*Sus scrofa domestica*) with a body weight of 48 ± 2 kg were used in this study.

A. Anesthesia and preparation

The animals were premedicated with azaperone (2 mg/kg IM). Anesthesia was initiated with ketamine hydrochloride (20 mg/kg IM) and atropine sulphate (0.02 mg/kg IM), followed by boluses of morphine (0.1 mg/kg IV) and propofol (2 mg/kg IV). A cuffed endotracheal tube (I.D. 7.5 mm) was used for intubation. Anesthesia was maintained with propofol (8 to 10 mg/kg/h IV) in combination with morphine (0.1 mg/kg/h IV) and heparin (40 U/kg/h IV). To suppress spontaneous breathing, myorelaxant pipecuronium bromide (4 mg boluses every 45 min) was administered during mechanical lung ventilation. Initially, rapid infusion of 1 000 mL of saline was administered intravenously, followed by a continuous IV administration of 250 mL/h to reach and maintain central venous pressure of 6 to 7 mmHg.

Mixed venous blood oxygen saturation and continuous cardiac output were measured by Vigilance (Edwards Lifesciences, Irvine, CA, USA) monitor. Arterial blood gases, i.e. arterial partial pressure of oxygen, carbon dioxide (PaCO_2) and pH, were continuously measured by CDI 500 (Terumo, Tokyo, Japan). The arterio-venous extracorporeal circuit for CDI 500 monitor was established between the femoral artery and the femoral vein using a mechanical blood pump (peristaltic roller pump with a blood flow set to 400 mL/min).

In one animal, repeated whole lung lavage (normal saline, 30–40 mL/kg, 37°C) was performed to induce the surfactant deficiency similar to acute respiratory distress syndrome (ARDS) [8].

B. Ventilation

Conventional ventilator Hamilton G5 (Hamilton Medical AG, Bonaduz, Switzerland) was used in the CMV mode with the following setting: respiratory rate 18 bpm, FiO_2 21%, I:E 1:2 with initial positive end-expiratory pressure (PEEP) of 5 cmH_2O and pressure limit set to 40 cmH_2O . The initial V_T was set to 8.5 mL/kg of the actual body weight and was titrated to reach normocapnia (PaCO_2 40 ± 3 mmHg). During the study protocol four increasing PEEP steps of 5 cmH_2O

were performed in animals with healthy lungs and three increasing PEEP steps of 4 cmH_2O with initial value of 10 cmH_2O were performed in the ARDS model. Each PEEP level was maintained at least for 3 minutes.

C. EIT measurements

EIT system PulmoVista 500 (Dräger Medical, Lübeck, Germany) was used for data acquisition. The electrode belt (size S) was attached to the chest of the animal at the level of the 6th intercostal space. The frequency of the applied current was set to 110 kHz with amplitude of 9 mA. EIT images were recorded continuously with a frame rate of 50 Hz during the entire PEEP maneuver.

D. Data Processing

The acquired data were pre-processed in Dräger EIT Data Analysis Tool 6.1 (Dräger Medical, Lübeck, Germany). Baseline frame was set automatically for each animal as a frame that corresponds with the global minimum of impedance waveform. Reconstructed data were processed in MATLAB 2014b (MathWorks, Natick, MA, USA).

At each PEEP level, EIT data from 30 consecutive breaths were used for analysis. The breaths were selected in the phases where the values of end-expiratory lung impedance were the most stable. Tidal variation (TV) images were calculated as a difference between end-inspiratory and end-expiratory EIT images. In consequence, 30 TV images were obtained for each PEEP level.

Functional ROI was defined based on the standard deviation (SD) of individual pixel values in time [12], [14]. Six threshold levels ranging from 15% to 40% of maximum pixel SD with 5% step were used for image segmentation. For each set of 30 TV images, a common ROI was applied. The index called Center of Gravity (CoG) was defined as a weighted mean of row sums obtained from TV image [13]:

$$\text{CoG} = \frac{1}{N+1} \cdot \frac{\sum_{x=1}^N \sum_{y=1}^N y \cdot TV_{xy}}{\sum_{x=1}^N \sum_{y=1}^N TV_{xy}} \quad (1)$$

where N stands for both the number of pixel rows and pixel columns in the TV image ($N = 32$ for EIT images provided by PulmoVista 500) and TV_{xy} stands for the value of the pixel with coordinates x, y .

For the purposes of this study, Center of Ventilation (CoV) index was defined as a vertical coordinate that divides the sum of fractional ventilation in two equal halves [8] (Fig. 1). Our implementation of the algorithm for calculation of CoV can be summarized as follows:

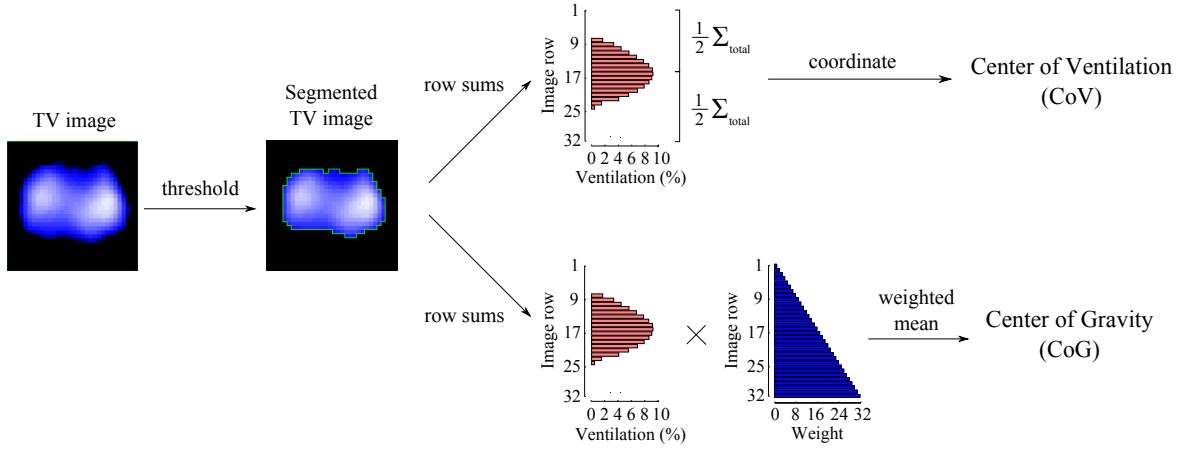


Fig. 1: Computation of Center of Ventilation (CoV) and Center of Gravity (CoG). Tidal variation (TV) images were segmented and a region of interest (ROI) was defined. Row sums were calculated from the segmented TV image. CoV was calculated as a coordinate that divides row sums in two equal halves. CoG was calculated as a weighted mean of image row sums.

1. Normalize the pixel values in the TV image:

$$TV_{xy}^* = \frac{TV_{xy}}{\sum_{x=1}^N \sum_{y=1}^N TV_{xy}} \cdot 100 \quad (2)$$

where TV_{xy}^* expresses the value of the original pixel TV_{xy} as a percentage of the total sum of the TV image.

2. Calculate row sums of the normalized TV image and save them into the array \mathbf{r} .
3. Find the highest index $n \in \mathbb{N}$ for which holds:

$$\sum_{i=1}^n \mathbf{r}_i \leq 50 \quad (3)$$

4. Calculate the ratio k :

$$k = \frac{50 - \sum_{i=1}^n \mathbf{r}_i}{\mathbf{r}_n} \quad (4)$$

5. Calculate the value of CoV:

$$\text{CoV} = \frac{n + k + 0.5}{N + 1} \quad (5)$$

For calculation of both CoV and CoG, a coordinate system with the top left pixel represented by coordinates $x = 1$, $y = 1$ was used. In the following text the abbreviations “CoV” and “CoG” refer to the indices described above and the unabbreviated term “Center of Ventilation” represents the index in general.

Paired two-tailed t-test was used for evaluation of statistical differences between CoV and CoG. The values of both indices obtained at different PEEP levels were visualized as a box plot.

III. RESULTS

EIT data from 4 animals were studied. The highest PEEP step was omitted in two subjects due to their hemodynamic instability. In total 510 TV images were analyzed.

In general, the values of CoV were significantly higher ($p < 0.05$) than the corresponding values of CoG in all subjects. As shown in Table 1, there were four cases where the difference between CoV and CoG was not statistically significant and three cases where the mean value of CoG was higher than the corresponding mean value of CoV.

Box plots were created for each animal to visualize the effect of image segmentation upon values of both CoV and CoG. Figure 2 shows typical values of these indices during incremental PEEP steps. Both CoV and CoG move dorsally when a higher PEEP level is applied. When calculated from segmented TV images, variation in values of both indices decreases with higher threshold.

The effect of image segmentation upon the values of CoV and CoG is rather small when the indices are calculated from mean TV image, as illustrated in Fig. 3 and 4. The influence of PEEP upon both indices is much higher when compared to the changes caused by application of different image segmentation thresholds.

IV. DISCUSSION

The results of this study show, that in general, there is a statistically significant difference between the values obtained using different methods for calculation of Center of Ventilation. Both presented algorithms for its calculation show relatively low sensitivity to lung segmentation.

Table 1: The differences CoV–CoG (mean \pm SD). Statistically insignificant differences (paired t-test, $p > 0.05$) are marked as *. The cases where the mean value of CoG is higher than the value of CoV are marked as †. Repeated whole lung lavage was performed in pig 4.

Pig	PEEP level (cmH ₂ O)	Threshold (% of max. SD)					
		15	20	25	30	35	40
1	5	0.290 \pm 0.049	0.315 \pm 0.043	0.361 \pm 0.045	0.392 \pm 0.053	0.509 \pm 0.047	0.509 \pm 0.040
	10	0.477 \pm 0.089	0.434 \pm 0.046	0.387 \pm 0.028	0.383 \pm 0.057	0.308 \pm 0.048	0.308 \pm 0.043
	15	0.348 \pm 0.112	0.193 \pm 0.058	0.166 \pm 0.012	0.191 \pm 0.027	0.090 \pm 0.027	0.090 \pm 0.027
	20	0.507 \pm 0.333	0.034 \pm 0.179*	0.062 \pm 0.054	0.098 \pm 0.036	0.047 \pm 0.036	0.047 \pm 0.031
	25	1.131 \pm 0.434	0.539 \pm 0.374	0.088 \pm 0.243*	0.066 \pm 0.093	0.057 \pm 0.051	0.057 \pm 0.049
2	5	0.770 \pm 0.122	0.823 \pm 0.112	0.908 \pm 0.110	0.845 \pm 0.101	0.719 \pm 0.091	0.719 \pm 0.086
	10	1.158 \pm 0.063	1.174 \pm 0.054	0.972 \pm 0.050	0.635 \pm 0.056	0.513 \pm 0.055	0.513 \pm 0.044
	15	0.851 \pm 0.056	0.314 \pm 0.023	0.186 \pm 0.026	0.138 \pm 0.025	0.080 \pm 0.021	0.080 \pm 0.019
	20	0.507 \pm 0.017	0.093 \pm 0.026	0.026 \pm 0.028	−0.001 \pm 0.030†*	−0.039 \pm 0.029†	−0.039 \pm 0.033†
3	5	0.193 \pm 0.122	0.186 \pm 0.121	0.181 \pm 0.118	0.186 \pm 0.117	0.052 \pm 0.122	0.052 \pm 0.110*
	10	0.498 \pm 0.098	0.448 \pm 0.098	0.407 \pm 0.103	0.355 \pm 0.105	0.221 \pm 0.107	0.221 \pm 0.102
	15	0.647 \pm 0.106	0.532 \pm 0.063	0.358 \pm 0.050	0.320 \pm 0.055	0.198 \pm 0.057	0.198 \pm 0.059
	20	0.460 \pm 0.233	0.307 \pm 0.159	0.246 \pm 0.067	0.240 \pm 0.040	0.146 \pm 0.041	0.146 \pm 0.036
4	10	0.304 \pm 0.206	0.351 \pm 0.199	0.234 \pm 0.129	0.166 \pm 0.078	0.106 \pm 0.081	0.106 \pm 0.084
	14	0.528 \pm 0.255	0.497 \pm 0.231	0.385 \pm 0.176	0.341 \pm 0.138	0.264 \pm 0.127	0.264 \pm 0.113
	18	1.116 \pm 0.474	1.088 \pm 0.479	0.930 \pm 0.448	0.730 \pm 0.392	0.449 \pm 0.312	0.449 \pm 0.237
	22	1.338 \pm 0.376	1.197 \pm 0.387	1.051 \pm 0.380	0.742 \pm 0.324	0.311 \pm 0.220	0.311 \pm 0.134

Although statistically significant, the differences between the values of CoV and CoG presented in this study are mostly at the edge of clinical relevance or even negligible. However, as shown in Fig. 5, there might be considerable differences in some subjects.

When functional ROI is applied to TV image, the variation in values of both CoV and CoG and the difference between their mean values decrease with an increasing threshold of lung segmentation. This is mainly due to the fact that the pixels with low change of relative impedance in time represent poorly ventilated lung regions or tissues that does not participate in ventilation at all. When these pixels are excluded from the ROI, only the lung regions that substantially contribute to ventilation are used for the calculation. In consequence, this may result in cases where CoV and CoG switch their positions when a high segmentation threshold is applied, as shown in Table 1. Similarly, the mean difference between CoV and CoG values substantially decreases when large insufficiently ventilated lung regions are omitted from the calculation because of the use of high segmentation threshold, as shown in the values of the ARDS model in Table 1.

Contrary to the effect of lung segmentation, when incremental PEEP steps are performed, the lung area that is pre-

dominantly ventilated moves dorsally. Therefore, the changes of both CoV and CoG values caused by PEEP setting are more pronounced.

For the purposes of this study we expressed both CoV and CoG in percentage as we consider this as the most common way [6]–[9], [12]. However, the expression as a value from the interval $(1, N)$, where N stands for the number of image row is also possible and correct [13].

To enable the comparison of two different approaches for calculation of Center of Ventilation, we modified the published algorithms to provide the value of 50% for a homogeneous image and also for images that are symmetrical along vertical axis. Both algorithms are also shift invariant for the structures that are symmetrical along vertical axis (top row of Fig. 5). Therefore, the biggest differences between CoV and CoG occur for the images with a strong horizontal asymmetry as shown in the bottom row of Fig. 5.

We used the abbreviation “CoV” for the method presented by van Heerde et al. [8] as it is in our opinion closer to the original idea of geometrical center of ventilation [5], [6]. The methods for calculation of this index presented in [7], [9], [11], [12] are closer to the idea of Center of Gravity index [13]. Therefore, abbreviation “CoG” was used for this

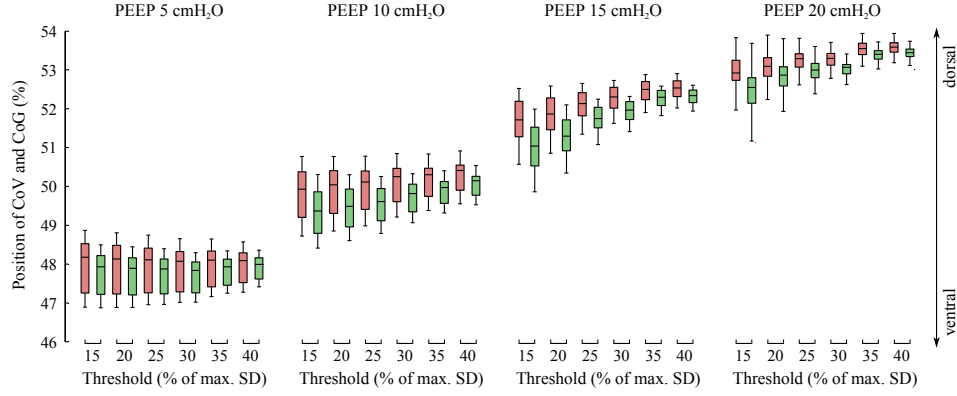


Fig. 2: Values of Center of Ventilation (red) and Center of Gravity (green) calculated from EIT images that were segmented using thresholds in the range of 15% – 40% of maximum pixel standard deviation (SD). The data obtained at four different PEEP levels are presented as box-and-whisker plot (minimum – lower quartile – median – upper quartile – maximum).

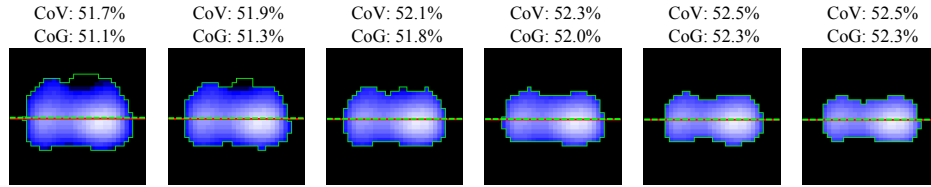


Fig. 3: Thresholding effect upon mean tidal variation (TV) image in the range from 15% to 40% in 5% steps (fig 3, PEEP 15 cmH₂O). The position of Center of Ventilation (CoV) and Center of Gravity (CoG) is depicted with red solid line and green dashed line, respectively. The pixel values of the image were obtained as a mean of 30 consecutive TV images.

method. In this study we did not evaluate the method presented by Blankman et al. [10].

Segmentation of TV images based on SD values of individual pixels is one of the most common approaches used for definition of functional ROI [14]. For this method, there is a recommended range of threshold values from 20% to 35% of maximum pixel SD. In this study we used threshold values ranging from 15% to 40% to assess also the effect of ROIs that are produced by setting of the threshold criteria outside the recommended range.

V. CONCLUSION

This study shows that there is a statistically significant difference between the values provided by the two studied methods for calculation of Center of Ventilation. The differences occurred in healthy animals as well as in the model of lung injury. In consequence, assessment of ventral-to-dorsal shifts in lung ventilation may be compromised. However, both algorithms that were evaluated are relatively insensitive to the segmentation of EIT images.

ACKNOWLEDGEMENTS

The authors thank the employees of the animal laboratory of the Department of Physiology, FFM CU, where the animal trial was performed. The study was supported by grants VG20102015062 and SGS14/216/OHK4/3T/17.

The authors declare that they have no conflict of interest.

REFERENCES

1. Frerichs I., Hinz J., Herrmann P., et al. Detection of local lung air content by electrical impedance tomography compared with electron beam CT *J Appl Physiol.* 2002;93:660-666.
2. Holder D.S.. *Electrical Impedance Tomography: methods, history and applications.* Philadelphia: Institute of Physics Pub. 2005.
3. Putensen C., Wrigge H., Zinserling J.. Electrical impedance tomography guided ventilation therapy *Curr Opin Crit Care.* 2007;13:344-350.
4. Adler A., Amato M.B., Arnold J.H., et al. Whither lung EIT: Where are we, where do we want to go and what do we need to get there? *Physiol Meas.* 2012;33:679-694.
5. Frerichs I., Hahn G., Golisch W., Kurpitz M., Burchardi H., Hellige G.. Monitoring perioperative changes in distribution of pulmonary ventilation by functional electrical impedance tomography *Acta Anaesthesiol Scand.* 1998;42:721-726.
6. Frerichs I., Dargaville P.A., Van Genderingen H., Morel D.R., Rimensberger P.C.. Lung volume recruitment after surfactant administration

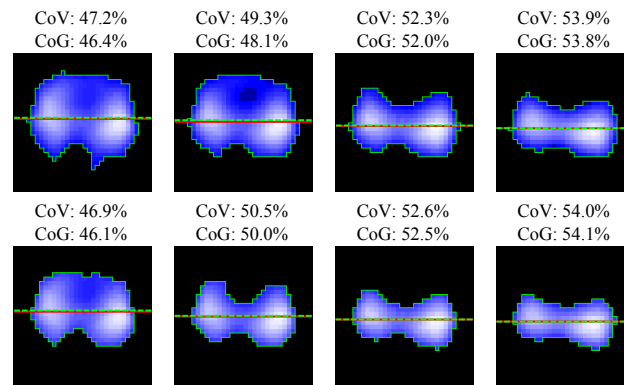


Fig. 4: The effect of PEEP and lung segmentation upon mean tidal variation (TV) images. Distribution of ventilation at four PEEP levels (from left to right, 5 to 20 cmH₂O with a step of 5 cmH₂O). Top row: thresholding set to 20% of maximum SD, bottom row: threshold set to 35% of maximum SD. The position of Center of Ventilation (CoV) and Center of Gravity (CoG) is depicted with red solid line and green dashed line, respectively. The pixel values of the image were obtained as a mean of 30 consecutive TV images.

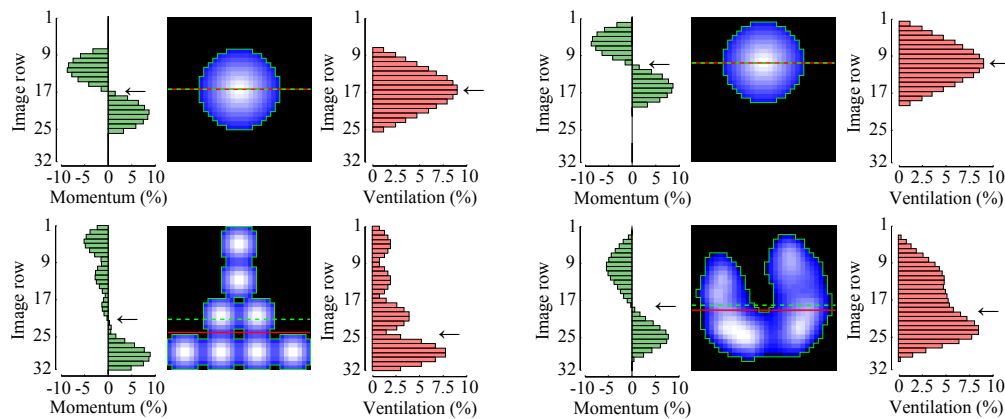


Fig. 5: The position of Center of Ventilation (CoV) and Center of Gravity (CoG) for the image structures that are symmetrical (top row) and asymmetrical (bottom row) along vertical axis. For each image, the left bar graph represents the distribution of momentum (weighted means) along vertical axis and the right bar graph shows the row sums in the normalized tidal variation (TV) image. The right bottom image is an example of TV image obtained in a spontaneously breathing healthy volunteer. The position of CoV and CoG is depicted with red solid line and green dashed line, respectively.

- modifies spatial distribution of ventilation *Am J Respir Crit Care Med*. 2006;174:772-779.
- Schibler A., Yuill M., Parsley C., Pham T., Gilshenan K., Dakin C.. Regional ventilation distribution in non-sedated spontaneously breathing newborns and adults is not different *Pediatr Pulmonol*. 2009;44:851-858.
 - Van Heerde M., Roubik K., Kopelent V., Kneyber M.C.J., Markhorst D.G.. Spontaneous breathing during high-frequency oscillatory ventilation improves regional lung characteristics in experimental lung injury *Acta Anaesthesiol Scand*. 2010;54:1248-1256.
 - Radke O.C., Schneider T., Heller A.R., Koch T.. Spontaneous breathing during general anesthesia prevents the ventral redistribution of ventilation as detected by electrical impedance tomography: A randomized trial *Anesthesiology*. 2012;116:1227-1234.
 - Blankman P., Hasan D., Erik G.J., Gommers D.. Detection of 'best' positive end-expiratory pressure derived from electrical impedance tomography parameters during a decremental positive end-expiratory pressure trial *Crit Care*. 2014;18.
 - Zhao Z., Frerichs I., Pulletz S., Müller-Lisse U., Möller K.. The influence of image reconstruction algorithms on linear thorax EIT image analysis of ventilation *Physiol Meas*. 2014;35:1083-1093.
 - Schaefer M.S., Wania V., Bastin B., et al. Electrical impedance tomography during major open upper abdominal surgery: A pilot-study *BMC Anesthesiol*. 2014;14.
 - Luepschen H., Meier T., Grossherr M., Leibecke T., Karsten J., Leonhardt S.. Protective ventilation using electrical impedance tomography *Physiol Meas*. 2007;28:S247-S260.
 - Pulletz S., Van Genderingen H.R., Schmitz G., et al. Comparison of different methods to define regions of interest for evaluation of regional lung ventilation by EIT *Physiol Meas*. 2006;27:S115.

Author: Vladimir Sobota
 Institute: Faculty of Biomedical Engineering,
 Czech Technical University in Prague
 Street: Sitna Sq. 3105
 City: Kladno
 Country: Czech Republic
 Email: vladimir.sobota@fbmi.cvut.cz

Appendix C

POSTER 2016 conference paper

A conference paper presented at the 20th International Conference on Electrical Engineering (POSTER 2016), May 24th, 2016, Faculty of Electrical Engineering, Czech Technical University in Prague.

Regional Time Constants Determined by Electrical Impedance Tomography are Affected by Ventilatory Parameters

Vladimír SOBOTA¹, Marek LANGER¹

¹Dept. of Biomedical Technology, Czech Technical University in Prague, Nám. Sítná 3105, 272 01 Kladno, Czech Republic

vladimir.sobota@fbmi.cvut.cz, marek.langer@fbmi.cvut.cz

Abstract. *Electrical impedance tomography (EIT) is a non-invasive radiation free imaging modality that enables bedside monitoring of regional lung aeration dynamics. Recently published study has shown that EIT-derived time constants (τ) can be obtained from the data acquired during mechanical ventilation. Moreover, it suggested that τ could be used to distinguish lung pathologies. The aim of our study is to investigate whether setting of ventilatory parameters can affect the values of τ . An animal trial ($n=3$) with anesthetized mechanically ventilated pigs was conducted. In one animal, acute respiratory distress syndrome was induced by repeated whole lung lavage. Changes of tidal volume (V_T), respiratory rate (RR) and inspiratory-to-expiratory (I:E) ratio were performed. For each ventilatory setting, 20 consecutive breath cycles were used for analysis. EIT data were segmented in spatial domain and mean breath cycles were calculated. Regional values of τ were obtained for each ventilatory setting. The main result of this study is that values of τ are significantly affected by settings of ventilatory parameters. In a consequence, assessment of lung pathologies by means of τ may be compromised when various ventilatory settings are applied.*

a considerable alternative to computed tomography (CT), especially in monitoring of lung ventilation and perfusion [1], [2]. Unfortunately, when compared to CT, EIT suffers from low spatial resolution and the provided information may be rather difficult to interpret [3]. Therefore, it still seeks new approaches of data processing and visualization.

Monitoring of regional lung aeration dynamics is probably one of the most promising areas for clinical use of EIT. It has been shown that in patients with chronic obstructive pulmonary disease (COPD) the values of expiratory time constant derived from pneumotachometer data are significantly higher when compared to patients without COPD [4]. However, these pulmonary function tests provide values that are representative for the whole lungs only. To assess regional dynamics of lung aeration, a concept of regional EIT-derived time constants (τ) was introduced [5]. In this approach, EIT data are recorded continuously during spirometry and τ is calculated from a forced expiration maneuver. Subsequently, color-coded maps representing regional values of τ are generated. Moreover, recently published feasibility study [6] suggested that τ obtained in mechanically ventilated patients can be used to distinguish lung pathologies such as acute respiratory distress syndrome (ARDS) or COPD.

Hence the original idea for determination of τ uses EIT data that were recorded during defined ventilatory maneuver (forced expiration performed in Tiffeneau test), ventilatory parameters are set individually for each mechanically ventilated patient. Therefore, we hypothesized that the values of τ calculated from EIT data acquired in mechanically ventilated patients may be influenced by setting of ventilatory parameters.

The aim of this study is to investigate whether setting of ventilatory parameters can affect the values of EIT-derived regional time constants.

Keywords

Electrical impedance tomography, mechanical ventilation, respiratory mechanics, time constants.

1. Introduction

In the last two decades, electrical impedance tomography (EIT) made a big leap from a research technology to imaging modality for intensive care units. It is a safe, radiation-free technique that enables long-term bedside monitoring of patients. The principle of EIT is based on application of small alternating currents using skin electrodes attached to the patient's chest, measurement of the resulting voltages and consequent calculation of the distribution of tissue impedance within the selected body cross-section. Many studies have shown that EIT could offer

2. Methods

The study protocol was approved by the Institutional Review Board of the First Faculty of Medicine, Charles

University in Prague (FFM CU) and is in accordance with Act No. 246/1992 Coll., on the protection of animals against cruelty. The measurements were performed at an accredited animal laboratory of the FFM CU.

Three crossbred Landrace female pigs (*Sus scrofa domestica*) with a body weight of 47 ± 2 kg were used in the study.

2.1. Anesthesia and preparation

The animals were premedicated with azaperone (2 mg/kg IM), followed by anesthesia with ketamine hydrochloride (20 mg/kg IM) and atropine sulphate (0.02 mg/kg IM). When placed on the operating table, initial boluses of morphine (0.1 mg/kg IV) and propofol (2 mg/kg IV) were administered. A cuffed endotracheal tube (I.D. 7.5 mm) was used for intubation. Anesthesia was maintained with propofol (8 to 10 mg/kg/h IV) in combination with heparin (40 U/kg/h IV) and morphine (0.1 mg/kg/h IV). Myorelaxant pipecuronium bromide (4 mg boluses every 45 min) was administered during mechanical lung ventilation to suppress spontaneous breathing. Initial rapid infusion of 1 000 mL of normal saline was administered intravenously, followed by a continuous IV drip of 250 mL/h to reach and maintain central venous pressure of 6 to 7 mmHg.

Heart rate, arterial blood pressure, central venous pressure, body temperature and ECG were monitored using MU-631 RK (Nihon Kohden, Tokyo, Japan) patient monitor. Continuous cardiac output and mixed venous blood oxygen saturation were measured by Vigilance (Edwards Lifesciences, Irvine, CA, USA) monitor. Arterial blood gases, i.e. arterial partial pressure of oxygen, carbon dioxide (PaCO_2) and pH, were measured continuously by CDI 500 (Terumo, Tokyo, Japan). The arterio-venous extracorporeal circuit for CDI 500 monitor was established between the femoral artery and the femoral vein using peristaltic roller pump with a blood flow set to 400 mL/min.

In one animal, repeated whole lung lavage (normal saline, 40 mL/kg, 37°C) was performed to induce surfactant deficiency similar to ARDS [7].

2.2. Ventilation

Conventional ventilator Engström (Datex-Ohmeda, GE Healthcare, Finland) was used in the VCV mode with the following initial setting: respiratory rate (RR) 18 min^{-1} , FiO_2 21%, inspiratory-to-expiratory ratio (I:E) 1:2, positive end-expiratory pressure (PEEP) of 5 cmH_2O and pressure limit set to 40 cmH_2O . Tidal volume (V_T) was set to 8.5 mL/kg of the actual body weight and was titrated to reach normocapnia (PaCO_2 40 ± 3 mmHg).

2.3. EIT measurements

PulmoVista 500 (Dräger Medical, Lübeck, Germany) was used for continuous EIT data acquisition during the whole study protocol. The electrode belt of size S was attached to the chest of the animal at the level of the 6th intercostal space. The frequency of the applied current was set to 110 kHz and the frame rate to 50 Hz.

2.4. Study protocol

After animal preparation, myorelaxation and instrumentation, calibration of the EIT system was performed. A steady phase of 30 minutes was introduced. The study protocol consisted of three phases separated by stabilization periods. In each phase, several different settings of a selected ventilatory parameter were used while keeping the values of remaining ventilatory parameters unchanged. Each setting was kept at least for 2 minutes. The stabilization periods lasted from 3 to 4 minutes. In the first phase, the values of V_T were set in a range from 6 to 12 mL/kg with a step of 2 mL/kg. In the second phase, six different values of RR were used, ranging from 12 to 22 breaths per minute with a step of 2. Changes of I:E were performed in the third phase, setting the values of the parameter to 1:1, 1:1.5, 1:2, 1:2.5 and 1:3. The study protocol is summarized in the scheme in Fig. 1.

In the ARDS subject, different setting of ventilatory parameters was used to prevent severe hypercapnia and hypoxemia. PEEP was set to 15 cmH_2O during the whole protocol. In the first phase, RR was set to 30 min^{-1} and the highest value of V_T (12 mL/kg) was omitted. In the second phase, RR was set to 30, 35, 40, 45 and 50 min^{-1} with V_T of 8 mL/kg. The third phase was performed with RR set to 30 min^{-1} and V_T of 8 mL/kg.

2.5. Data analysis and statistics

The acquired EIT data were pre-processed using Dräger EIT Data Analysis Tool 6.1 (Dräger Medical, Lübeck, Germany). Reference frames (often referred to as baseline frames) were set automatically for each animal as frames that corresponds with the global minima of the global impedance waveforms. Reconstructed data were processed in MATLAB 2014b (MathWorks, Natick, MA, USA). For each ventilatory setting, a data set representing 20 consecutive breaths was created and used for analysis.

Functional region of interest (ROI) was determined in each data set, based on the approach of linear regression coefficient [8]. For each pixel, the relative impedance values in time (impedance waveforms) were used as a dependent variable while the global impedance waveform, determined

	Time →														
	Steady phase	Phase 1: Changes of V_T				Stabilization	Phase 2: Changes of RR					Stabilization	Phase 3: Changes of I:E		
V_T (mL/kg)	8	6	8	10	12	8	10	10	10	10	10	8	10	10	10
RR (min ⁻¹)	20	20	20	20	20	20	12	14	16	18	20	20	20	20	20
I:E (-)	1:2	1:2	1:2	1:2	1:2	1:2	1:2	1:2	1:2	1:2	1:2	1:2	1:1	1:1.5	1:2

Fig.1. Study design and the settings of ventilatory parameters during the protocol. For each phase, the changes in parameter setting are highlighted by light gray background of the parameter value. V_T —tidal volume; RR—respiratory rate; I:E—inspiratory-to-expiratory time ratio.

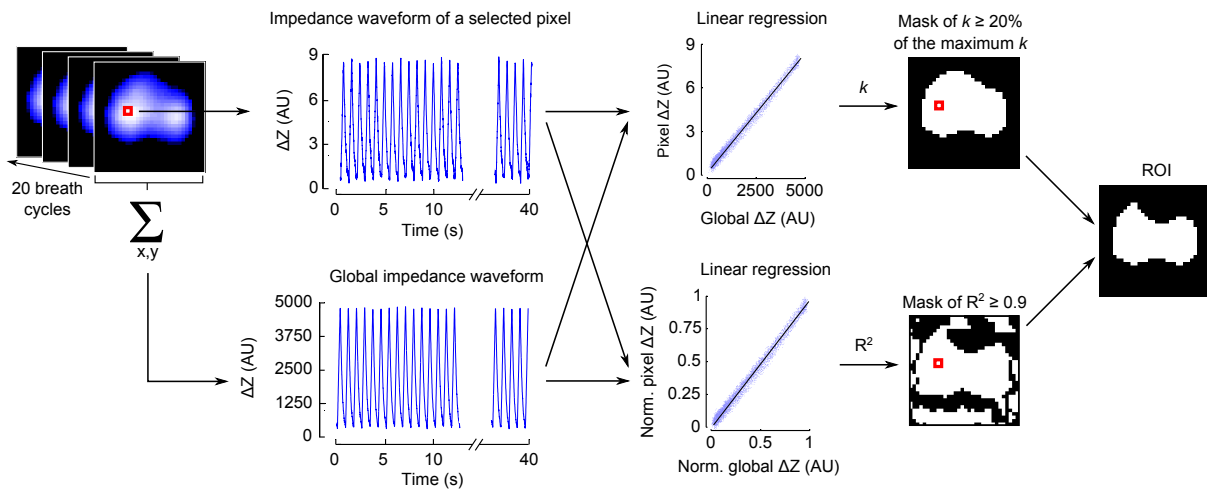


Fig.2. Determination of the region of interest (ROI). For each pixel, impedance waveform represents a time course of the relative impedance (ΔZ). Global impedance waveform is obtained as a sum of impedance waveforms of all pixels. Linear regression coefficient (k) is determined using the pixel and the global impedance waveform as a dependent and independent variable, respectively. Similarly, coefficient of determination (R^2) is calculated when the normalized values are used. Based on the given criteria, two masks are obtained from the values of k and R^2 . The final ROI is obtained as an intersection of both masks.

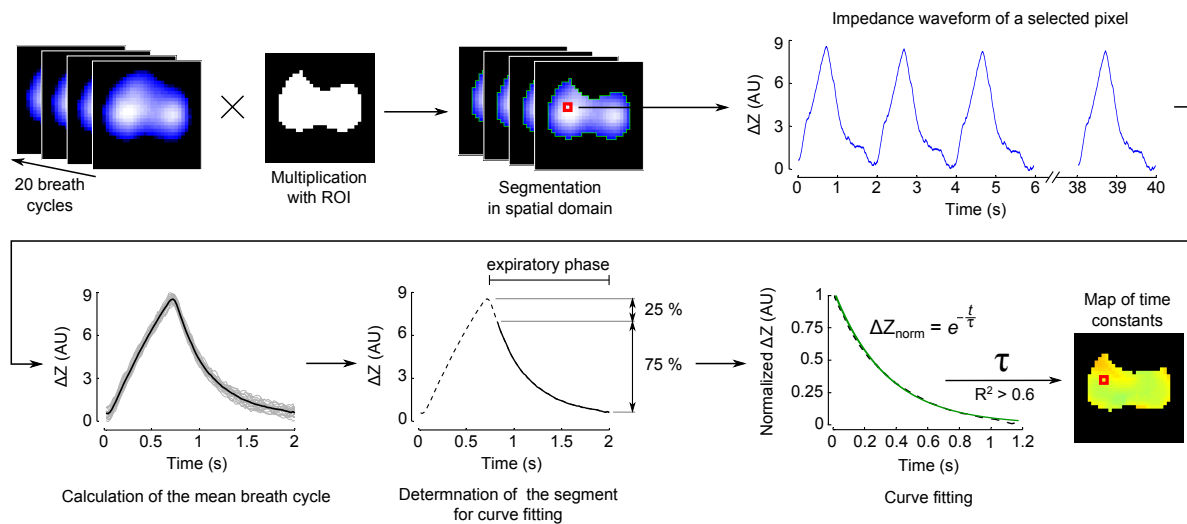


Fig.3. Data processing scheme. EIT data set is segmented in a spatial domain by multiplication of each frame with the region of interest (ROI). Impedance waveform of each pixel within the ROI is divided in 20 separated breath cycles from which one mean breath cycle is calculated. The expiratory phase of the mean breath cycle is determined and the part with the values lower than 75% of the mean breath amplitude is fitted with an exponential curve. The values of time constants (τ) obtained from the curve fitting with coefficient of determination (R^2) higher than 0.6 are visualized as a map of time constants.

as a sum of impedance waveforms of all pixels, was used as an independent variable. Consequently, linear regression coefficient was calculated. The set of all pixels with the values of regression coefficient larger than 20% of the maximum resulted in a segmentation mask. For the purposes of this study, this approach was enhanced by computation of another mask, based on the values of coefficient of determination (R^2). For each image point, both pixel and global impedance waveforms were normalized and R^2 of linear regression was calculated. The final ROI was obtained as an intersection of both masks. Determination of the ROI is schematically depicted in Fig. 2.

The ROI was applied to the data set and the segmented data were further processed. For each pixel, impedance waveform was segmented in time domain, resulting in 20 separated breath cycles from which one mean breath cycle was calculated. An expiratory phase was determined in the mean breath cycle and the part with the values higher than 75% of the mean breath amplitude was cropped [6]. The resulting part of the expiratory phase was normalized and fitted with an exponential curve:

$$\Delta Z_{\text{norm}} = e^{-\frac{t}{\tau}} \quad (1)$$

where ΔZ_{norm} is normalized relative impedance, t is time and τ is a time constant. Only the values of τ that resulted from a curve fitting with $R^2 > 0.6$ were considered [6]. The whole procedure of obtaining the time constants is depicted in Fig. 3.

For each ventilatory setting the values of τ were visualized as a color-coded maps and as a box-and-whisker-plot. To enable pairwise comparisons within each pig, only the pixels with nonzero τ for all ventilatory settings were considered for statistical analysis. The Shapiro-Wilk test was used to confirm the normality of evaluated data. The differences between the values of τ were assessed by repeated measures ANOVA. A value of $p < 0.05$ was considered as statistically significant. The statistical analysis was performed with STATISTICA (StatSoft, Inc., Tulsa, OK, USA).

3. Results

EIT data from 3 animals were analyzed according to the study protocol. In one healthy animal the values of RR were set to 12, 15, 18, 20, 22 and 24 min^{-1} in the second phase of the protocol to investigate greater range of settings. In total, 44 data sets were analyzed.

In general, the values of τ differed significantly in each phase of the protocol as shown in Fig. 4. There were only three cases where the changes in τ were statistically insignificant with $p > 0.05$ and one case with $p > 0.01$. The box plots in Fig. 4 show that V_T has an increasing effect upon values of τ while the effect of RR is exactly the opposite. Similarly, the values of τ are higher when the

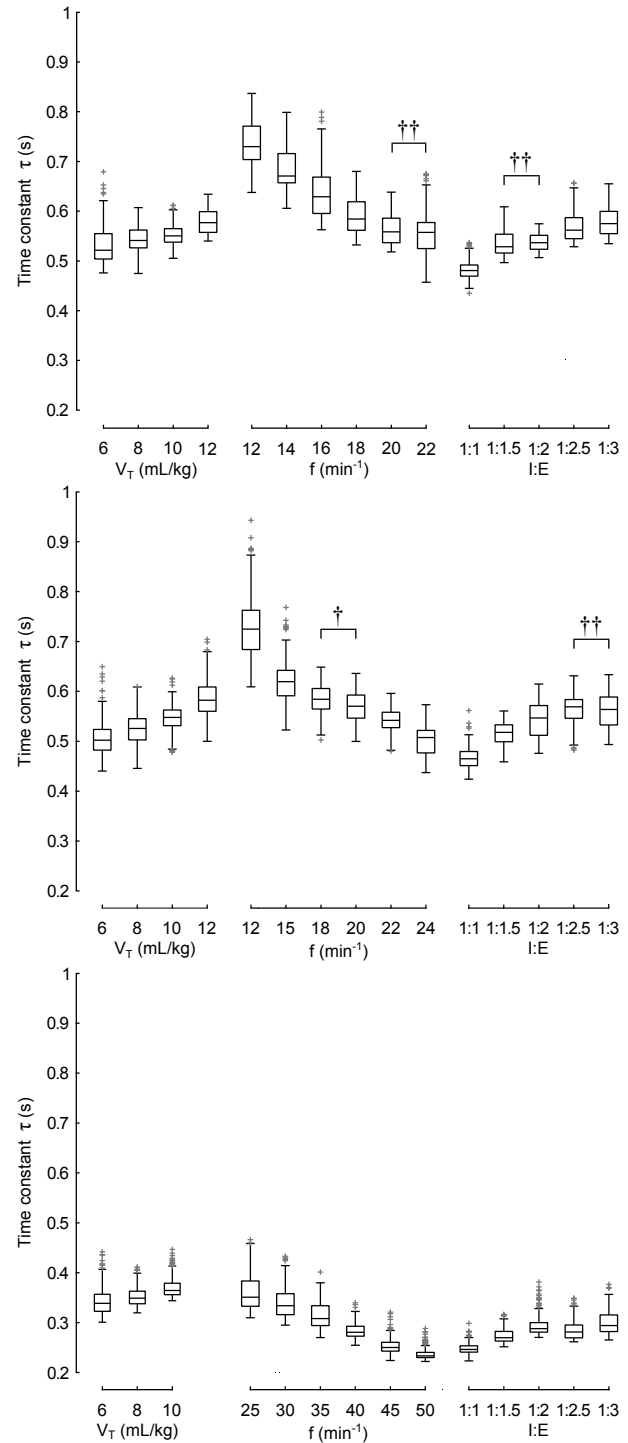


Fig. 4. Values of regional time constants (τ) for different ventilatory settings. The top and the middle graph represent the values obtained in healthy animals, the bottom graph presents τ calculated in the animal with induced acute respiratory distress syndrome. Statistically insignificant differences are marked as † ($p > 0.01$) and †† ($p > 0.05$). V_T , tidal volume; RR, respiratory rate; I:E, inspiratory-to-expiratory ratio.

value of I:E is increased on the side of expiratory time. In the ARDS animal, τ was significantly lower as shown in Fig. 4 and in the color-coded maps presented in Fig. 5 and 6.

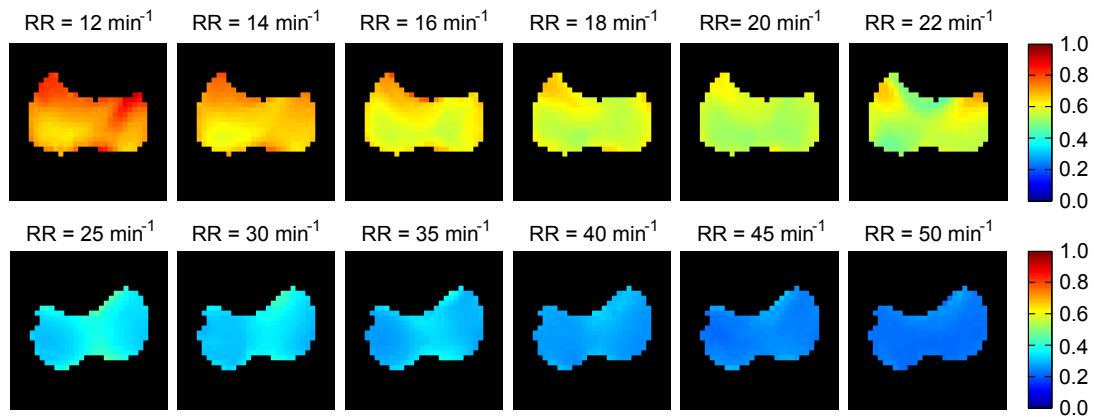


Fig.5. Color-coded maps of time constants obtained during the second phase of the study protocol. Top row: changes of respiratory rate (RR) in healthy animal—positive end-expiratory pressure (PEEP) 5 cmH₂O, tidal volume (V_T) 10 mL/kg, inspiratory-to-expiratory ratio (I:E) 1:2. Bottom row: animal with induced acute respiratory distress syndrome—PEEP 15 cmH₂O, V_T 8 mL/kg, I:E 1:2.

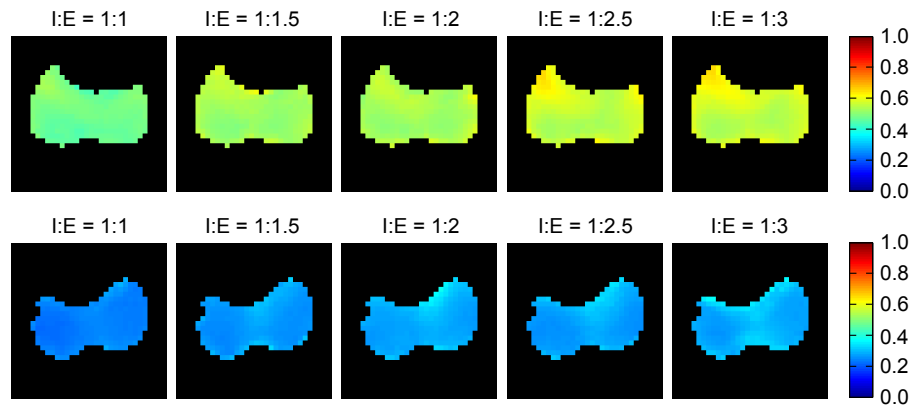


Fig.6. Color-coded maps of time constants obtained during the third phase of the study protocol. Top row: changes of inspiratory-to-expiratory ratio (I:E) in healthy animal—positive end-expiratory pressure (PEEP) 5 cmH₂O, tidal volume (V_T) 10 mL/kg, respiratory rate (RR) 20 min^{-1} . Bottom row: animal with induced acute respiratory distress syndrome—PEEP 15 cmH₂O, V_T 8 mL/kg, RR 30 min^{-1} .

4. Discussion

The main result of this study is that values of regional EIT-derived time constants τ are affected by setting of ventilatory parameters. Statistically significant changes of τ were observed for different settings of V_T , RR and I:E in healthy animals as well as in the animal with artificially induced ARDS.

The values of τ obtained in healthy animals are comparable with the values presented in recently published study [6]. However, we observed more pronounced decrease of τ in the ARDS animal. This was probably caused by the setting of RR which was relatively high during the whole study protocol. Because the results show that RR has a decreasing effect upon τ , it is rather difficult to distinguish how much the values of τ are affected by the ventilatory setting and what is the effect of the lung injury itself.

Despite the observed dependency of τ upon settings of ventilatory parameters, we do not reject the idea that different lung pathologies could be distinguished

by assessment of regional dynamics of lung aeration as determined by EIT. However, the results of our study indicate that a defined ventilatory maneuver or ventilatory setting is necessary to obtain comparable values for different subjects.

There are numerous outliers above the box plots depicted in Fig. 4, especially in the graph of the ARDS animal. Analysis of the maps of time constants presented in Fig. 5 and 6 showed that the corresponding pixels are predominantly located at the ventral edge of the ROI. Therefore, we speculate that the high values of τ in these pixels are caused by the presence of cardiac-related artifacts in the impedance waveforms.

Although the original idea of regional time constants considered calculation of τ on a breath-to-breath basis, we decided to use mean breath cycles for our calculations. The main advantage of this approach is that averaging attenuates the artifacts in the impedance waveforms that are related to cardiac activity and lung perfusion.

In this study we used a modified approach for calculation of ROI. Multiplication of the original ROI with the mask that is based on the values of R^2 resulted in most of the cases in neglecting of cardiac-related pixels. In a consequence, there were only few pixels where the value of τ was omitted due to poor curve fitting ($R^2 < 0.6$).

Despite the fact the study was performed using data from three animals only, we do not consider this number as insufficient. Rather than evaluation of τ in individual animals, we wanted to assess the changes caused by different ventilatory settings. Thus, the applied range of selected ventilatory parameters was more important for the study design than the total number of evaluated subjects. For this reason, we considered higher number of animals involved in the study as ethically inappropriate.

5. Conclusion

This study shows that setting of ventilatory parameters significantly affects the values of EIT-derived regional time constants. In a consequence, assessment of lung pathologies by means of regional time constants may be compromised when various ventilatory settings are applied.

Acknowledgements

The authors thank to employees of the animal laboratory of the Department of Physiology, FFM CU, where the animal trial was performed. Especially, we would like to express our gratitude to Mikuláš Mlček, MD, PhD. The study was supported by grant SGS16/258/OHK4/3T/17.

References

- [1] VICTORINO, J.A., BORGES, J.B., OKAMOTO, V.N., MATOS, G.F., TUCCI, M.R., CARAMEZ, M.P., TANAKA, H., SIPMANN, F.S., SANTOS, D.C., BARBAS, C.S., CARVALHO, C.R., AMATO, M.B. Imbalances in regional lung ventilation: a validation study on electrical impedance tomography. In *American Journal of Respiratory and Critical Care Medicine*, 2004, vol. 169, no. 7, pp. 791-800.
- [2] FRERICHS, I., HINZ, J., HERMANN, P., WEISSER, G., HAHN, G., QUINTEL, M., HELBIGE, G. Regional Lung Perfusion as Determined by Electrical Impedance Tomography in Comparison With Electron Beam CT Imaging. In *IEEE Transactions on Medical Imaging*, 2002, vol. 21, no. 6, pp. 646-52.
- [3] PUTENSEN, C., WRIGGE, H., ZINSERLING, J. Electrical impedance tomography guided ventilation therapy. In *Current Opinion in Critical Care*, 2007, vol. 13, no. 3, pp. 344-50.
- [4] LOURENS, M.S., VAN DEN BERG, B., AERTS, J.G., VERBRAAK, A.F., HOOGSTEDEN, H.C., BOGAARD, J.M. Expiratory time constants in mechanically ventilated patients with and without COPD. In *Intensive Care Medicine*, 2000, vol. 26, no. 11, pp. 1612-8.
- [5] PIKKEMAAT, R., TENBROCK, K., LEHMANN, S., LEONHARDT, S. Electrical impedance tomography: New diagnostic possibilities using regional constant maps *Applied Cardiopulmonary Pathophysiology*, 2012, vol. 16, pp. 212-225.
- [6] RÓKA, P.L., WALDMANN, A.D., MÜLLER, B., ENDER, F., BÖHM, S.H., WINDISCH, W., STRASSMANN, S., KARAGIANNIDIS, C. Breath-by-breath regional expiratory time constants by electrical impedance tomography – a feasibility study. In *Proceedings of the 16th International Conference on Biomedical Applications of Electrical Impedance Tomography*. Neuchâtel (Switzerland), 2015, p. 50.
- [7] VAN HEERDE, M., ROUBÍK, K., KOPELANT, V., KNEYBER, M.C.J., MARKHORST, D.G. Spontaneous breathing during high-frequency oscillatory ventilation improves regional lung characteristics in experimental lung injury *Acta Anaesthesiologica Scandinavica*, 2010, vol. 54, pp. 1248-1234.
- [8] PULLETZ, S., VAN GENDERINGEN, H.R., SCHMITZ, G., ZICK, G., SCHÄDLER, D., SCHOLZ, J., WEILER, N., FRERICHS, I. Comparison of different methods to define regions of interest for evaluation of regional lung ventilation by EIT *Physiological Measurement*, 2006, vol. 27, no. 5, pp. S115-27.

About Authors...

Vladimír SOBOTA was born in Vrchlabí, Czech Republic, in 1990. He received his bachelor (Bc.) degree from the Faculty of Biomedical Engineering, Czech Technical University in Prague, where he is currently working towards his master degree. His research activities are aimed at electrical impedance tomography.

Marek LANGER was born in Ostrava, Czech Republic, in 1993. Currently, he is working towards his bachelor degree at Faculty of Biomedical Engineering, Czech Technical University in Prague. His research is focused on electrical impedance tomography.

Appendix D

CD contents

Description	Name of the file
Abstract (Czech)	abstract_cz.pdf
Abstract (English)	abstract_en.pdf
Keywords (Czech)	keywords_cz.pdf
Keywords (English)	keywords_en.pdf
Master thesis	master_thesis.pdf
Master thesis assignment (Czech)	thesis_assignment_cz.pdf
Master thesis assignment (English)	thesis_assignment_en.pdf